UiT
THE ARCTIC
UNIVERSITY
OF NORWAY

Faculty of Science and Technology
Department of Physics and Technology

Stochastic modelling of intermittent scrape-off layer plasma fluctuations

Audun Theodorsen

FYS-3900 Master's thesis in physics May 2015

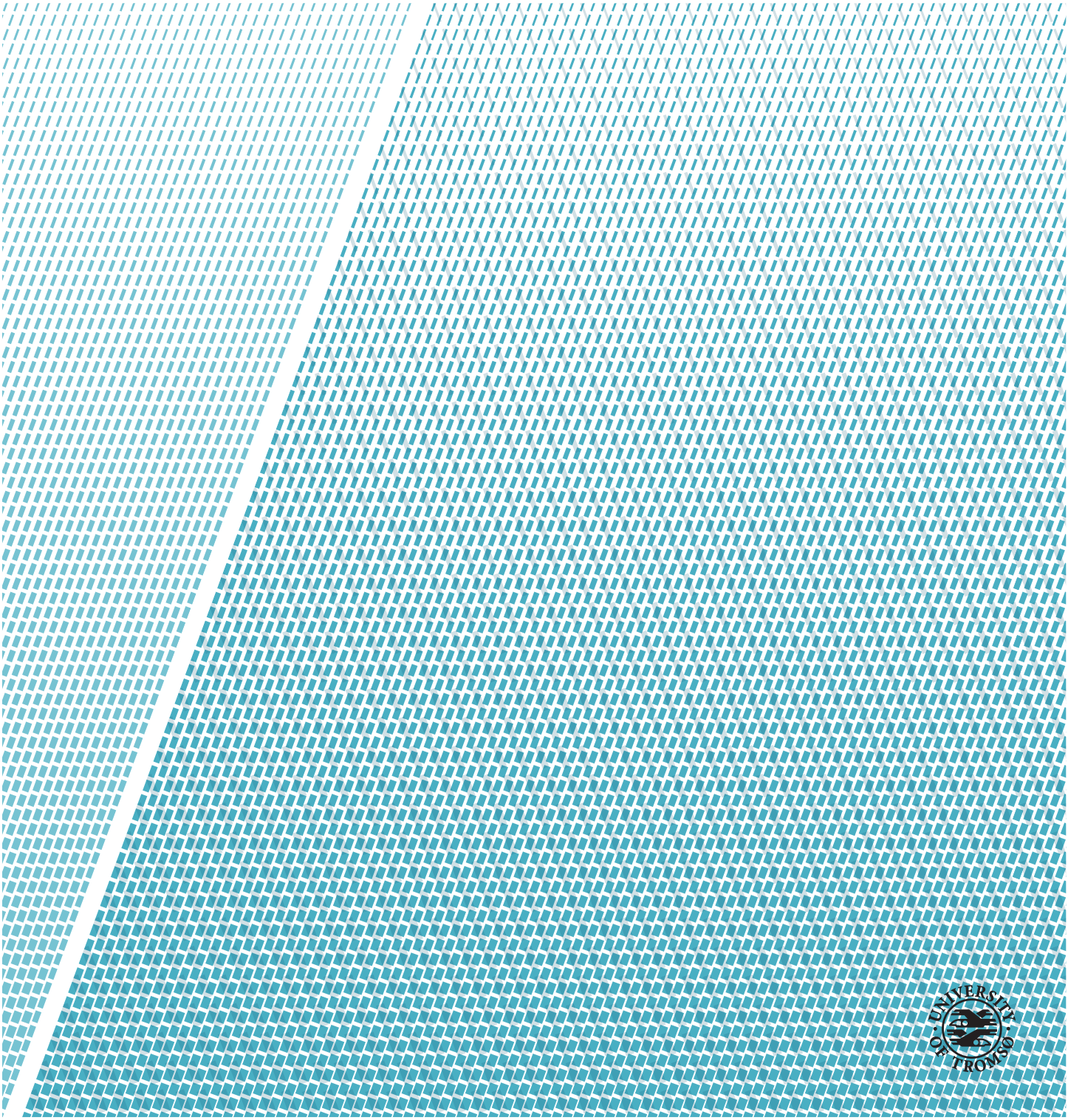

Abstract

In the tokamak scrape-off layer, radial motion of blob-like structures is the dominant mechanism for transport of particles and heat. Fixed point probe measurements in the Tokamak à Configuration Variable scrape-off layer reveal highly intermittent fluctuations in the ion saturation current. These measurements are well described by a shot noise process with exponential pulse shapes, exponentially distributed pulse amplitude and pulses arriving according to a Poisson process.

The statistical properties of this shot noise process is explored in this thesis. Characteristic functions and probability density functions of the shot noise process have been derived, as well as the joint probability density function between the resulting signal and its derivative. These probability density functions have then been used to derive a general model for the excess statistics of a shot noise process. This model has been explored using synthetically generated shot noise time series.

Synthetically generated shot noise time series have also been used to compare results of conditional averaging using various pulse amplitude and waiting time distributions, as well as different pulse shapes. While the pulse shape is well preserved after conditional averaging, the pulse waiting time and amplitude distributions are not.

Excess time statistics have been analyzed for the ion saturation current measured by a Langmuir probe at a fixed point in the Tokamak à Configuration Variable scrape-off layer. The general model gives a qualitatively better fit to the data from the measurements than the normal limit does. Probability density functions of the time above threshold per upcrossing have been computed, and reveal exponential tails. It is found that both the average time above threshold per upcrossing and the root mean square value of the time above threshold per upcrossing have very slow decay for large threshold values, underlining the importance of intermittent fluctuations for plasma-wall interactions for tokamak plasmas.

Acknowledgements

First, I would like to thank my supervisor, Professor Odd Erik Garcia, for guidance, advice and always finding the time for lengthly discussions.

I would also like to thank Ralph Kube, for startup help, python-support and the nice figure layout.

I am grateful to Bjørn Fjukstad, Erlend Graff (and anyone else who worked on it) for the UiT thesis LaTeX template.

Also my parents and grandparents for support, meta advice and dinners.

And finally Martine Johansen Lerbukt for love, motivation and making sure I take a break every now and then.

Contents

Abstract i

Acknowledgements iii

List of Figures ix

List of Tables xi

1 Introduction and motivation 1
- 1.1 Transport and turbulence in the SOL . . . 2
- 1.2 The TCV Tokamak . . . 5
  - 1.2.1 The TCV Discharge 27601 data set . . . 5
  - 1.2.2 Motivation from the TCV results . . . 10
- 1.3 Thesis Structure . . . 12
- 1.4 List of symbols . . . 13

2 Stochastic modelling by shot noise processes 15
- 2.1 Shot noise processes . . . 15
  - 2.1.1 Signal formulation and assumptions . . . 16
  - 2.1.2 General expression for the mean of $\Phi(t)$ . . . 20
  - 2.1.3 Expressions for the variance . . . 21
  - 2.1.4 Distribution and characteristic functions of $\Phi(t)$ . . . 30
  - 2.1.5 Autocorrelation function and power spectral density of the shot noise process . . . 37
- 2.2 The normalized time derivative of a shot noise process . . . 41
  - 2.2.1 Variance of the time derivative of a shot noise process 43
  - 2.2.2 Moments of the time derivative of a shot noise process 44
  - 2.2.3 The PDF of the time derivative of a shot noise process for the double exponential waveform . . . 45
- 2.3 The joint PDF $P_{\Phi\Theta}(\Phi,\Theta)$ . . . 50
  - 2.3.1 The characteristic function of $P_{\Phi\Theta}(\Phi,\Theta)$ . . . 50
  - 2.3.2 The full joint PDF $P_{\Phi\Theta}(\Phi,\Theta)$ . . . 51
  - 2.3.3 Correlation and dependencies in the joint PDF . . . 52
  - 2.3.4 Reduction of the joint PDF to the marginal PDFs . . . 53

2.3.5 Discussion 55

3 Excess time statistics **59**
3.1 Definition of total time above threshold, number of upcrossings and average time above threshold 60
3.1.1 The models 61
3.1.2 The normalized threshold 62
3.1.3 Another way to the number of upwards crossings . . 63
3.2 The general model 64
3.2.1 Total time above threshold 64
3.2.2 The total number of upwards threshold crossings . . 65
3.2.3 The average time above the threshold 65
3.2.4 The limit of large γ 66
3.2.5 The limit of the one-sided waveform 66
3.2.6 The limit of $\zeta \gg 1$ 68
3.3 The normal limit $\gamma \gg 1$ 68
3.3.1 The total time above threshold 69
3.3.2 The total number of upwards crossings 69
3.3.3 The average time above threshold 70
3.4 The strong intermittency limit $\gamma \ll 1$ 70
3.4.1 The total time above threshold 71
3.4.2 The total number of upwards crossings 71
3.4.3 The average time above threshold 72
3.4.4 The PDF of $\mathcal{T}$ and another way to $\langle \mathcal{T} \rangle(C)$ 72
3.5 Comparisons 76
3.5.1 Comparisons of expressions for $\zeta \gg 1$ 78
3.6 Excess time statistics of synthetic data 78
3.6.1 Method 79
3.6.2 Total time above threshold from synthetic data 79
3.6.3 Number of upwards crossings from synthetic data . . 80
3.6.4 Average time above threshold from synthetic data . . 80
3.6.5 The rms-value of the time above threshold 84
3.6.6 The PDF of the time above threshold 86

4 Conditional averaging **87**
4.1 Theory and methods 87
4.1.1 Problems and prospects 89
4.1.2 Choice of threshold 89
4.2 Conditional averaging of synthetic data 90
4.2.1 Preservation of waiting time distribution 92
4.2.2 Preservation of amplitude distribution 94
4.2.3 Preservation of the pulse waveform 97
4.2.4 Conclusion 100

5 Results from TCV **103**
5.1 Moments of the normalized ion saturation current 104
5.2 Moments of the derivative of the normalized ion saturation current 105
5.3 Excess time statistics for the TCV data 107
5.3.1 Fraction of time above threshold 107
5.3.2 Rate of positive threshold crossings 107
5.3.3 Average time above threshold 109
5.3.4 Rms-value of time above threshold 110
5.3.5 PDF of time above threshold 110

6 Conclusion **113**
6.1 Future work and prospects 115

Appendices

A Special Functions **117**
A.1 The Fourier transform $\mathcal{F}$ 117
A.2 The gamma function $\Gamma(s)$ 118
A.2.1 Large arguments 118
A.2.2 Small argument 118
A.2.3 The incomplete gamma functions 118
A.2.4 The limit of large x 119
A.2.5 The limit of small x 119
A.3 The error function 119
A.3.1 The limit $x \to \infty$ 120
A.4 A useful limit 120

B Statistical Concepts **121**
B.1 The cumulative distribution function 121
B.2 The probability density function 122
B.3 Moments of X 122
B.3.1 The mean value $\langle X \rangle$ 123
B.3.2 The variance and rms values 123
B.3.3 Skewness 123
B.3.4 Kurtosis 123
B.3.5 Preserving S_X and F_X under normalization 124
B.3.6 Estimation of moments 124
B.4 The characteristic function 125
B.5 Commonly used distribution functions 125
B.5.1 The exponential distribution 126
B.5.2 The Rayleigh distribution 126
B.5.3 The degenerate distribution 127
B.5.4 The uniform distribution 127

B.5.5 Other relevant distributions 128
B.6 The connection between the Poisson distribution, the uniform distribution and the exponential distribution 130
B.7 Equivalence of Gamma distribution and Gaussian distribution in the limit of large shape parameter 131
B.8 Truncated distributions 133

C Source Code **137**

Bibliography **149**

List of Figures

1.1 Schematics of the tokamak configuration. 2
1.2 Puff of neutral deuterium gas in the edge plasma region of the NSTX experiment. The area is $(23\text{cm})^2$, and there are $10\mu s$ between each frame. Image courtesy of Stuart Zweben. . . . 3
1.3 Large-scale fluctuations in the SOL 4
1.4 TCV Discharge 27601: a) Poloidal cross-section of the TCV. b) Detail around the probe. c) The Langmuir probe head [Horacek et al., 2005]. 5
1.5 TCV Discharge 27601: The derivative of the signal in Figure 1.3a, normalized by the correlation time $\tau_d = 15.9\mu s$. . . 6
1.6 TCV Discharge 27601: Probability density function of the normalized ion saturation current, logarithmic scale. 7
1.7 TCV Discharge 27601: Complementary cumulative distribution function of the waiting time between large amplitude events in the normalized, detrended electron density. 8
1.8 TCV Discharge 27601: Complementary cumulative distribution function of the amplitudes of conditionally averaged bursts. 8
1.9 TCV Discharge 27601: The conditionally averaged waveforms. 9
1.10 TCV Discharge 27601: Autocorrelation function of the normalized, detrended plasma electron density 11
1.11 TCV Discharge 27601: Power spectral density of the normalized, detrended plasma electron density 11

2.1 Several realizations of the shot noise process with $\gamma = \tau_d/\tau_w$ as the intermittency parameter. The waveform Eq. (2.5) with $\tau_r = 0.25$, $\tau_f = 0.75$ has been used, and $\langle A \rangle = 1$. 16
2.2 The normalized, analytic derivatives of the shot noise processes in Figure 2.1. The form of this derivative is covered in Section 2.2. 17
2.3 Comparisons of the relative fluctuation level for exponential, Rayleigh and degenerate waiting time distributions. The amplitudes are exponentially distributed. 31
2.4 Logarithmic scale of Figure 2.3 to see behaviour for $\gamma \to 0$ and $\gamma \to \infty$. 31

2.5 The PDF of a shot noise process for various γ-values 34
2.6 Auto-correlation function for the centered and scaled signal for a range of τ_r. 40
2.7 Power spectral density for the centered and scaled signal for a range of τ_r. 40
2.8 The PDF of the time derivative of a shot noise process, from equation (2.100). Above, $\lambda = 1/2$ for various γ. Below,$\gamma = 2$ for various λ. 48
2.9 Joint PDF between Φ and Θ for $\gamma = 5$ with changing λ. . . . 56
2.10 Joint pdf (left) and product of the marginal pdfs (right) between Φ and Θ for $\lambda = 0.25$ and various γ. 57

3.1 Example of excess times over the threshold $\zeta = \widehat{\Phi}/2$ for a synthetic signal with $\gamma = 1$ and $\lambda = 0.25$. 60
3.2 Excess times for a shot noise process with $\gamma = 0.1$ and $\lambda = 0.5$ 73
3.3 The PDF of time above threshold in the strong intermittency limit where pulse overlap can be neglected, for various threshold values. 75
3.4 The average time above threshold in the strong intermittency limit where pulse overlap can be neglected, with bounds of rms-value of time above threshold. 75
3.5 Comparison of analytic expressions for excess times for $\lambda = 0.25$ and various intermittency parameters. 77
3.6 Fraction of time above threshold for $\lambda = 0.25$ and varying γ. 79
3.7 Rate of upwards crossings over threshold for $\lambda = 0.25$ and varying γ. 80
3.8 Average time above threshold for $\lambda = 0.25$ and varying γ. . . 81
3.9 Comparison of average time above threshold for $\lambda = 0$ and $\lambda > 0$ calculated from synthetic data. 82
3.10 Average time above threshold for large threshold. $\lambda = 0.25$ and γ varies. 83
3.11 The second raw moment of time above threshold for changing γ 85
3.12 The second raw moment of time above threshold for changing λ 85
3.13 The PDF of time above threshold for $\lambda = 0.25$ and changing γ 86

4.1 Left: A synthetically generated shot noise process with $\lambda = 0.25$ and $\gamma = 1$ (blue lime), threshold (black dotted line), found peak values (red stars) and corresponding subintervals (green horizontal bars). Right: The average from all subintervals. 88
4.2 Graphical representation of complementary CDFs 91
4.3 Waiting time distributions of conditionally averaged signals with $\gamma = 1$, with fitted exponential and Rayleigh distributions. 92

4.4 Comparisons of waiting time distributions for large-amplitude events. 93
4.5 Comparison of conditionally averaged waiting times with intermittency parameter $\gamma = 0.1$. 93
4.6 Conditionally averaged amplitude distributions with fitted exponential and Rayleigh distributions. $\gamma = 1$ and the pulse waiting times are exponentially distributed. 95
4.7 Comparison of conditionally averaged amplitude distributions. The pulse waiting times are degenerately distributed. 95
4.8 Comparison of conditionally averaged amplitude distributions with non-degenerate pulse waiting time distributions. 96
4.9 Comparison of conditionally averaged amplitude distributions with uniformly distributed pulse amplitudes and varying pulse waiting time distribution. 96
4.10 Conditionally averaged amplitude distributions fitted to exponential and Rayleigh distributions. $\gamma = 0.5$ and pulse amplitude distribution is uniform. 96
4.11 An example of a conditionally averaged signal with threshold $\alpha = 2.5$. 98
4.12 Conditionally averaged signals with $K = 10^5$ and $\gamma = 10$. Pulse amplitudes and waiting times are exponentially distributed. The conditionally averaged signal has been normalized to fall off towards 0 and to have a peak at 1 99
4.13 Comparisons of λ and waveforms after conditional averaging and normalization. 100

5.1 PDF of the normalized particle density 104
5.2 PDF of the normalized derivative of the ion saturation current from TCV Discharge 27601. Note the logarithmic scale used for the y-axis. 105
5.3 TCV Discharge 27601: Fraction of time above threshold as a function of the normalized threshold, compared to the general model and the non-intermittent limit. 108
5.4 TCV Discharge 27601: Rate of positive threshold crossings as a function of the normalized threshold, compared to the general model and the non-intermittent limit. 108
5.5 TCV Discharge 27601: Average time above threshold as a function of the normalized threshold, compared to the general model and the non-intermittent limit. 109
5.6 TCV Discharge 27601: Rms-value of time above threshold as a function of the normalized threshold. 110
5.7 TCV Discharge 27601: PDF of time above threshold as a function of time above threshold for different threshold values. . 111

B.1 Comparison of the normal distribution to the Gamma distribution for three different values of the scale parameter k. . . 133

List of Tables

5.1 Comparison of moments of the derivative of the normalized ion saturation current. 105

1

Introduction and motivation

Since the discovery some 80 years ago that nuclear fusion of small elements releases large amounts of energy, controlling and harnessing this power has been a goal for the scientific community. While the challenges were great (great enough to see collaboration between Nato and Soviet during the Cold War), today nuclear fusion is one of our most promising paths towards a clean and sustainable energy source. One particularly promising design for a fusion reactor is the tokamak, invented by Igor Tamm and Andrei Sakharov in the Soviet Union [Fowler, 1999].

The tokamak is a torus-shaped device which uses magnetic fields to confine the hot plasma which sustains the fusion reactions. The magnetic fields are created by magnetic coils as well as currents in the plasma, as presented in Figure 1.1a. Toroidal magnetic coils are used to create a toroidal magnetic field, while currents within the plasma together with the poloidal coils create a poloidal magnetic field. Together, these fields result in a helical magnetic field which confines the plasma particles to helical paths within the tokamak. However, due to the toroidal shape of the tokamak, forces are generated which push the plasma outwards along the major radius of the device, towards its outer walls [Freidberg, 2007, p. 271]. This is undesirable, as plasma-wall interactions causes damage to the walls and release of impurities back into the plasma. To avoid plasma-wall interactions, divertor targets are set up below the plasma

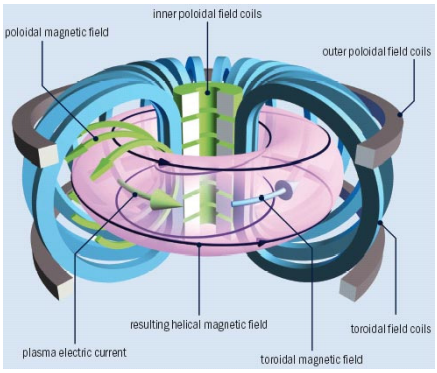

(a) Magnetic coils and the resulting current and helical magnetic field.

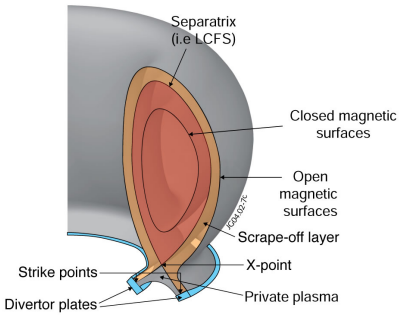

(b) Poloidal cross-section of the diverted tokamak plasma.

Figure 1.1: Schematics of the tokamak configuration.

core where plasma exhaust and removal of impurities can be controlled. A schematic of the poloidal cross-section of the magnetic field lines in a tokamak with divertor targets is presented in Figure 1.1b. In the plasma core, the magnetic field lines are closed. Closer to the wall, outside the separatrix (or last closed flux surface), the magnetic field lines intersect the divertor targets. This area of open magnetic field lines is called the *scrape-off layer* (SOL). Outside of the SOL is the *wall shadow*, where the magnetic field lines hit the tokamak walls instead of the divertor targets. Ideally, plasma moving across the separatrix will follow the magnetic field lines ending at the divertor targets instead of hitting the tokamak walls [Stangeby, 2000a,b].

1.1 Transport and turbulence in the SOL

Unfortunately, it turns out that the plasma moving into the SOL does not always simply flow towards the divertor targets. An example is seen in Figure 1.2, where a neutral deuterium gas has been injected into the edge region of a plasma and the resulting emission is recorded by a fast camera [Maqueda et al., 2011]. The solid line is the location of the last closed flux surface (see Figure 1.1b), while the dotted line marks the beginning of the wall shadow, where magnetic field lines hit the main chamber wall of the tokamak. A blob of plasma escaping across the separatrix reaches the wall shadow in about 70μs, and dissipates at the wall instead of at the divertor targets. The radial motion of such blob-like structures is the dominant mechanism for transport of particles and heat in the SOL [D'Ippolito et al., 2011, Garcia, 2009].

Figure 1.3a shows the ion saturation current fluctuations measured by a Lang-

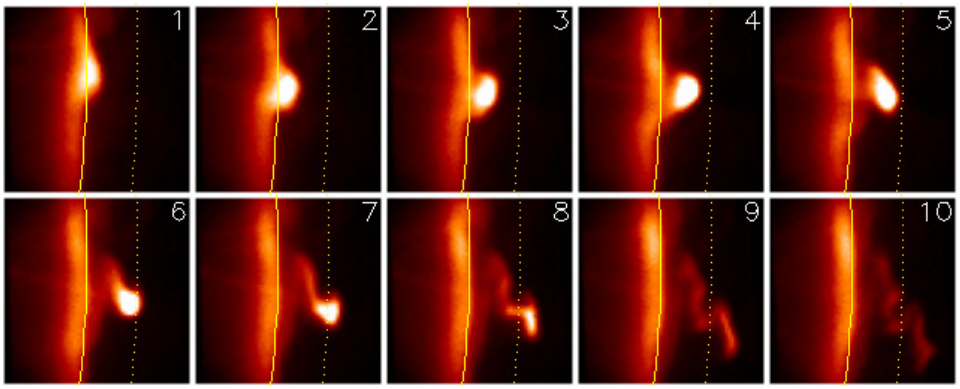

Figure 1.2: Puff of neutral deuterium gas in the edge plasma region of the NSTX experiment. The area is $(23\text{cm})^2$, and there are $10\mu s$ between each frame. Image courtesy of Stuart Zweben.

muir probe at a fixed point in the SOL of the Tokamak á Configuration Variable (TCV) tokamak. Here, fluctuations often reach values above 4 times the root mean square (rms)-value, (which is very unlikely for a Gaussian process, a probability of less than 3×10^{-5}). Figure 1.3a is a time series; the bursts seen are due to the radial motion of blob-like structures such as the one seen in Figure 1.2. That such large-scale fluctuations exist in the SOL is a well-known result. In Figure 1.3b, the rms-values of electron density, electric potential, electron temperature and magnetic field strength in the SOL are presented as functions of radius. $r/a = 1$ corresponds to the last closed magnetic flux surface, so $r/a > 1$ corresponds to the SOL. It is evident that while there exists fluctuations in the electron density and electric potential in the plasma core, the fluctuation levels increase rapidly with distance in the SOL, and the same behaviour is seen in the electron temperature.

The large-amplitude fluctuations caused by the motion of blob-like structures in the SOL present considerable engineering challenges. We need to be capable of describing these fluctuations in a coherent manner. The focus of this thesis will be to approach the problem by using statistical modelling to describe fluctuations seen in time series from single-point measurements. The analytical work will be motivated by and compared to the TCV tokamak discharge 27601 ion saturation current (Figure 1.3a). The model presented here and its predictions are general. While we apply the model to the plasma scrape-off layer in tokamaks, it can be applied to many other physical systems. Examples include shot effect in vacuum tubes, thermal agitation of electrons in resistors [Rice, 1944] and atmospheric wind gusts [Kristensen et al., 1991].

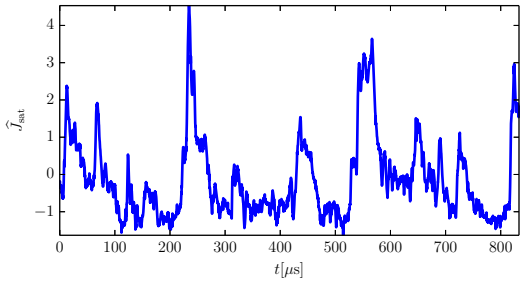

(a) TCV Discharge 27601: Excerpt of the normalized, detrended ion saturation current at the probe position in the SOL.

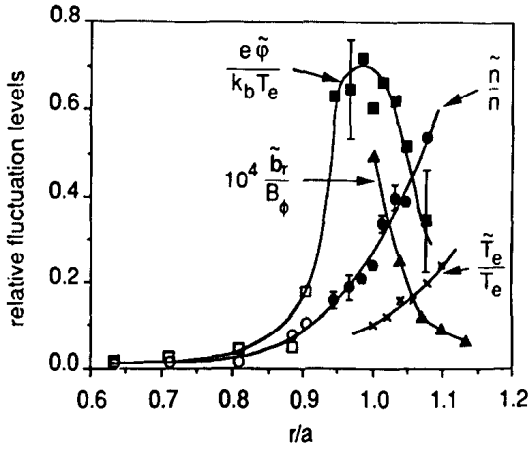

(b) The radial dependencies of the normalized rms fluctuating amplitudes of density ($\widetilde{n}/n$), potential ($\widetilde{\phi}/k_b T_e$), temperature ($\widetilde{T_e}/T_e$) and magnetic field ($\widetilde{b_r}/B_\phi$) in a trial in the TEXT-tokamak [Wootton, 1990].

Figure 1.3: Large-scale fluctuations in the SOL

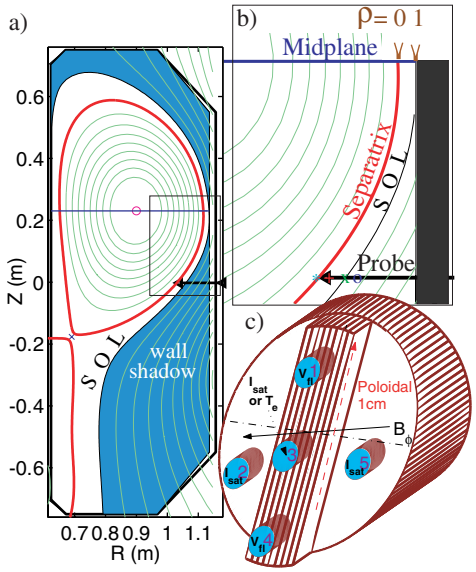

Figure 1.4: TCV Discharge 27601: a) Poloidal cross-section of the TCV. b) Detail around the probe. c) The Langmuir probe head [Horacek et al., 2005].

1.2 The TCV Tokamak

The TCV Tokamak is a medium sized tokamak with major plasma radius $R_0 = 0.89$m and minor plasma radius $a = 0.25$m. In the experiment discussed here, the toroidal magnetic field was $B_{\text{tor}} = 1.4$T, and a standard 5-pin Langmuir probe was used for measurement of plasma fluctuations. The probe head is fixed 10mm below the midplane, and 3mm in front of the main chamber wall [Garcia et al., Forthcoming 2015]. A graphical representation of the poloidal cross-section of the TCV tokamak is presented in Figure 1.4, where the blue lines show the magnetic field lines and the broken blue lines represent the SOL magnetic field. The black arrow in the right mid-plane shows how the Langmuir probe enters the plasma, although in this figure it is about 23cm below the midplane. More detailed, technical discussions of the tokamak and probe setups can be found in Horacek et al. [2005] and Garcia et al. [Forthcoming 2015].

1.2.1 The TCV Discharge 27601 data set

The Langmuir probe recorded (among other data) the ion saturation current J_{sat} in the SOL plasma. The probe recorded at a frequency of 6Mhz for about one second, an unprecedented length of time. During this time, all plasma parameters were constant except for a slow drift of the plasma column, causing

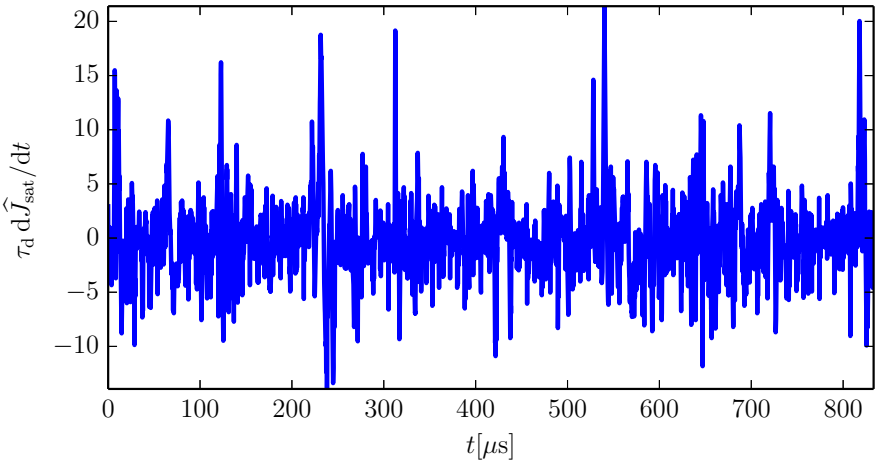

Figure 1.5: TCV Discharge 27601: The derivative of the signal in Figure 1.3a, normalized by the correlation time $\tau_d = 15.9\mu s$.

a linear trend in J_{sat}. In addition, due to errors in measurement of low frequency variations, negative values of the saturation current appears in the time series. In order to counteract these problems, the linear trend was first removed and then the signal was normalized according to $\widehat{J}_{sat} = (J_{sat} - \langle J_{sat} \rangle)/J_{rms}$. The trend was $-6.23\text{mAs}^{-1}t[\text{s}] + 6.43\text{mA}$ and the rms-value was $J_{rms} = 4.89\text{mA}$. The moments of $\widehat{J}_{sat}$ are presented below. Trivially, the first two moments are very close to 0 and 1, respectively. $\widehat{J}_{sat}$ has a positive skewness and a flatness which is 3.65 higher than the flatness of a normal distribution. Thus, the ion saturation current is far from being normally distributed,

$$S_{\widehat{J}_{sat}} = 1.51, \tag{1.1}$$

$$F_{\widehat{J}_{sat}} = 6.65. \tag{1.2}$$

An excerpt of the detrended, normalized signal is presented in Figure 1.3a. Note the bursty nature of this signal with frequent appearances of amplitudes much larger than the rms-value of the signal. In Figure 1.5, the normalized derivative of $\widehat{J}_{sat}$ is presented, $\tau_d d\widehat{J}_{sat}/dt$, where τ_d is the correlation time of the signal, which is later in this section shown to be $15.9\mu s$. This derivative has been calculated using a five-point polynomial method.

In Figure 1.6, the probability density function (from here on denoted PDF) of the normalized, detrended ion saturation current is presented, along with a fitted normalized gamma distribution [see appendix, Eq. (B.25)]. The gamma distribution is a good fit for $\widehat{J}_{sat} > 0$, but fails for lower values of $\widehat{J}_{sat}$, most likely due to the negative values in the original data set. Here and in the following, all fits are made on a logaritmic scale to a truncated PDF or cumulative dis-

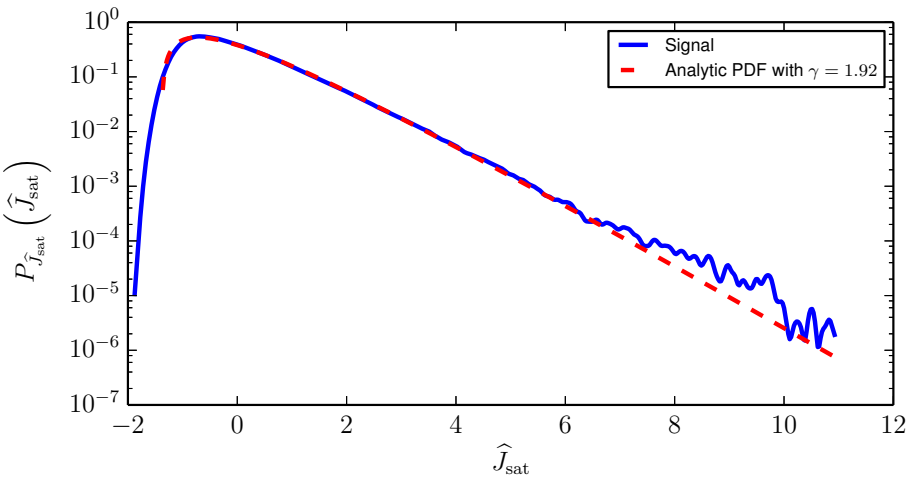

Figure 1.6: TCV Discharge 27601: Probability density function of the normalized ion saturation current, logarithmic scale.

tribution function (from here on denoted CDF). Truncated distributions are covered in the appendix, Section B.8. Usually, the truncation parameter is fixed at the lowest data set value and other parameters are fit parameters. Here, the truncation parameter has been set higher (at -1.75) to avoid the discrepancies between the signal and a gamma distribution for small signal values.

Conditional averaging of the TCV Discharge 27601 data set

Figures 1.7, 1.8 and 1.9 present results from conditional averaging of $\widehat{J}_{\mathrm{sat}}$. Conditional averaging is a method for elucidating the statistical properties of large amplitude fluctuations in a signal, detailed in Section 4.1. In these figures, large-amplitude fluctuations are defined as bursts with peak values of $\widehat{J}_{\mathrm{sat}} > 2.5$. 2041 such bursts were recorded. In Figure 1.7, the complementary cumulative distribution function of the waiting time between large-scale fluctuations is presented, along with an exponential fit to the data. The excellent fit suggests that the number of large-amplitude bursts follows a Poisson distribution, and thus that the individual bursts are uncorrelated. In Figure 1.8, the complementary cumulative distribution function of the peak amplitudes of the large-amplitude fluctuations, along with an exponential fit, is presented. Again, the fit describes the data well.

As well as the time between peaks and the amplitudes of the peaks, the conditional average gives the average shape of all recorded bursts. The result is presented in Figure 1.9a, along with exponential fits to both the rising and falling parts of the waveform. The fit gives a characteristic rise time $\tau_{\mathrm{r}} = 5.14\mu s$ and

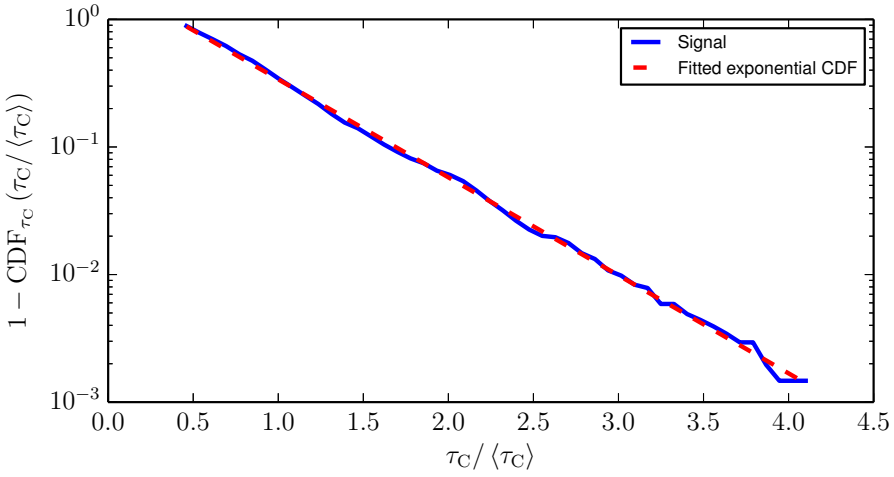

Figure 1.7: TCV Discharge 27601: Complementary cumulative distribution function of the waiting time between large amplitude events in the normalized, detrended electron density.

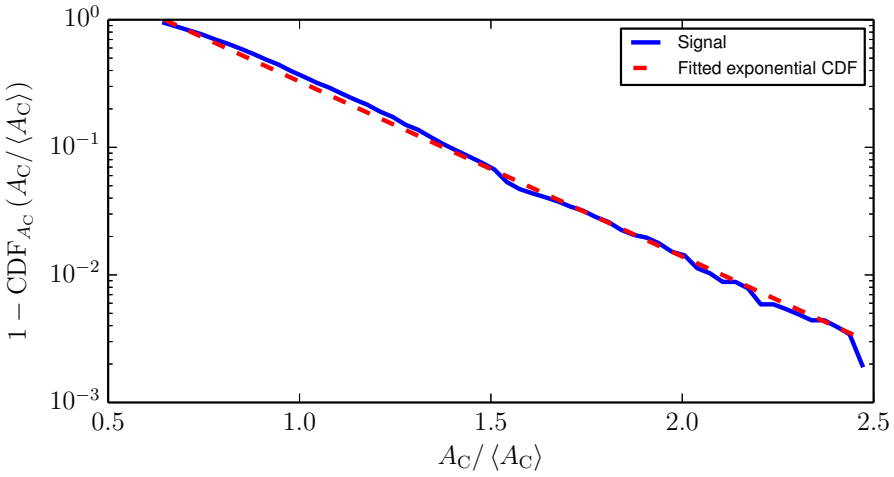

Figure 1.8: TCV Discharge 27601: Complementary cumulative distribution function of the amplitudes of conditionally averaged bursts.

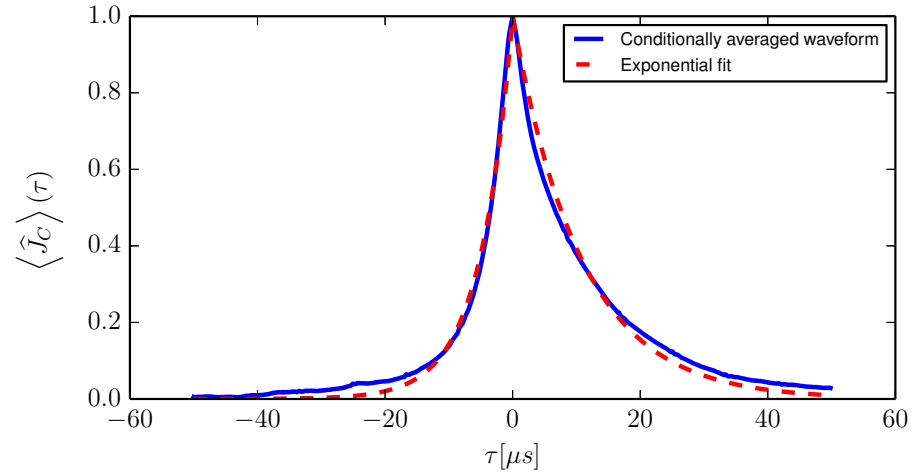

(a) Wave form of conditionally averaged bursts of the detrended, normalized electron density with exponential fit.

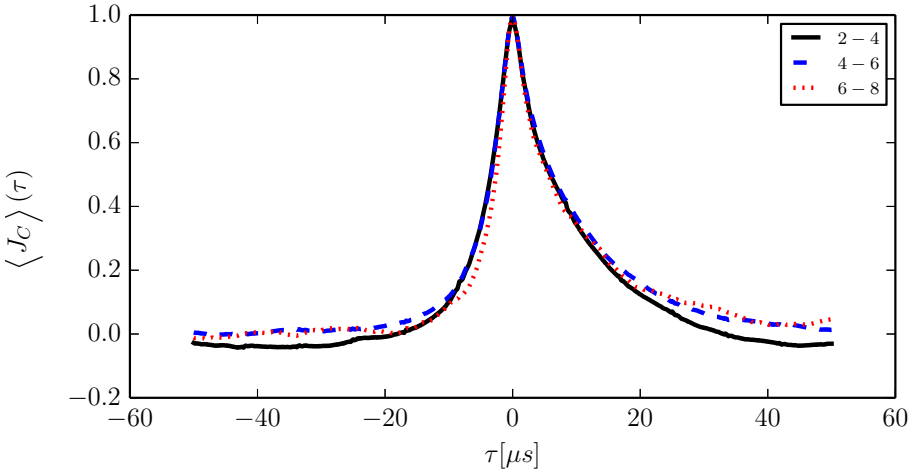

(b) Wave forms of conditionally averaged bursts of the detrended, normalized electron density for varying threshold ranges.

Figure 1.9: TCV Discharge 27601: The conditionally averaged waveforms.

a characteristic fall time $\tau_f = 10.7\mu s$, giving the estimated duration time, or correlation time, as $\tau_d = \tau_r + \tau_f = 15.9\mu s$. In Figure 1.9b, the waveforms from conditional averaging with several different ranges of threshold is presented, the black line is the average of peaks for $2 < \widehat{J}_{sat} < 4$, the blue dashed line is the average of waveforms with peaks in the range $4 < \widehat{J}_{sat} < 6$ and the red dotted line is for peaks with values $6 < \widehat{J}_{sat} < 8$. This figure shows that all three ranges give approximately the same resulting waveform, and that the shape does not depend on the burst amplitudes.

Autocorrelation function and power spectral density of the TCV Discharge 27601 data set

An analytic expression for the autocorrelation function of a shot noise process will be discussed in Section 2.1.5. In Figure 1.10, the autocorrelation function of $\widehat{J}_{sat}$ is presented, together with the autocorrelation function of a normalized shot noise process with τ_r and τ_f equal to the characteristic rise and fall time found from the waveform of the conditionally averaged signal (black dotted line) and the same analytic expression fitted to the experimental data with τ_r and τ_f as fit parameters (red dashed line). Fitting the function gives $\tau_r = 0.615\mu s$ and $\tau_f = 15.3\mu s$. Even though these are quite different from the values from conditional averaging, they still give $\tau_d = \tau_r + \tau_f = 15.9\mu s$, making this a robust result. That a sharp pulse rise time in general becomes less sharp after conditional averaging is a result presented in Section 4.2, and this is consistent with the difference in the fit parameters. Figure 1.11 shows the power spectral density of $\widehat{J}_{sat}$, calculated by Welch's method. The black dotted line and red dashed line are the analytic results with τ_r and τ_f from conditional averaging and fitted to the autocorrelation function, respectively. Again, the fit to the autocorrelation function gives better correspondence to the experimental data than the values from conditional averaging.

1.2.2 Motivation from the TCV results

A shot noise process is a stochastic process consisting of the superposition of identical pulse shapes with randomly distributed amplitudes and arrival times. Figure 1.6 shows that the ion saturation current fluctuations have the same probability density function as a shot noise process with Poisson distribution of pulse events, exponentially distributed pulse amplitudes and an exponential waveform [Garcia, 2012]. Conditional averaging of the ion saturation current agrees with these results, as the large-amplitude events in the density fluctuations have exponentially distributed amplitudes and waiting times, and the event shapes are well described by exponential functions. This motivates both

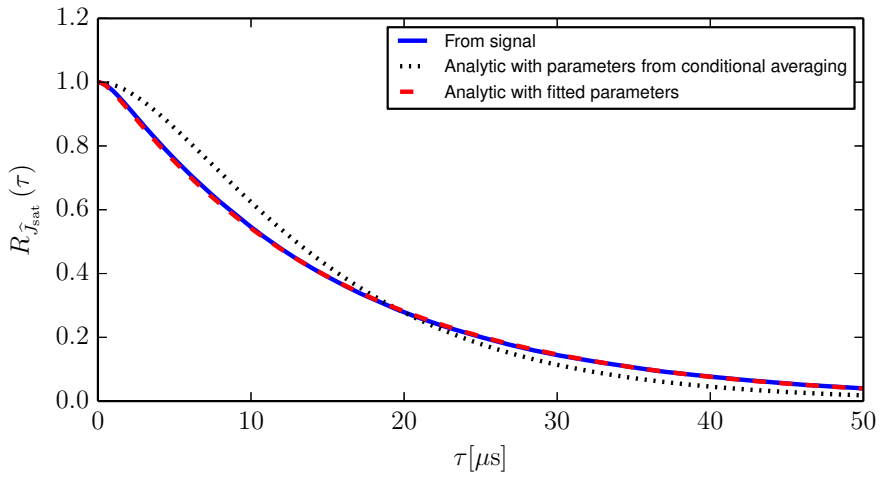

Figure 1.10: TCV Discharge 27601: Autocorrelation function of the normalized, detrended plasma electron density

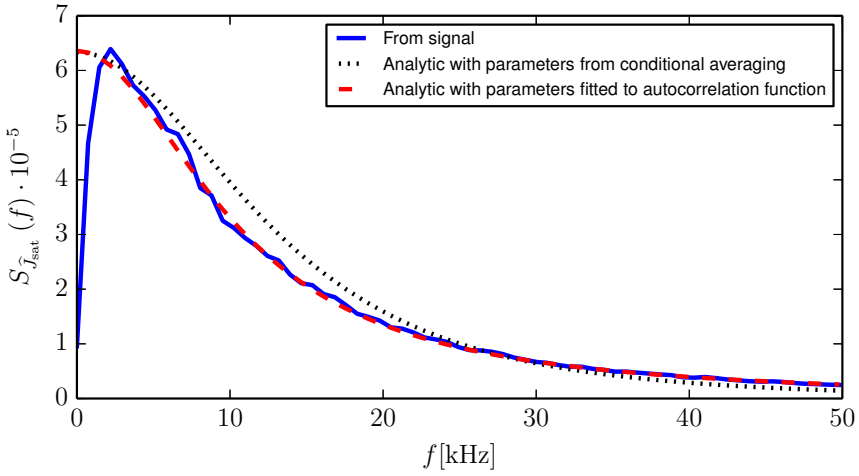

Figure 1.11: TCV Discharge 27601: Power spectral density of the normalized, detrended plasma electron density

an investigation into the statistical properties of the shot noise model, as well as an investigation of how the amplitude- and waiting time distribution of large-amplitude events depends on the underlying amplitude- and waiting time distribution of the pulses in the shot noise process. The choice of materials for the divertor targets and the main chamber walls depends heavily on the size and duration of the particle- and heat flux they are expected to endure. Therefore, investigation of the statistical properties of the time a shot noise process spends above a given amplitude, called *excess time statistics*, is of particular interest.

1.3 Thesis Structure

In Chapter 2, the shot noise model is introduced. The one-sided exponential pulse shape, common in the literature, is extended to a double-sided exponential pulse shape. Campbell's theorem is presented and discussed for some choices of waiting time distributions. The autocorrelation function and power spectral density of the shot noise process with a double-sided exponential pulse shape are discussed. The moments of both the shot noise process and the derivative of the shot noise process are discussed, and the PDFs for these are found for Poisson distribution of pulse events, exponentially distributed pulse amplitudes and the double-sided exponential pulse shape.Lastly, the joint PDF of the shot noise process and its derivative is found for the same pulse distributions and pulse shape.

In Chapter 3, excess time statistics of the shot noise process is discussed. A general model, based on the joint PDF between the shot noise process and its derivative, is presented. The non-intermittent and strong intermittency limits of this general model are discussed, as well as the limit of large threshold. In the strong intermittency limit, a PDF of the time above threshold is found. The results are compared to synthetically generated shot noise processes.

Chapter 4 considers the method of conditional averaging and investigates how well the pulse waiting time distribution, pulse amplitude distribution and pulse shape are preserved under conditional averaging. In this chapter, conditionally averaged shot noise processes with four different pulse amplitudes and pulse waiting times are compared.

In Chapter 5, excess time statistics of the TCV Discharge 27601, introduced in Chapter 1, is discussed. Comparisons are made between the experimental results, the analytic model obtained from the joint PDF between the shot noise process and its derivative and the non-intermittent limit. The rms-value of time above threshold and PDF of time above threshold are also discussed.

Lastly, Chapter 6 concludes the thesis and outlines future work and prospects.

Additionally, there are three appendices. Appendix A presents the gamma function and the error function with connections between them and some limits for both. In addition, the Fourier transform is defined and the limit of an oft used function is derived. In appendix B, statistical concepts such as probability density function, cumulative distribution function, characteristic function and moments are defined. Some distributions with possible normalizations are presented, as well as some connections between these. Appendix C presents the python code for generating and analyzing synthetic time series.

1.4 List of symbols

Shot noise process

$\Phi(t)$	Shot noise process
$\phi_k(t)$	Pulse event k of the shot noise process
$\varphi(t)$	Pulse waveform of the shot noise process
$\Theta(t)$	The normalized derivative of the shot noise process $\Phi(t)$
$\theta_k(t)$	Pulse event k of $\Theta(t)$
$\vartheta(t)$	Pulse waveform of $\Theta(t)$
A_k	Pulse amplitude of event k
t_k	Pulse time of event k
T	Duration of $\Phi(t)$
K	Burst events in time $[0, T]$
τ_d	Waveform duration time
τ_r	Waveform rise time
τ_f	Waveform fall time
$\tau_k = t_k - t_{k-1}$	Waiting time between bursts
τ_w	Average waiting time
$\gamma = \tau_\mathrm{d}/\tau_\mathrm{w}$	Intermittency parameter

Conditional average and excess time statistics

Φ_C	Conditionally averaged signal with condition C
A_C	Amplitudes of burst events fulfilling condition C
$\tau_{k,\mathrm{C}}$	Waiting time between burst events fulfilling condition C
C	Threshold value (as variable)
$\mathscr{T}(C)$	Total time a signal spends above the threshold value C
$\mathscr{N}(C)$	Total number of times the signal crosses C upwards
$\langle\mathcal{T}\rangle(C)$	Average time a signal spends above the threshold value C

Plasma Physics

R	Major plasma radius
a	Minor plasma radius
B, E	Magnetic and electric fields
$\widehat{\phi}$	Toroidal direction
$\widehat{\theta}$	Poloidal direction
n	Particle density
T_e	Electron temperature
Γ	Particle flux
V	Electric potential
U	$E \times B$-velocity
J_{sat}	Ion saturation current
C_s	Ion acoustic speed

Mathematical and statistical concepts

$H(t)$	Heaviside step function
$\mathcal{F}[x(t)](\omega)$	Fourier transform of $x(t)$
$\mathcal{F}^{-1}[X(\omega)](t)$	Fourier transform of $X(\omega)$
$\widehat{\bullet}$	Normalized value
$\langle \bullet \rangle$	Average value
$\bullet_{\text{rms}} = \left\langle (\bullet - \langle \bullet \rangle)^2 \right\rangle^{1/2}$	rms-value
S	Skewness
F	Flatness
$P_X(x)$	Probability distribution function (PDF) of X
$CDF_X(x)$	Cumulative distribution function (CDF) of X
$\langle \exp(iXu) \rangle$	Characteristic function of X
$R_\Phi(t) = \langle \Phi(\tau)\Phi(\tau + t) \rangle$	Autocorrelation function of Φ
$S_\Phi(\omega) = \mathcal{F}[R_\Phi(t)](\omega)$	Power spectral density of Φ

2

Stochastic modelling by shot noise processes

2.1 Shot noise processes

The shot noise process is a versatile model, and is constructed from superpositions of basic pulse shapes $\varphi(t)$, arriving at times t_k with amplitudes A_k. The pulse shape (also called a pulse waveform) can be any function which is appreciabely different from o only on a finite domain and which is characterized by a parameter τ_d, called the pulse duration time. τ_d is defined as

$$\tau_\mathrm{d} = \int_{-\infty}^{\infty} \mathrm{d}t \, |\varphi(t)|. \tag{2.1}$$

t_k and A_k are random variables with known distributions. The shot noise process consists of K *pulses* $\phi_k(t) = A_k\varphi(t - t_k)$ arriving in a time interval $[0, T]$, and can be written as

$$\Phi_K(t) = \sum_{k=1}^{K(T)} \phi_k(t - t_k) = \sum_{k=1}^{K(T)} A_k\varphi(t - t_k). \tag{2.2}$$

In the following, we will refer to the waiting time between consecutive pulses as $\tau_k = t_{k+1} - t_k$. The waiting times are assumed to have the mean value $\langle\tau_k\rangle = \tau_\mathrm{w}$ and the amplitudes are assumed to have the mean value $\langle A\rangle$. The

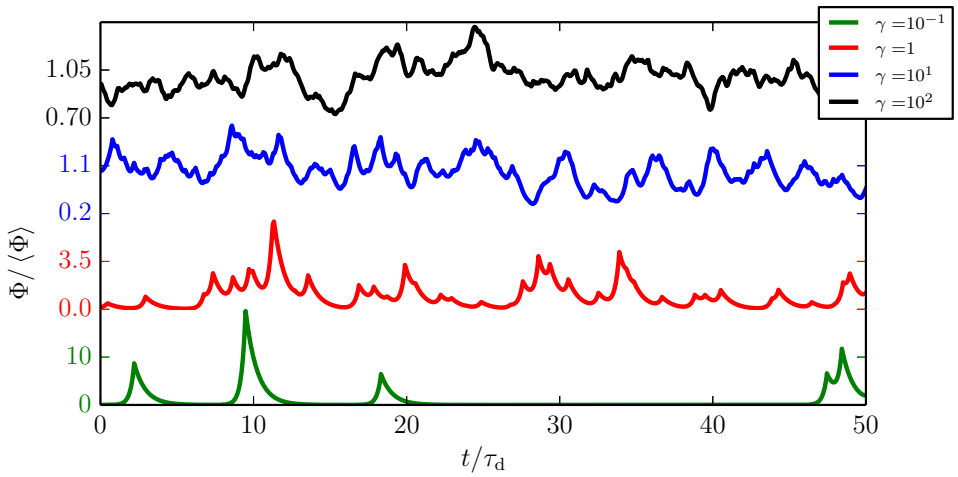

Figure 2.1: Several realizations of the shot noise process with $\gamma = \tau_d/\tau_w$ as the intermittency parameter. The waveform Eq. (2.5) with $\tau_r = 0.25$, $\tau_f = 0.75$ has been used, and $\langle A \rangle = 1$.

ratio between pulse duration time and average waiting time $\gamma = \tau_d/\tau_w$ is called the *intermittency parameter*, a name which will be justified later.

Some examples of the shot noise process for various values of γ are presented in Figure 2.1. For small γ, the pulses are separated and the shot noise process is strongly intermittent, with small mean value and large relative fluctuation level (that is, large rms-value compared to the mean value. For large γ, there is significant pulse overlap, givig a high mean value with small relative fluctuation level. For $\gamma \gg 1$, the signal resembles random noise. Thus, γ describes relative fluctuation level and can be used as an indication of on-off intermittency.

In Figure 2.2, the derivative of the processes in Figure 2.1 is presented, normalized by the pulse duration time τ_d. The on-off intermittency is clearer for small γ-values, while the derivative resembles random noise at smaller values of γ than the shot noise process itself, due to the irregular nature of the derivative.

2.1.1 Signal formulation and assumptions

In the following, we introduce useful concepts related to the pulse waveform $\varphi(t)$. These are generalizations of concepts found in Garcia [2012], Pécseli [2000] and Rice [1944].

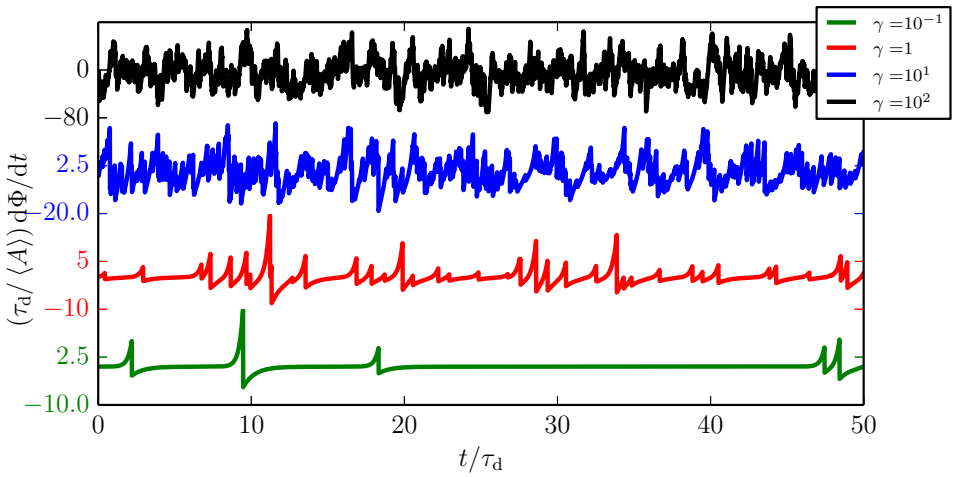

Figure 2.2: The normalized, analytic derivatives of the shot noise processes in Figure 2.1. The form of this derivative is covered in Section 2.2.

The pulse shape $\varphi(t)$

In the previous section, the duration time τ_d of the pulse shape was defined. In addition to assuming a finite pulse duration time, it will also be advantageous to assume that the waveform has finite integrals over its n'th power

$$I_n = \frac{1}{\tau_d} \int_{-\infty}^{\infty} dt\, [\varphi(t)]^n, \quad n = 1, 2, 3, \ldots, \tag{2.3}$$

and a finite convolution

$$R_\varphi(\tau) = \frac{1}{\tau_d} \int_{-\infty}^{\infty} dt\, \varphi(t)\varphi(t-\tau). \tag{2.4}$$

Finite I_n is not strictly required for a well-defined signal, but is required for calculating the moments or the PDF of $\Phi(t)$. Note that there is no absolute value sign in the formulation of I_n, so although $I_1 = 1$ for a positive $\varphi(t)$, I_1 is not required to have any particular value. In both cases above, we are dividing by τ_d to normalize the result, making sure we end up with a unitless number. τ_d is chosen as the normaization factor as it is the fundamental waveform parameter. We will also only consider waveforms with a finite convolution, since the convolution is needed when calculating the rms-value of the signal, Φ_{rms}.

The exponential waveform We will be using an exponential waveform, which has a good basis in conditional averaging of experimental data:

$$\varphi(t) = \exp\left(\frac{t}{\tau_\mathrm{r}}\right) H_{1/2}(-t) + \exp\left(-\frac{t}{\tau_\mathrm{f}}\right) H_{1/2}(t), \tag{2.5}$$

where τ_r is the rise time, τ_f is the fall time, $\tau_\mathrm{r} + \tau_\mathrm{f} = \tau_\mathrm{d}$ is the pulse duration time and $H_a(t)$ is the step function

$$H_a(t) = \begin{cases} 0 & t < 0 \\ a & t = 0 \\ 1 & t > 0 \end{cases}. \tag{2.6}$$

Note that the Heaviside function only takes dimensionless input values, so we should use t/τ_d instead of t inside the Heaviside functions. This is omitted for the sake of simplicity and, since $\tau_\mathrm{d} > 0$, does not affect the function value.

We will also consider one-sided versions of this waveform, either with $\tau_\mathrm{r} = \tau_\mathrm{d}$, $\tau_\mathrm{f} = 0$:

$$\varphi_\mathrm{r}(t) = \exp\left(\frac{t}{\tau_\mathrm{d}}\right) H_1(-t), \tag{2.7}$$

or with $\tau_\mathrm{r} = 0$, $\tau_\mathrm{f} = \tau_\mathrm{d}$:

$$\varphi_\mathrm{f}(t) = \exp\left(-\frac{t}{\tau_\mathrm{d}}\right) H_1(t). \tag{2.8}$$

The waveform in Eq. (2.5) will be referred to as the "double-sided exponential waveform" while Eq. (2.7) and Eq. (2.8) will both be called a "one-sided exponential waveform". Note that we use different step functions for the double-sided exponential waveform compared to the two one-sided exponential waveforms. This is to ensure that $\varphi(0) = \varphi_\mathrm{r}(0) = \varphi_\mathrm{f}(0) = 1$.

Integrals of the exponential waveforms For all the exponential waveforms above, the integral in Eq. (2.3) is simple to calculate and gives the result

$$I_n = \frac{1}{n}. \tag{2.9}$$

In particular, $I_1 = 1$, as should be the case for positive pulse shapes.

Convolution of the exponential waveforms The convolution is different for the dobule-sided exponential waveform and the one-sided waveforms. The double exponential waveform gives the convolution

$$R_\varphi(\tau) = \frac{\tau_\mathrm{f}}{2(\tau_\mathrm{f} - \tau_\mathrm{r})} \exp\left(-\frac{|\tau|}{\tau_\mathrm{f}}\right) - \frac{\tau_\mathrm{r}}{2(\tau_\mathrm{f} - \tau_\mathrm{r})} \exp\left(-\frac{|\tau|}{\tau_\mathrm{r}}\right), \tag{2.10}$$

from which it follows that $R_\varphi(0) = 1/2$. The one-sided exponential waveforms, on the other hand, both give the convolution

$$R_{\varphi_\mathrm{r}}(\tau) = R_{\varphi_\mathrm{f}}(\tau) = \frac{1}{2}\exp\left(-\frac{|\tau|}{\tau_\mathrm{d}}\right). \tag{2.11}$$

As above, $R_{\varphi_\mathrm{r}}(0) = 1/2$. Also note that $\lim_{\tau_\mathrm{r}\to 0} R_\varphi(\tau) = R_{\varphi_\mathrm{f}}(\tau)$ and $\lim_{\tau_\mathrm{f}\to 0} R_\varphi(\tau) = R_{\varphi_\mathrm{r}}(\tau)$.

To get the convolution for the symmetric waveform, $\tau_\mathrm{f} = \tau_\mathrm{r}$, we need to take the limit $\tau_\mathrm{f} \to \tau_\mathrm{r}$ in Eq. (2.10) and use L'Hôpital's rule:

$$\begin{aligned}
&\lim_{\tau_\mathrm{f}\to\tau_\mathrm{r}} \frac{\tau_\mathrm{f}\exp(-|\tau|/\tau_\mathrm{f}) - \tau_\mathrm{r}\exp(-|\tau|/\tau_r)}{2(\tau_\mathrm{f}-\tau_\mathrm{r})} \\
&= \lim_{\tau_\mathrm{f}\to\tau_\mathrm{r}} \frac{1}{2}\exp\left(-\frac{|\tau|}{\tau_\mathrm{f}}\right) + \frac{|\tau|}{2\tau_\mathrm{f}}\exp\left(-\frac{|\tau|}{\tau_\mathrm{f}}\right) \\
&= \left(\frac{1}{2} + \frac{|\tau|}{2\tau_\mathrm{f}}\right)\exp\left(-\frac{|\tau|}{\tau_\mathrm{f}}\right).
\end{aligned}$$

Setting $\tau_\mathrm{f} = \tau_\mathrm{r} = \tau_\mathrm{d}/2$, we get

$$R_\varphi(\tau) = \left(\frac{1}{2} + \frac{|\tau|}{\tau_\mathrm{d}}\right)\exp\left(-\frac{2|\tau|}{\tau_\mathrm{d}}\right), \tag{2.12}$$

which also has $R_\varphi(0) = 1/2$. This is as it should be, since we see from Eq. (2.3) and Eq. (2.4) that $R_\varphi(0) = I_2$, and $I_2 = 1/2$ from Eq. (2.9).

The distribution of pulse events

$K(T)$ is the number of pulse events arriving in a time interval $[0, T]$. We state that pulses don't arrive at the same time, since two pulses with amplitudes A_k and $A_{\mathrm{k}+1}$ arriving at the same time are superposed and counted as a single pulse with amplitude $A_\mathrm{k} + A_{\mathrm{k}+1}$. In addition, we assume that the PDF of $K(T)$ only depends on the length of the interval $[0, T]$ (and not, for instance, on how many pulses have arrived before the start of the interval) and that the number of pulses in any given interval is independent of the number of pulses in other, disjoint, intervals. In other words, we assume that the process $K(T)$ has independent, stationary increments. Under these assumptions, we know that $K(T)$ has a poisson distribution [Walpole et al., 2007]:

$$P_K(K;T) = \frac{1}{K!}\left(\frac{T}{\tau_\mathrm{w}}\right)^K \exp\left(-\frac{T}{\tau_\mathrm{w}}\right). \tag{2.13}$$

Here, $1/\tau_\mathrm{w}$ is the mean rate of pulse arrivals (so $\langle K(T)\rangle = T/\tau_\mathrm{w}$). We show in Section B.6 that when the number of pulse arrivals is Poisson distributed, the

waiting time between pulses is exponentially distributed:

$$P_\tau(\tau) = \frac{1}{\tau_\mathrm{w}} \exp\left(-\frac{\tau}{\tau_\mathrm{w}}\right) H_1(\tau) \tag{2.14}$$

where the mean waiting time between pulses is $\langle \tau \rangle = \tau_\mathrm{w}$.

The assumptions on $K(T)$ (stationary and independent increments) may not be satisfied; it is possible to imagine that the intensity of pulse arrivals oscillates in time, for instance, or that after many large pulses there will be a quiet interval since the energy reservoir for large pulses is depleted (such that the number of pulses in a given interval depends on the number of pulses in a previous interval). But the Poisson process represents the most basic assumption we can make: that the pulses arrive completely independently of each other and that the rate at which they arrive is constant. The choise of $P_K(K;T)$ as a poisson distribution is advantageous and has precendence in the literature [Garcia, 2012, Pécseli, 2000] since it makes for ease of calculation and exponentially distributed waiting times has good agreement with experimental results. While this distribution will be our primary focus, we will in Section 2.1.3 and Section 4.2 compare some results using degenerate, Rayleigh and uniform waiting time distributions.

2.1.2 General expression for the mean of $\Phi(t)$

Campbell's theorem [Pécseli, 2000, Rice, 1944] is a general result for the first two moments of the shot noise process. The first part states that the mean of a shot noise process is

$$\langle \Phi \rangle = \frac{\langle A \rangle}{\tau_\mathrm{w}} \int_{-\infty}^{\infty} \mathrm{d}t\, \varphi(t), \tag{2.15}$$

where $\langle \Phi \rangle$ is the time average of the signal. $\langle \Phi \rangle$ can be written as

$$\langle \Phi \rangle = \gamma \langle A \rangle I_1 = \gamma \langle A \rangle, \tag{2.16}$$

where $I_1 = 1$ is given by Eq. (2.3). This result is universal, as it does not depend on any assumptions of the pulse amplitude or waiting time distributions and it is independent of waveform [except the requirement Eq. (2.1)]. This result is intuitive: $\gamma = \tau_\mathrm{d}/\tau_\mathrm{w}$, and as τ_d increases in relation to τ_w, the pulses appear closer together or last longer. This obviously leads to a lager degree of pulse overlap and an increase in the average value of the resulting signal. Moreover, $\langle A \rangle$ is independent of the intermittency parameter γ, so the mean value of the signal is proportional to the mean value of the pulse amplitudes. It can also be shown [Pécseli, 2000, Rice, 1944] that the shot noise process is an ergodic process, and thus that the moments of the shot noise process are independent of time.

2.1.3 Expressions for the variance

The second part of Campbell's theorem gives the variance of a shot noise process. With $P_\tau(\tau)$ as the PDF of the pulse waiting time distribution, the general expression for the variance is [Pécseli, 2000, Rice, 1944]:

$$\left\langle \Phi^2(t) \right\rangle = \gamma \left\langle A^2 \right\rangle R_\varphi(0) + 2\gamma \langle A \rangle^2 \left[\int_0^\infty \mathrm{d}\tau \, P_\tau(\tau) R_\varphi(\tau) + \int_0^\infty \mathrm{d}\tau_1 \int_0^\infty \mathrm{d}\tau_2 \, P_\tau(\tau_1) P_\tau(\tau_2) R_\varphi(\tau_1 + \tau_2) + \ldots \right]. \quad (2.17)$$

This result is valid for arbitrary amplitude distribution, and waiting time distributions, provided the first two moments of the amplitude distribution exists and that the waiting time distribution has a well-defined PDF. It is also valid for any pulse shape with finite convolution. We will in the following investigate special cases for this expression, using different assumptions.

Influence of the pulse shape

Due to the convolutions in Eq. (2.17), the first assumption we will make is that the pulse waveform is one of the exponential waveform found in Section 2.1.1. Using one of these, the convolutions can be split and the infinite sum can be calculated. We first present results for all cases, then discuss them together.

The double-sided waveform With the double sided waveform, we have $R_\varphi(\tau)$ from Eq. (2.10) and $R_\varphi(0) = 1/2$. We can then write:

$$\int_0^\infty \mathrm{d}\tau \, P_\tau(\tau) R_\varphi(\tau) = \frac{\tau_\mathrm{f}}{2(\tau_\mathrm{f} - \tau_\mathrm{r})} q_\mathrm{f} - \frac{\tau_\mathrm{r}}{2(\tau_\mathrm{f} - \tau_\mathrm{r})} q_\mathrm{r}, \quad (2.18)$$

where

$$q_\mathrm{f} \equiv \int_0^\infty \mathrm{d}\tau \, P_\tau(\tau) \exp\left(-\frac{\tau}{\tau_\mathrm{f}}\right), \quad (2.19)$$

$$q_\mathrm{r} \equiv \int_0^\infty \mathrm{d}\tau \, P_\tau(\tau) \exp\left(-\frac{\tau}{\tau_\mathrm{r}}\right). \quad (2.20)$$

We can then split the second integral in Eq. (2.17) into two parts:

$$\begin{aligned}
&\int_0^\infty \mathrm{d}\tau_1 \int_0^\infty \mathrm{d}\tau_2\, P_\tau(\tau_1) P_\tau(\tau_2) R_\varphi(\tau_1+\tau_2) \\
&= \frac{\tau_\mathrm{f}}{2(\tau_\mathrm{f}-\tau_\mathrm{r})} \int_0^\infty \mathrm{d}\tau_1 \int_0^\infty \mathrm{d}\tau_2\, P_\tau(\tau_1) P_\tau(\tau_2) \exp\!\left(-\frac{\tau_1}{\tau_\mathrm{f}}\right) \exp\!\left(-\frac{\tau_2}{\tau_\mathrm{f}}\right) \\
&- \frac{\tau_\mathrm{r}}{2(\tau_\mathrm{f}-\tau_\mathrm{r})} \int_0^\infty \mathrm{d}\tau_1 \int_0^\infty \mathrm{d}\tau_2\, P_\tau(\tau_1) P_\tau(\tau_2) \exp\!\left(-\frac{\tau_1}{\tau_\mathrm{r}}\right) \exp\!\left(-\frac{\tau_2}{\tau_\mathrm{r}}\right) \\
&= \frac{\tau_\mathrm{f}}{2(\tau_\mathrm{f}-\tau_\mathrm{r})} q_\mathrm{f} q_\mathrm{f} - \frac{\tau_\mathrm{r}}{2(\tau_\mathrm{f}-\tau_\mathrm{r})} q_\mathrm{r} q_\mathrm{r}
\end{aligned}$$

We can split the rest of the infinite series likewise, and we get from Eq. (2.17):

$$\begin{aligned}
\Phi_\mathrm{rms}^2 &= \left\langle \Phi^2 \right\rangle - \langle \Phi \rangle^2 = \left\langle \Phi^2 \right\rangle - \gamma^2 \langle A \rangle^2 \\
&= \gamma \left\langle A^2 \right\rangle R_\varphi(\tau) - \gamma^2 \langle A \rangle^2 + \frac{\gamma \langle A \rangle^2}{\tau_\mathrm{f}-\tau_\mathrm{r}} \left[\tau_\mathrm{f}\left(q_\mathrm{f} + q_\mathrm{f}^2 + \cdots\right) - \tau_\mathrm{r}\left(q_\mathrm{r} + q_\mathrm{r}^2 + \cdots\right) \right] \\
&= \frac{\gamma \left\langle A^2 \right\rangle}{2} - \gamma^2 \langle A \rangle^2 + \frac{\gamma \langle A \rangle^2}{\tau_\mathrm{f}-\tau_\mathrm{r}} \left[\tau_\mathrm{f}\left(\frac{1}{1-q_\mathrm{f}} - 1\right) - \tau_\mathrm{r}\left(\frac{1}{1-q_\mathrm{r}} - 1\right) \right] \\
&= \frac{\gamma \left\langle A^2 \right\rangle}{2} + \gamma^2 \langle A \rangle^2 \left[\frac{1}{(\tau_\mathrm{f}-\tau_\mathrm{r})\gamma} \left(\tau_\mathrm{f} \frac{q_\mathrm{f}}{1-q_\mathrm{f}} - \tau_\mathrm{r} \frac{q_\mathrm{r}}{1-q_\mathrm{r}} \right) - 1 \right]
\end{aligned} \tag{2.21}$$

The double-sided waveform with $\tau_\mathrm{r} = \tau_\mathrm{f}$ Starting from Eq. (2.21) and taking $\tau_\mathrm{r} \to \tau_\mathrm{f}$, we get (where we use L'Hôpital's rule in the second line)

$$\begin{aligned}
&\lim_{\tau_\mathrm{r}\to\tau_\mathrm{f}} \frac{1}{(\tau_\mathrm{f}-\tau_\mathrm{r})\gamma} \left(\tau_\mathrm{f} \frac{q_\mathrm{f}}{1-q_\mathrm{f}} - \tau_\mathrm{r} \frac{q_\mathrm{r}}{1-q_\mathrm{r}} \right) \\
&= \lim_{\tau_\mathrm{r}\to\tau_\mathrm{f}} \frac{1}{\gamma} \left(\frac{q_\mathrm{r}}{1-q_\mathrm{r}} + \frac{q_\mathrm{r}}{(1-q_\mathrm{r})^2} \right) \\
&= \frac{1}{\gamma} \frac{q_\mathrm{f}(2-q_\mathrm{f})}{(1-q_\mathrm{f})^2},
\end{aligned} \tag{2.22}$$

and with $\tau_\mathrm{f} = \tau_\mathrm{d}/2$, we arrive at

$$\Phi_\mathrm{rms}^2 = \frac{\gamma \left\langle A^2 \right\rangle}{2} + \gamma^2 \langle A \rangle^2 \left[\frac{q_\mathrm{s}(2-q_\mathrm{s})}{\gamma (1-q_\mathrm{s})^2} - 1 \right], \tag{2.23}$$

where q_s is the integral for the symmetric waveform

$$q_\mathrm{s} \equiv \int_0^\infty \mathrm{d}\tau\, P_\tau(\tau) \exp\!\left(-\frac{2\tau}{\tau_\mathrm{d}}\right). \tag{2.24}$$

The one-sided waveform Note that since $\lim_{\tau_r \to 0} \tau_r \, q_r/(1-q_r) = 0$ and $\lim_{\tau_f \to 0} \tau_f \, q_f/(1-q_f) = 0$, we find that in both limits $\tau_f \to \tau_d$ and $\tau_r \to \tau_d$, equation (2.21) reduces to

$$\Phi_{\text{rms}}^2 = \frac{\gamma\left\langle A^2 \right\rangle}{2} + \gamma^2 \langle A \rangle^2 \left[\frac{q}{\gamma(1-q)} - 1 \right], \tag{2.25}$$

where

$$q = \int_0^\infty \mathrm{d}\tau \, P_\tau(\tau) \exp(-\tau/\tau_d). \tag{2.26}$$

This equation can be found by using the one-sided waveform with finite fall time directly, as seen in Pécseli [2000]. In this case the convolution is given by Eq. (2.11). We find from Eq. (2.17) that Φ_{rms}^2 becomes

$$\begin{aligned} \Phi_{\text{rms}}^2 &= \left\langle \Phi^2 \right\rangle - \langle \Phi \rangle^2 = \gamma \left\langle A^2 \right\rangle R_\varphi(\tau) - \gamma^2 \langle A \rangle^2 + \gamma \langle A \rangle^2 \left[q + q^2 + \cdots \right] \\ &= \frac{\gamma\left\langle A^2 \right\rangle}{2} - \gamma^2 \langle A \rangle^2 + \gamma \langle A \rangle^2 \left[\frac{1}{1-q} - 1 \right] \\ &= \frac{\gamma\left\langle A^2 \right\rangle}{2} + \gamma^2 \langle A \rangle^2 \left[\frac{q}{\gamma(1-q)} - 1 \right], \end{aligned} \tag{2.27}$$

and using the one-sided waveform with finite rise time yields the same result.

Discussion We see from Eq. (2.21) and Eq. (2.27) that the rms-value of Φ consists of one part independent of th details of the signal (amplitude and waiting time distribution), $\gamma\langle A^2 \rangle/2$, and one part that depends on the pulse waveform and pulse waiting time distribution $P_\tau(\tau)$. If we now divide Φ_{rms}^2 by $\langle \Phi \rangle^2$, we will get a measure for the relative fluctuation level of the signal: A signal with large rms-value compared to the mean value is an intermittent signal, while a signal with low rms-value compared to the mean value is a non-intermittent signal. Using Φ_{rms} as given by Eq. (2.27) and $\langle \Phi \rangle$ given by Eq. (2.16), we have

$$\frac{\Phi_{\text{rms}}^2}{\langle \Phi \rangle^2} = \frac{\dfrac{\gamma\left\langle A^2 \right\rangle}{2} + \gamma^2 \langle A \rangle^2 \left(\dfrac{q}{\gamma(1-q)} - 1 \right)}{\gamma^2 \langle A \rangle^2} = \frac{1}{\gamma} \left(\frac{\left\langle A^2 \right\rangle}{2\langle A \rangle^2} - \gamma + \frac{q}{1-q} \right), \tag{2.28}$$

where the pre-factor shows that the relative fluctuation will be large for small γ. This agrees with the intuition: If γ is large, $\tau_d \gg \tau_w$ and we have a signal with long pulses arriving frequently. This means that the pulses superimpose significantly and increase the mean value while decreasing the variation around the mean. If, on the other hand, γ is small, $\tau_w \gg \tau_d$ and we have a signal with

short pulses arriving far apart, leaving very little superposition of the pulses and a strongly fluctuating signal.

To discover the influence of the waiting time and amplitude distributions on the intermittency of the signal, we will consider some special cases.For the sake of simplicity, we will consider the one-sided exponential waveform, that is we will use Eq. (2.28) with the rms-value from Eq. (2.27) and not Eq. (2.21). (We will see later, in Section 2.1.4, that for exponentially distributed amplitudes and Poisson distribution of events the rms-value is independent of the ratio τ_r/τ_f).

Influence of the pulse amplitude distribution

The amplitude distribution only enters Eq. (2.28) through the factor $\langle A^2\rangle/2\langle A\rangle^2$. Using the example distributions in the Appendix, Section B.5, we see that:

$$\text{Exponential}: \frac{\left\langle A^2\right\rangle}{2\langle A\rangle^2} = 1, \tag{2.29}$$

$$\text{Rayleigh}: \frac{\left\langle A^2\right\rangle}{2\langle A\rangle^2} = \frac{2}{\pi} \approx 0.63, \tag{2.30}$$

$$\text{Degenerate}: \frac{\left\langle A^2\right\rangle}{2\langle A\rangle^2} = \frac{1}{2}, \tag{2.31}$$

$$\text{Uniform}: \frac{\left\langle A^2\right\rangle}{2\langle A\rangle^2} = \frac{3}{2}. \tag{2.32}$$

Since all these one-parameter distributions can be defined based on the mean value, $\langle A^2\rangle$ is proportional to $\langle A\rangle^2$, and we are only left with a numerical factor that (for these distributions) is of the order of unity. Thus the underlying amplitude distribution has comparatively little effect on the relative fluctuation level of the signal.

Influence of the pulse waiting time distribution

We have seen in the introduction that exponentially distributed waiting times is a particularly intersting case. We will now compare exponentially distributed waiting times to Rayleigh, uniformly and degenerately distributed waiting times, and especially look at the asymptotic behaviour of $\Phi_{\text{rms}}/\langle\Phi\rangle$ in the limits $\gamma \to 0$ and $\gamma \to \infty$.

Exponentially distributed waiting times

The exponential distribution is given by Eq. (B.16):

$$P_\tau(\tau) = \frac{1}{\tau_\mathrm{w}} \exp\left(-\frac{\tau}{\tau_\mathrm{w}}\right) H_1(\tau). \tag{2.33}$$

We insert this into Eq. (2.26) and find that:

$$\begin{aligned} q &= \int_0^\infty \mathrm{d}\tau\, P_\tau(\tau) \exp\left(-\frac{\tau}{\tau_\mathrm{d}}\right) = \int_0^\infty \frac{1}{\tau_\mathrm{w}} \exp\left(-\frac{\tau}{\tau_\mathrm{w}}\right) \exp\left(-\frac{\tau}{\tau_\mathrm{d}}\right) \\ &= \frac{1}{\tau_\mathrm{w}/\tau_\mathrm{d} + 1} = \frac{1}{1/\gamma + 1}, \end{aligned} \tag{2.34}$$

and the fraction in Eq. (2.28) becomes

$$\frac{q}{1-q} = \frac{\dfrac{1}{1/\gamma + 1}}{1 - \dfrac{1}{1/\gamma + 1}} = \frac{1}{1/\gamma + 1 - 1} = \gamma.$$

Note that the only difference between the q from Eq. (2.26) and q_f and q_r from respectively Eq. (2.19) and Eq. (2.24) is that τ_d changes to τ_f and τ_r. Therefore, we also have

$$q_\mathrm{f} = \frac{1}{\tau_\mathrm{w}/\tau_\mathrm{f} + 1}, \tag{2.35}$$

$$q_\mathrm{r} = \frac{1}{\tau_\mathrm{w}/\tau_\mathrm{r} + 1}, \tag{2.36}$$

and

$$\begin{aligned} \frac{q_\mathrm{f}}{1-q_\mathrm{f}} &= \frac{\tau_\mathrm{f}}{\tau_\mathrm{w}}, \\ \frac{q_\mathrm{r}}{1-q_\mathrm{r}} &= \frac{\tau_\mathrm{r}}{\tau_\mathrm{w}}. \end{aligned}$$

This means that both Eq. (2.28) and $\Phi_\mathrm{rms}^2/\langle\Phi\rangle^2$ with Φ_rms^2 from Eq. (2.21) becomes

$$\frac{\Phi_\mathrm{rms}^2}{\langle\Phi\rangle^2} = \frac{1}{\gamma} \frac{\left\langle A^2 \right\rangle}{2\langle A\rangle^2}. \tag{2.37}$$

In this case, we clearly have γ as an intermittency parameter, as discussed above. This discussion holds completely up to the numerical factor provided by $\langle A^2\rangle/2\langle A\rangle^2$. This relation will be used as the basis for comparison with the other waiting time distributions.

Rayleigh distributed waiting times

Eq. (B.17) gives us the Rayleigh distribution:

$$P_\tau(\tau) = \frac{\pi\tau}{2{\tau_\mathrm{w}}^2}\exp\left(-\frac{\pi\tau^2}{(4{\tau_\mathrm{w}}^2)}\right)H_1(\tau). \tag{2.38}$$

This, we insert into Eq. (2.19):

$$q = \int_0^\infty \mathrm{d}\tau\, P(\tau)\exp\left(-\frac{\tau}{\tau_\mathrm{d}}\right) = \int_0^\infty \mathrm{d}\tau\, \frac{\pi\tau}{2{\tau_\mathrm{w}}^2}\exp\left(-\frac{\pi\tau^2}{4{\tau_\mathrm{w}}^2}\right)\exp\left(-\frac{\tau}{\tau_\mathrm{d}}\right),$$

which we solve by Mathematica to get

$$q = 1 - \frac{\tau_\mathrm{w}}{\tau_\mathrm{d}}\exp\left(\frac{\tau_\mathrm{w}^2}{\pi\tau_\mathrm{d}^2}\right)\mathrm{erfc}\left(\frac{\tau_\mathrm{w}}{\sqrt{\pi}\tau_\mathrm{d}}\right) = 1 - \frac{1}{\gamma}\exp\left(\frac{1}{\pi\gamma^2}\right)\mathrm{erfc}\left(\frac{1}{\sqrt{\pi}\gamma}\right),$$

where $\mathrm{erfc}(\cdot)$ is the complementary error function (see Section A.3) . Defining

$$f(\gamma) = \exp\left(1/\pi\gamma^2\right)\mathrm{erfc}\left(1/\sqrt{\pi}\gamma\right),$$

we see that the fraction in Eq. (2.28) is:

$$\frac{q}{1-q} = \frac{1 - f(\gamma)/\gamma}{1 - (1 - f(\gamma)/\gamma)} = \frac{\gamma - f(\gamma)}{f(\gamma)}.$$

From Eq. (2.28), we then have:

$$\frac{\Phi_\mathrm{rms}^2}{\langle\Phi\rangle^2} = \frac{1}{\gamma}\left[\frac{\left\langle A^2\right\rangle}{2\langle A\rangle^2} - \gamma + \frac{\gamma}{\exp(1/\pi\gamma^2)\,\mathrm{erfc}\left(1/\sqrt{\pi}\gamma\right)} - 1\right]. \tag{2.39}$$

We next show that the asymptotic behaviour of this equation is determined by the $1/\gamma$ pre-factor, with the terms inside the square brackets only contributing a numerical factor.

The limit $\gamma \to 0$ The error function can be written as $\mathrm{erfc}(x) = \Gamma_U\left(1/2, x^2\right)/\sqrt{\pi}$, where $\Gamma_U(\cdot,\cdot)$ is the upper incomplete gamma function (see Sections A.2 and A.3). Then, we have

$$\begin{aligned}
&\lim_{\gamma\to 0}\frac{1}{\gamma}\exp\left(\frac{1}{\pi\gamma^2}\right)\mathrm{erfc}\left(\frac{1}{\sqrt{\pi}\gamma}\right)\\
&= \lim_{\gamma\to 0}\frac{1}{\gamma\sqrt{\pi}}\exp\left(\frac{1}{\pi\gamma^2}\right)\Gamma_U\left(\frac{1}{2},\frac{1}{\pi\gamma^2}\right)\\
&= \lim_{\gamma\to 0}\frac{1}{\gamma\sqrt{\pi}}\exp\left(\frac{1}{\pi\gamma^2}\right)\left(\sqrt{\pi}\gamma\right)\exp\left(-\frac{1}{\pi\gamma^2}\right)\\
&= 1.
\end{aligned}$$

This means that in the limit $\gamma \to 0$, Eq. (2.39) becomes

$$\lim_{\gamma\to 0} \gamma \frac{\Phi_{\text{rms}}^2}{\langle\Phi\rangle^2} = \lim_{\gamma\to 0} \frac{\left\langle A^2\right\rangle}{2\langle A\rangle^2} - \gamma + 1 - 1 = \frac{\left\langle A^2\right\rangle}{2\langle A\rangle^2}, \tag{2.40}$$

and we have the same dependency on γ as for exponentially distributed waiting times, Eq. (2.37).

The limit $\gamma \to \infty$ In the limit of $\gamma \to \infty$,we have $\exp\left[1/\left(\pi\gamma^2\right)\right] \sim 1$ and

$$\begin{aligned}
&\lim_{\gamma\to\infty} \operatorname{erfc}\left[\frac{1}{\sqrt{\pi}\gamma}\right] \\
&= \lim_{\gamma\to\infty} \frac{1}{\sqrt{\pi}} \Gamma_U\left(\frac{1}{2}, \frac{1}{\pi\gamma^2}\right) \\
&= \frac{1}{\sqrt{\pi}}\left(\sqrt{\pi} - \frac{2}{\sqrt{\pi}\gamma}\right) = 1 - \frac{2}{\pi\gamma}.
\end{aligned}$$

If we insert these into Eq. (2.39), we have:

$$\lim_{\gamma\to\infty} \gamma \frac{\Phi_{\text{rms}}^2}{\langle\Phi\rangle^2} = \frac{\left\langle A^2\right\rangle}{2\langle A\rangle^2} - \gamma + \frac{\gamma}{1 - 2/(\pi\gamma)} - 1 = \frac{\left\langle A^2\right\rangle}{2\langle A\rangle^2} - \frac{\pi - 2}{\pi}. \tag{2.41}$$

While the γ-dependency is the same in this limit as for the exponentially distributed waiting times, the numerical value is slightly different ($(\pi - 2)/\pi \approx 0.36$, for exponentially distributed amplitudes we have $\Phi_{\text{rms}}^2/\langle\Phi\rangle^2 \approx 0.64/\gamma$). We have a Rayleigh distribution with a parameter proportional to τ_{w}, so when $\gamma \to \infty$, the waiting time distribution parameter becomes very small, leading to a sharply peaked, narrow distribution. Thus, the pulses arrive more clumped together than for an exponential distribution, leading to a higher ratio of mean signal value compared to the rms-value.

The uniform distribution

We use the uniform distribution

$$P_\tau(\tau) = \frac{1}{2\tau_{\text{w}}}, \quad 0 \le \tau \le 2\tau_{\text{w}}, \tag{2.42}$$

giving in Eq. (2.26)

$$q = \int_0^\infty \mathrm{d}\tau\, P_\tau(\tau) \exp\left(-\frac{\tau}{\tau_{\text{d}}}\right) = \frac{\gamma}{2}\left(1 - \exp\left[-\frac{2}{\gamma}\right]\right).$$

Inserting this expression into Eq. (2.28), we find:

$$\frac{\Phi_{\text{rms}}^2}{\langle\Phi\rangle^2} = \frac{1}{\gamma}\left[\frac{\left\langle A^2\right\rangle}{2\langle A\rangle^2} + \frac{(\gamma-1)-(\gamma+1)\exp(-2/\gamma)}{2/\gamma - 1 + \exp(-2/\gamma)}\right], \tag{2.43}$$

which has $1/\gamma$ as a pre-factor.

The limit $\gamma \to 0$ If we let $\gamma \to 0$, $\exp(-2/\gamma)$ goes to zero and the second term inside the square brackets in Eq. (2.43) goes to zero. Thus, in this limit

$$\lim_{\gamma\to 0} \gamma \frac{\Phi_{\text{rms}}^2}{\langle\Phi\rangle^2} = \frac{\left\langle A^2\right\rangle}{2\langle A\rangle^2}, \tag{2.44}$$

which is the same equation as for exponentially and Rayleigh distributed waiting times.

The limit $\gamma \to \infty$ For large values of γ, we can make the approximation $\exp(-2/\gamma) \approx 1 - 2/\gamma + 2/\gamma^2 - 4/\left(3\gamma^3\right)$, and Eq. (2.43) becomes

$$\lim_{\gamma\to\infty} \gamma \frac{\Phi_{\text{rms}}^2}{\langle\Phi\rangle^2} = \frac{\left\langle A^2\right\rangle}{2\langle A\rangle^2} - \frac{1}{3}. \tag{2.45}$$

Thus we subtract about the same factor in Eq. (2.45) as we do in Eq. (2.41). The interpretation is the same, $\gamma \to \infty$ leads to $\tau_{\text{w}} \to 0$, giving a sharply peaked uniform distribution leading to a lower $\Phi_{\text{rms}}^2/\langle\Phi\rangle^2$ compared to the exponential waiting time distribution.

The degenerate distribution

We use the degenerate distribution

$$P_\tau(\tau) = \delta(\tau - \tau_{\text{w}}), \tag{2.46}$$

giving in Eq. (2.26)

$$q = \int_0^\infty \mathrm{d}\tau\, P_\tau(\tau) \exp\left(-\frac{\tau}{\tau_{\text{d}}}\right) = \exp\left(-\frac{\tau_{\text{w}}}{\tau_{\text{d}}}\right) = \exp\left(-\frac{1}{\gamma}\right).$$

Inserting this expression into Eq. (2.28), we find:

$$\frac{\Phi_{\text{rms}}^2}{\langle\Phi\rangle^2} = \frac{1}{\gamma}\left(\frac{\left\langle A^2\right\rangle}{2\langle A\rangle^2} - \gamma + \frac{1}{\exp(1/\gamma)-1}\right), \tag{2.47}$$

which again has $1/\gamma$ as a pre-factor.

The limit $\gamma \to 0$ If we let $\gamma \to 0$, $\exp(1/\gamma)$ goes to infinity and the fraction in Eq. (2.47) goes to zero. Thus, in this limit

$$\lim_{\gamma \to 0} \gamma \frac{\Phi_{\text{rms}}^2}{\langle \Phi \rangle^2} = \frac{\left\langle A^2 \right\rangle}{2\langle A \rangle^2}. \tag{2.48}$$

as for the previous cases considered. Again, at some point a small enough γ-value ensures pulse separation and the exact waiting time distribution matters less and less for the relative fluctuation level of the signal. When the waiting time becomes much larger than the pulse duration time, the only thing affecting the relation $\Phi_{\text{rms}}/\langle \Phi \rangle$ is how long, on average, there is between pulses.

The limit $\gamma \to \infty$ For large values of γ, we can make the approximation $\exp(1/\gamma) \approx 1 + 1/\gamma + 1/\left(2\gamma^2\right)$, and Eq. (2.47) becomes

$$\lim_{\gamma \to \infty} \gamma \frac{\Phi_{\text{rms}}^2}{\langle \Phi \rangle^2} = \frac{\left\langle A^2 \right\rangle}{2\langle A \rangle^2} - \frac{1}{2}. \tag{2.49}$$

We subtract $1/2$, where we in Section 2.1.3 subtracted $1 - 2/\pi$ and in Section 2.1.3 subtracted $1/3$. When the waiting times are degenerately distributed, the waiting time distribution is the sharpest, most narrow peak of all the four distributions we have considered. The intervals between pulses is exactly the same. Thus, when the pulses arrive very close to each other, the mean of the signal is much larger than the rms-value, compared to the exponential distribution. (This also implies that this is the lowest intermittency relation possible for any waiting time distribution, since no distribution has a sharper peak than the degenerate distribution.

Comparisons

We have in the previous sections seen how, in the limit of very large and very small γ, all the four waiting time distributions have the same dependency on γ, justifying this as the intermittency parameter of the signal. What remains is investigating the behaviour of Eqs. (2.37), (2.39), (2.43) and (2.47) for γ of the order of unity, which is the most relvant for comparisons with the experimental data discussed in Section 1.2. In Figure 2.3, we present the relative fluctuation level as a function of γ for various waiting time distributions. In Figure 2.4 the same results are presented, but with double logarithmic axes in order to reveal the similar asymptotic behaviour for small and large γ. From Figure 2.3 it is evident that while there are differences, they are not huge; the $1/\gamma$-behaviour is still the strongest part of $\Phi_{\text{rms}}^2/\langle\Phi\rangle^2$. From figure 2.4 we see that the analytic results in the limits of very low and very large γ hold; for $\gamma \to 0$, $\Phi_{\text{rms}}^2/\langle\Phi\rangle^2$ converges. For $\gamma \to \infty$, the process with the exponentially distributed waiting times have the highest relative fluctuation level, while the process with the degenerately distributed waiting times have the lowest relative fluctuation level.

2.1.4 Distribution and characteristic functions of $\Phi(t)$

We will now determine the characteristic function and the PDF of $\Phi(t)$ in the case when pulses arrive in accordance with a Poisson process. This discussion follows Garcia [2012] closely. The characteristic function of a random variable Φ is the Fourier transform of its PDF $P_\Phi(\Phi)$:

$$\langle \exp(i\Phi u)\rangle = \int_{-\infty}^{\infty} \mathrm{d}\Phi\, P_\Phi(\Phi) \exp(i\Phi u), \tag{2.50}$$

and then the probability that Φ takes a value in the range between Φ and $\Phi + \Delta\Phi$ is given by the inverse transform:

$$P_\Phi(\Phi)\Delta\Phi = \frac{\Delta\Phi}{2\pi} \int_{-\infty}^{\infty} \mathrm{d}u\ \exp(-i\Phi u)\langle \exp(i\Phi u)\rangle.$$

A basic property of the characteristic function for a stochastic process is that adding random variables corresponds to multiplying their characteristic functions. If we have a sum $\Phi_K = \sum_{k=1}^{K} \phi_k$ of K pulses $\phi_k = A_k\varphi_k$, the characteristic function of Φ_K is:

$$\langle \exp(i\Phi_K u)\rangle = \prod_{k=1}^{K} \langle \exp(i\phi_k u)\rangle.$$

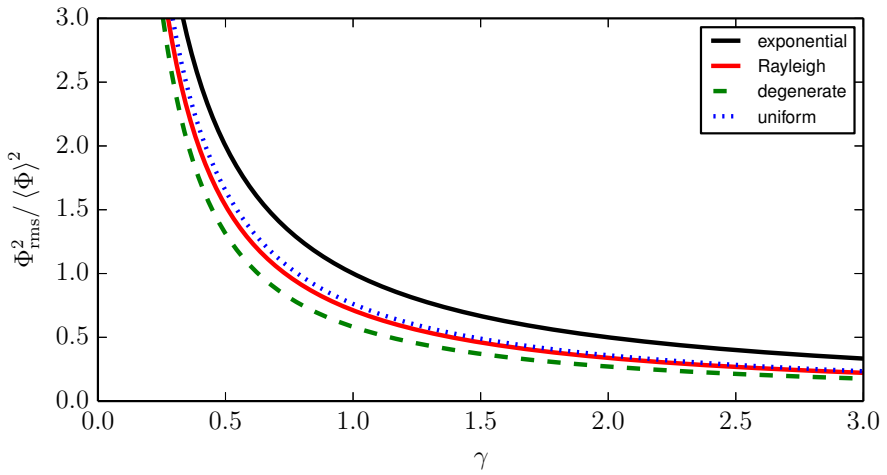

Figure 2.3: Comparisons of the relative fluctuation level for exponential, Rayleigh and degenerate waiting time distributions. The amplitudes are exponentially distributed.

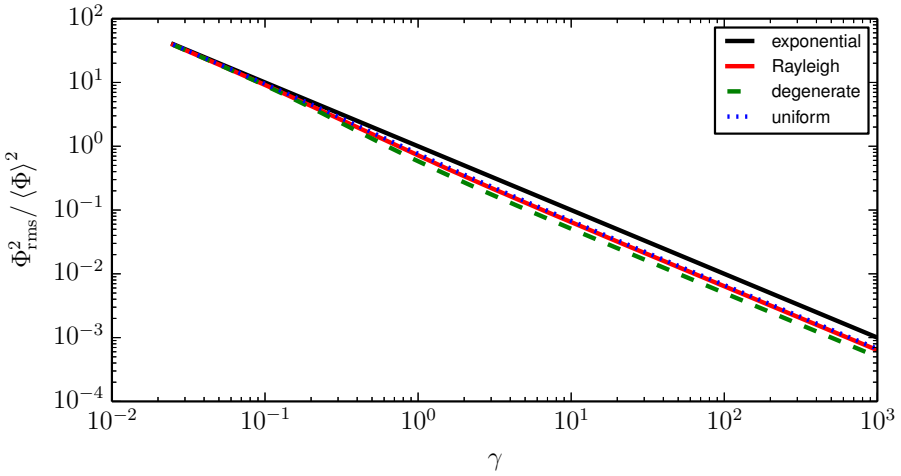

Figure 2.4: Logarithmic scale of Figure 2.3 to see behaviour for $\gamma \to 0$ and $\gamma \to \infty$.

The probability that this sum lies between values Φ_K and $\Phi_K + \Delta\Phi$ is then:

$$P_{\Phi_K}(\Phi_K)\Delta\Phi = \frac{\Delta\Phi}{2\pi}\int_{-\infty}^{\infty} \mathrm{d}u\ \exp(-i\Phi_K u)\prod_{k=1}^{K}\langle\exp(i\phi_k u)\rangle, \tag{2.51}$$

where as usual the angular brackets denote an average over all random variables. Since the pulses arrive in accordance with a Poisson process, the arrival times of the pulses are uniformly distributed (see Appendix, Section B.6 and thus $P_{t_k} = 1/T$ for all k. Therefore, we have

$$\langle\exp(i\phi_k u)\rangle = \frac{1}{T}\int_0^T \mathrm{d}t_k \int_{-\infty}^{\infty} \mathrm{d}A\, P_A(A)\exp(iA\varphi[t - t_k]u) \tag{2.52}$$

for general waveforms and amplitude distributions. If we again assume that the interval $[0,T]$ completely envelops $\varphi(t - t_k)$ for all t_k, all the characteristic functions above are equal, and we can write equation (2.51) as:

$$P_{\Phi_K}(\Phi_K) = \frac{1}{2\pi}\int_{-\infty}^{\infty} \mathrm{d}u\ \exp(-i\Phi_K u)\langle\exp(i\phi_k u)\rangle^K.$$

This distribution is conditional in the sense that it assumes exactly K pulses appear in the interval with duration T. To get the PDF of Φ instead of Φ_K, we sum over all K:

$$P_\Phi(\Phi) = \sum_{K=0}^{\infty} P_K(K;T)P_{\Phi_K}(\Phi_K), \tag{2.53}$$

where $P_K(K;T)$ is the probability density for K events in a realization of duration T. To get further, we need to make an assumption about $P_K(K;T)$, and we will assume it is a Poisson-distribution as detailed in Section 2.1.1. Taking $T \to \infty$ gives the stationary distribution. This gives the result [Garcia, 2012, Pécseli, 2000, Rice, 1944]

$$P_\Phi(\Phi) = \frac{1}{2\pi}\int_{-\infty}^{\infty} \mathrm{d}u\ \exp\left\{-i\Phi u + \frac{1}{\tau_\mathrm{w}}\int_{-\infty}^{\infty}\mathrm{d}A\, P_A(A)\int_{-\infty}^{\infty}\mathrm{d}t\,[\exp(iAu\varphi(t))]\right\}. \tag{2.54}$$

where the characteristic function of $P_\Phi(\Phi)$ is

$$\langle\exp(i\Phi u)\rangle = \exp\left\{\frac{1}{\tau_\mathrm{w}}\int_{-\infty}^{\infty}\mathrm{d}A\, P_A(A)\int_{-\infty}^{\infty}\mathrm{d}t\,[\exp(iAu\varphi(t))]\right\}. \tag{2.55}$$

By expanding the innermost exponential in Eq. (2.55), we can express the

logarithm of this characteristic function in simpler terms:

$$\begin{aligned}\ln(\langle\exp(i\Phi u)\rangle) &= \frac{1}{\tau_\mathrm{w}}\int_{-\infty}^{\infty} \mathrm{d}A\, P_A(A)\int_{-\infty}^{\infty}\mathrm{d}t\,[\exp(iAu\varphi(t))]\\ &= \sum_{n=1}^{\infty}\frac{1}{\tau_\mathrm{w}}\frac{(iu)^n}{n!}\int_{-\infty}^{\infty}\mathrm{d}A\,A^n P_A(A)\int_{-\infty}^{\infty}\mathrm{d}t\,[\varphi(t)]^n\\ &= \sum_{n=1}^{\infty}\gamma\frac{(iu)^n}{n!}\langle A^n\rangle I_n, \end{aligned} \tag{2.56}$$

where I_n is the integral defined in Eq. (2.3). The *cumulants* κ_n of a PDF are given by

$$\ln\langle\exp(i\Phi u)\rangle = \sum_{n=1}^{\infty}\kappa_n\frac{(iu)^n}{n!}, \tag{2.57}$$

and thus, for a shot noise process with Poisson-distributed pulses, we have that the cumulants are

$$\kappa_n = \gamma\langle A^n\rangle I_n. \tag{2.58}$$

These cumulants will be discussed in depth in section Section 2.1.4.

If we assume that the pulse amplitudes are exponentially distributed, we have $\langle A^n\rangle = n!\langle A\rangle^n$, and if we further assume that we have an exponential pulse shape, $I_n = 1/n$. Using these, we find that the characteristic function of $P_\Phi(\Phi)$ is

$$\begin{aligned}\ln(\langle\exp(i\Phi u)\rangle) &= \sum_{n=1}^{\infty}\gamma\frac{(i\langle A\rangle u)^n}{n}\\ &= -\gamma\sum_{n=1}^{\infty}-\frac{(i\langle A\rangle u)^n}{n}\\ &= -\gamma\ln(1-i\langle A\rangle u)\\ &= \ln\left[(1-i\langle A\rangle u)^{-\gamma}\right],\end{aligned}$$

giving

$$\langle\exp(i\Phi u)\rangle = (1-i\langle A\rangle u)^{-\gamma}. \tag{2.59}$$

This is the characteristic function of a Gamma distribution with shape parameter γ and scale parameter $\langle A\rangle$ (see Section B.5.5). Thus, we write the PDF of Φ as

$$P_\Phi(\Phi) = \frac{\Phi^{\gamma-1}}{\langle A\rangle^\gamma\Gamma(\gamma)}\exp\left(-\frac{\Phi}{\langle A\rangle}\right). \tag{2.60}$$

This PDF has the mean $\langle\Phi\rangle = \gamma\langle A\rangle$ and the rms-value $\Phi_\mathrm{rms} = \gamma^{1/2}\langle A\rangle$, in agreement with the results from Sections 2.1.2 and 2.1.3.

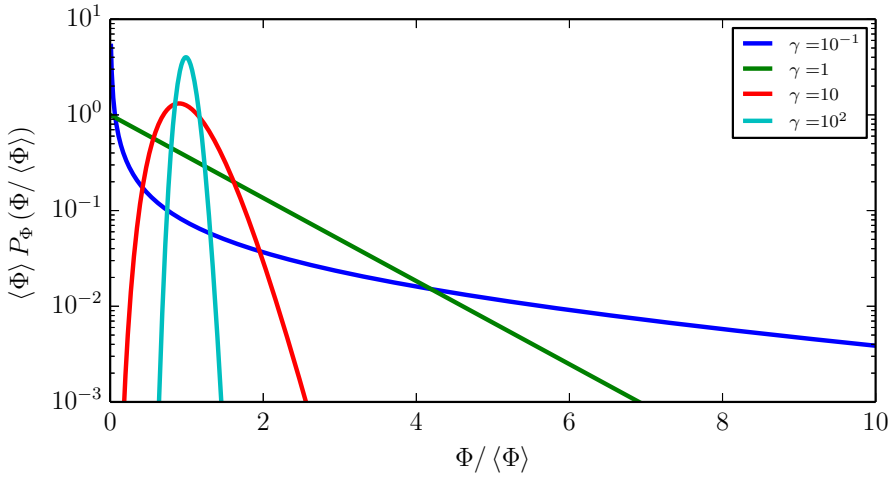

Figure 2.5: The PDF of a shot noise process for various γ-values

For $\gamma > 1$, the PDF of Φ is unimodal, with mode $(\gamma - 1)\langle A\rangle$. For $\gamma = 1$, it is an exponential distribution with parameter $1/\langle A\rangle$, and for $\gamma < 1$, it is monotonically decreasing and has a singularity at $\Phi = 0$. Writing the PDF in terms of the mean value $\langle\Phi\rangle$, we have

$$\langle\Phi\rangle P_\Phi(\Phi/\langle\Phi\rangle) = \frac{\gamma^\gamma}{\Gamma(\gamma)}\left(\frac{\Phi}{\langle\Phi\rangle}\right)^{\gamma-1}\exp\left(-\frac{\Phi}{\langle\Phi\rangle}\right).$$

This is effectively a one-parameter distribution with shape parameter γ. Some examples of this distribution for various γ is plotted in Figure 2.5. The essential features described above for the PDF of a shot noise process hold, and notice that the distribution seems to move towards a normal distribution for very large γ. This is discussed below.

$P_\Phi(\Phi)$ in the limit $\gamma \to \infty$

Let us return to Eq. (2.54), but replace the characteristic function (Eq. (2.55)) with the exponential of Eq. (2.56). The result is

$$P_\Phi(\Phi) = \frac{1}{2\pi}\int_{-\infty}^{\infty} \mathrm{d}u\, \exp\left\{-i\Phi u + \sum_{n=1}^{\infty}\frac{(iu)^n}{n!}\gamma\langle A^n\rangle I_n\right\}. \tag{2.61}$$

It can be shown [Rice, 1944, Pécseli, 2000, Garcia, 2012] that by expanding the characteristic function as a power series in u and integrating term wise, this function can be written as

$$\Phi_{\mathrm{rms}} P_\Phi(\Phi) = \frac{1}{\sqrt{2\pi}}\exp\left(-\frac{\widehat{\Phi}^2}{2}\right)\left[1 + \frac{\kappa_3\left(\widehat{\Phi}^3 - 3\widehat{\Phi}\right)}{3!\sqrt{2\pi}\Phi_{\mathrm{rms}}^3} + \mathcal{O}\left(\gamma^{-1}\right)\right], \tag{2.62}$$

where $\widehat{\Phi} = (\Phi - \langle\Phi\rangle)/\Phi_{\text{rms}}$ and R are the remaining terms in the expansion. The terms inside the square bracket are of order unity, $\gamma^{-1/2}$ and $1/\gamma$ respectively. Therefore, the PDF of any shot noise process with Poisson distribution of events approaches a normal distribution as γ increases. A specific example of this is that the limit of the Gamma distribution in Eq. (2.60) for $\gamma \to \infty$ is a normal distribution. This is a general result, shown in the appendix; Section B.7.

Moments of the shot noise process

Given a shot noise process with Poisson distribution of pulse arrivals, we have that the cumulants of the PDF of the shot noise process are (from Eq. (2.58)):

$$\kappa_n = \gamma \langle A^n \rangle I_n.$$

The four first central moments $\mu_n = \langle (\Phi - \langle\Phi\rangle)^n \rangle$ with $n \geq 2$ are related to the cumulants by (from Wolfram Math World):

$$\begin{aligned} \mu &= \kappa_1, \\ \mu_2 &= \kappa_2, \\ \mu_3 &= \kappa_3, \\ \mu_4 &= \kappa_4 + 3{\kappa_2}^2, \end{aligned}$$

where μ is the mean. This gives

$$\begin{aligned} \langle\Phi\rangle &= \mu = \gamma \langle A \rangle I_1, \\ \Phi_{\text{rms}}^2 &= \mu_2 = \gamma \left\langle A^2 \right\rangle I_2, \\ S_\Phi &= \frac{\mu_3}{\mu_2^{3/2}} = \gamma^{-1/2} \frac{I_3}{{I_2}^{3/2}} \frac{\left\langle A^3 \right\rangle}{\langle A^2 \rangle^{3/2}}, \\ F_\Phi &= \frac{\mu_4}{\mu_2^2} = 3 + \frac{\kappa_4}{\kappa_2^2} = 3 + \gamma^{-1} \frac{I_4}{I_2^2} \frac{\left\langle A^4 \right\rangle}{\langle A^2 \rangle^2}, \end{aligned}$$

where the expressions for skewness S_Φ and flatness F_Φ are found in the appendix (Section B.3). We see that $\langle\Phi\rangle$ is consistent with the first part of Campbell's theorem and we can express the flatness as a function of the skewness [Garcia, 2012]:

$$F_\Phi(S_\Phi) = 3 + \frac{I_2 I_4}{I_3^2} \frac{\left\langle A^2 \right\rangle \left\langle A^4 \right\rangle}{\langle A^3 \rangle^2} S_\Phi^2. \tag{2.63}$$

Thus, independent of the pulse shape and amplitude distribution, there is a parabolic relation between the skewness and kurtosis moments. Also note that if $\varphi(t)$ is positive, $S_\Phi \geq 0$ and $F_\Phi \geq 3$.

If we now assume that we have one of the exponential waveforms described in section Section 2.1.1, we have that $I_n = 1/n$, and the moments become

$$\begin{aligned}\langle\Phi\rangle &= \gamma\langle A\rangle,\\ \Phi_{\text{rms}}^2 &= \frac{\gamma}{2}\left\langle A^2\right\rangle,\\ S_\Phi &= \left(\frac{8}{9\gamma}\right)^{1/2}\frac{\left\langle A^3\right\rangle}{\langle A^2\rangle^{3/2}},\\ F_\Phi &= 3+\gamma^{-1}\frac{\left\langle A^4\right\rangle}{\langle A^2\rangle^2},\end{aligned}$$

we see that Φ_{rms} is consistent with Eq. (2.37), and the relation between skewness and kurtosis becomes:

$$F_\Phi(S_\Phi) = 3+\frac{9}{8}\frac{\left\langle A^2\right\rangle\left\langle A^4\right\rangle}{\langle A^3\rangle^2}S_\Phi^2. \tag{2.64}$$

With the additional assumption that the pulse amplitudes are exponentially distributed, we find that $\langle A^n\rangle = n!\langle A\rangle^n$, and we have:

$$\langle\Phi\rangle = \gamma\langle A\rangle, \tag{2.65}$$

$$\Phi_{\text{rms}}^2 = \gamma\langle A\rangle^2, \tag{2.66}$$

$$S_\Phi = \frac{2}{\gamma^{1/2}}, \tag{2.67}$$

$$F_\Phi = 3+\frac{6}{\gamma}. \tag{2.68}$$

Now, the relation between F_Φ and S_Φ takes on the simple form

$$F_\Phi(S_\Phi) = 3+\frac{3}{2}S_\Phi^2. \tag{2.69}$$

Application We have earlier stated that for the most common assumptions (Poisson distribution of events, exponentially distributed pulse amplitudes and an exponential waveform), $\langle\Phi\rangle^2/\Phi_{\text{rms}}^2 = \gamma$. This relation is not particularly useful when we consider the experimental data set, as we will wish to normalize the signal according to

$$\widehat{\Phi} = \frac{\Phi-\langle\Phi\rangle}{\Phi_{\text{rms}}},$$

which by construction has $\langle\widehat{\Phi}\rangle = 0$ and $\widehat{\Phi}_{\text{rms}} = 1$. Under this normalization, the statement $\left\langle\widehat{\Phi}\right\rangle^2/\widehat{\Phi}_{\text{rms}}^2 = \gamma$ is obviously no longer true. However, as shown in the appendix (Section B.3.5) $S_{\widehat{\Phi}} = S_\Phi$ and $F_{\widehat{\Phi}} = F_\Phi$, such that we can still find the intermittency parameter by $\gamma = 4/S_{\widehat{\Phi}}^2$ or $\gamma = 6/\left(F_{\widehat{\Phi}}-3\right)$.

2.1.5 Autocorrelation function and power spectral density of the shot noise process

The autocorrelation function

From Pécseli [2000] we have that the autocorrelation function of the shot noise process $\Phi(t)$ is

$$\begin{aligned} R_\Phi(\tau) &= \langle \Phi(t)\Phi(t+\tau)\rangle \\ &= \frac{\left\langle A^2\right\rangle}{\tau_\mathrm{w}} \int_{-\infty}^{\infty} \mathrm{d}t\, \varphi(t)\varphi(t+\tau) + \frac{\langle A\rangle^2}{\tau_\mathrm{w}^2}\left[\int_{-\infty}^{\infty} \mathrm{d}t\, \varphi(t)\right]^2 \\ &= \gamma\left\langle A^2\right\rangle R_\varphi(\tau) + \gamma^2\langle A\rangle^2, \end{aligned} \tag{2.70}$$

where $R_\varphi(\tau)$ is the convolution in Eq. (2.4). There are three separate cases to consider ($\tau_\mathrm{r} = 0$, $\tau_\mathrm{r} = \tau_\mathrm{f}$ and the general case with $\tau_\mathrm{r} > 0$ and $\tau_\mathrm{r} \neq \tau_\mathrm{f}$), with different convolutions given in Eq. (2.10), Eq. (2.11) and Eq. (2.12). Listing all cases gives:

$$R_\Phi(\tau) = \begin{cases} \dfrac{\gamma\left\langle A^2\right\rangle}{2}\exp\left(-\dfrac{|\tau|}{\tau_\mathrm{d}}\right) + \gamma^2\langle A\rangle^2 & \tau_\mathrm{r} = 0 \text{ or } \tau_\mathrm{f} = 0 \\ \dfrac{\gamma\left\langle A^2\right\rangle}{2}\left(1 + \dfrac{2|\tau|}{\tau_\mathrm{d}}\right)\exp\left(-\dfrac{2|\tau|}{\tau_\mathrm{d}}\right) + \gamma^2\langle A\rangle^2 & \tau_\mathrm{r} = \tau_\mathrm{f} = \tau_\mathrm{d}/2 \\ \dfrac{\gamma\left\langle A^2\right\rangle}{2(\tau_\mathrm{f}-\tau_\mathrm{r})}\left[\tau_\mathrm{f}\exp\left(-\dfrac{|\tau|}{\tau_\mathrm{f}}\right) - \tau_\mathrm{r}\exp\left(-\dfrac{|\tau|}{\tau_\mathrm{r}}\right)\right] + \gamma^2\langle A\rangle^2 & \text{otherwise} \end{cases} . \tag{2.71}$$

This is listed in full for convenience, although all cases can be derived from the last, most general case. In the following, only this general case will be used.

The power spectral density

According to the Wiener-Khinchin theorem, the power spectral density and autocorrelation function are a Fourier transform pair, $S_\Phi(\omega) = \mathcal{F}[R_\Phi(\tau)]$. Thus,

the power spectral density is readily calculated as

$$S_\Phi(\omega) = \begin{cases} \dfrac{\gamma\left\langle A^2\right\rangle}{2}\dfrac{2\tau_\mathrm{d}}{1+\tau_\mathrm{d}^2\omega^2} + 2\pi\gamma^2\langle A\rangle^2\delta(\omega) & \tau_\mathrm{r}=0 \text{ or } \tau_\mathrm{f}=0 \\ \dfrac{\gamma\left\langle A^2\right\rangle}{2}\dfrac{32\tau_\mathrm{d}}{\left(4+\tau_\mathrm{d}^2\omega^2\right)^2} + 2\pi\gamma^2\langle A\rangle^2\delta(\omega) & \tau_\mathrm{r}=\tau_\mathrm{f} \\ \dfrac{\gamma\left\langle A^2\right\rangle}{2}\dfrac{2\tau_\mathrm{d}}{\left(1+\tau_\mathrm{f}^2\omega^2\right)\left(1+\tau_\mathrm{r}^2\omega^2\right)} + 2\pi\gamma^2\langle A\rangle^2\delta(\omega) & \text{otherwise} \end{cases} . \tag{2.72}$$

Here, the delta function in the last term of each expression is the zero-frequency contribution due to the finite mean value of the signal. Also striking is the qualitative difference between the case of $\tau_\mathrm{r} = 0$ and $\tau_\mathrm{r} > 0$. In the first case, the power spectral density is proportional to $1/\omega^2$, while in the last case it is proportional to $1/\omega^4$. A shot noise process with a double-sided waveform has thus more energy in low frequencies compared to a process with a one-sided pulse shape.

The normalized autocorrelation and power spectral density

In the following, we will assume exponentially distributed waiting times and amplitudes such that $\langle\Phi\rangle = \gamma\langle A\rangle$ and $\Phi_\mathrm{rms}^2 = \gamma\langle A^2\rangle$. The autocorrelation of the normalized shot noise process $\widehat{\Phi}(t) = (\Phi(t) - \langle\Phi\rangle)/\Phi_\mathrm{rms}$ is $R_{\widehat{\Phi}}(\tau) = \langle\widehat{\Phi}(t)\widehat{\Phi}(t-\tau)\rangle$. The relation between R_Φ and $R_{\widehat{\Phi}}$ is then

$$\begin{aligned} R_{\widehat{\Phi}}(\tau) &= \left\langle\widehat{\Phi}(t)\widehat{\Phi}(t-\tau)\right\rangle \\ &= \left\langle\frac{\Phi(t)-\langle\Phi\rangle}{\Phi_\mathrm{rms}}\frac{\Phi(t-\tau)-\langle\Phi\rangle}{\Phi_\mathrm{rms}}\right\rangle \\ &= \frac{\langle\Phi(t)\Phi(t-\tau)\rangle - \langle\Phi\rangle^2}{\Phi_\mathrm{rms}^2} \\ &= \frac{R_\Phi(\tau)-\langle\Phi\rangle^2}{\Phi_\mathrm{rms}^2}, \end{aligned} \tag{2.73}$$

giving under the assumptions of exponentially distributed pulse amplitudes and waiting times

$$R_{\widehat{\Phi}}(\tau) = \frac{\tau_\mathrm{f}\exp(-|\tau|/\tau_\mathrm{f}) - \tau_\mathrm{r}\exp(-|\tau|/\tau_\mathrm{r})}{\tau_\mathrm{f}-\tau_\mathrm{r}}, \tag{2.74}$$

which has $R_{\widehat{\Phi}}(0) = 1$, as the normalization requires.

To get the normalization of the power spectral density, we again use the prop-

erty that $S_{\widehat{\Phi}}(\omega)$ and $R_{\widehat{\Phi}}(\tau)$ are a Fourier transform pair:

$$\begin{aligned} S_{\widehat{\Phi}}(\omega) &= \mathcal{F}\big[R_{\widehat{\Phi}}(\tau)\big] = \mathcal{F}\left[\frac{R_\Phi(\tau) - \langle\Phi\rangle^2}{\Phi_{\text{rms}}^2}\right] \\ &= \frac{1}{\Phi_{\text{rms}}^2}\big(\mathcal{F}[R_\Phi] - \mathcal{F}[\langle\Phi\rangle^2]\big) \\ &= \frac{1}{\Phi_{\text{rms}}^2}\big(S_\Phi(\omega) - 2\pi\langle\Phi\rangle^2\delta(\omega)\big). \end{aligned} \tag{2.75}$$

Under the assumptions stated previously, we then have that the normalized power spectral density is

$$S_{\widehat{\Phi}}(\omega) = \frac{2\tau_\text{d}}{\big(1 + \tau_\text{f}^2\omega^2\big)\big(1 + \tau_\text{r}^2\omega^2\big)}. \tag{2.76}$$

$R_{\widehat{\Phi}}(0) = 1$ gives a requirement on the normalized power spectral density: $\int_{-\infty}^{\infty} \text{d}\omega\, S_{\widehat{\Phi}}(\omega) = 2\pi$. This is easy to verify from Eq. (2.76).

In Figure 2.6, $R_{\widehat{\Phi}}(\tau)$ is plotted graphically for various values of $\tau_\text{r}/\tau_\text{d}$. It shows how the different cases in Eq. (2.71) blend into each other. Figure 2.7 shows the same for the normalized power spectral density. Note how, in Figure 2.7, the power spectral density for $\tau_\text{r} = 0$ is the lowest of the graphs plotted, with the least amount of energy in the low frequencies.

$R_{\widehat{\Phi}}(\tau)$ and $S_{\widehat{\Phi}}(\omega)$ for only positive values of τ and ω It is obvious that Eqns. (2.74) and (2.76) are symmetric around $\tau = 0$ and $\omega = 0$. They can therefore be formulated for only positive values of τ and ω, and the results are

$$R_{\widehat{\Phi}}(\tau) = \frac{\tau_\text{f}\exp(-\tau/\tau_\text{f}) - \tau_\text{r}\exp(-\tau/\tau_\text{r})}{\tau_\text{f} - \tau_\text{r}} H_0(\tau), \tag{2.77}$$

and

$$S_{\widehat{\Phi}}(\omega) = \frac{4\tau_\text{d}}{\big(1 + \tau_\text{f}^2\omega^2\big)\big(1 + \tau_\text{r}^2\omega^2\big)} H_0(\omega). \tag{2.78}$$

Here, we have multiplied $S_{\widehat{\Phi}}(\omega)$ by a factor of two to keep the requirement $\int_{-\infty}^{\infty} \text{d}\omega\, S_{\widehat{\Phi}}(\omega) = 2\pi$.

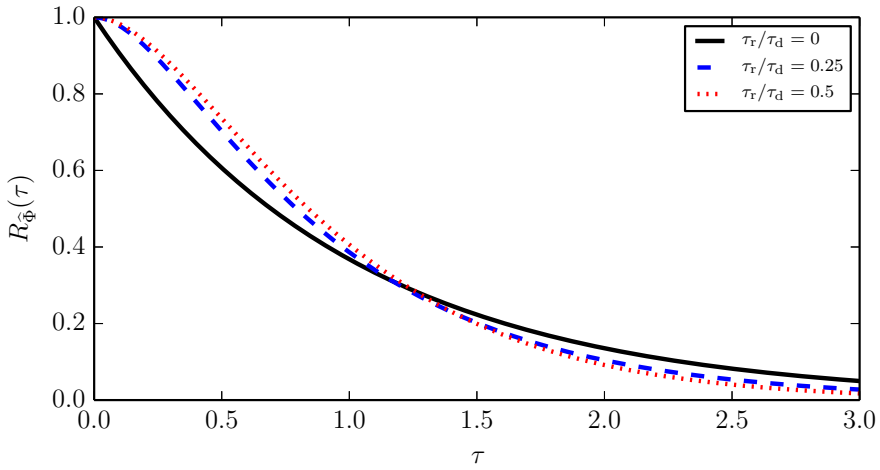

Figure 2.6: Auto-correlation function for the centered and scaled signal for a range of τ_r.

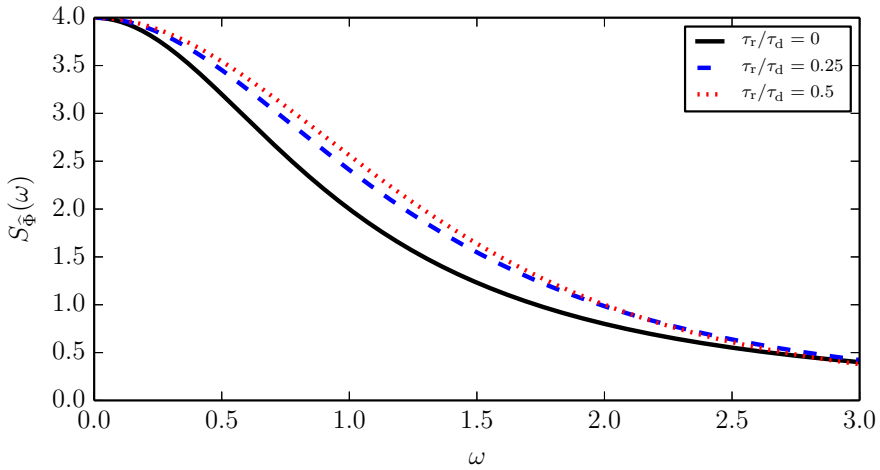

Figure 2.7: Power spectral density for the centered and scaled signal for a range of τ_r.

2.2 The normalized time derivative of a shot noise process

We define the normalized derivative of a shot noise process as

$$\Theta(t) = \tau_\mathrm{d}\frac{\mathrm{d}\Phi(t)}{\mathrm{d}t} = \sum_{k=1}^{K(T)} A_k \tau_\mathrm{d}\frac{\mathrm{d}\varphi(t-t_k)}{\mathrm{d}t} = \sum_{k=1}^{K(T)} A_k \vartheta(t-t_k), \tag{2.79}$$

where $\vartheta(t) = \tau_\mathrm{d}\mathrm{d}\varphi(t)/\mathrm{d}t$. The individual pulses of the normalized derivative are denoted $\theta_k(t) = A_k\vartheta(t-t_k)$. Analogous to Eq. (2.3), we will use J_n for the integral over the n'th power of $\vartheta(t)$:

$$J_n = \frac{1}{\tau_\mathrm{d}}\int_{-\infty}^{\infty}\mathrm{d}t\,[\vartheta(t)]^n, \quad n = 1,2,3,\ldots. \tag{2.80}$$

This process is a shot noise process as well, so Campbell's theorem (from Section 2.1.2) still holds, and we have for the mean value:

$$\langle\Theta\rangle = \gamma\langle A\rangle J_1,$$

where γ, $\langle A\rangle$ and τ_d are the same as for the process $\Phi(t)$. We do however have an additional restriction on the waveform of $\Theta(t)$: Since we are assuming that the shot noise process is stationary, we require $\langle\Phi\rangle$ to be independent of time, which implies that we require $\langle\Theta\rangle = \tau_\mathrm{d}\langle\mathrm{d}\Phi/\mathrm{d}t\rangle = 0$. Using the equation above, this means that we have a limitation on the waveform of the signal itself:

$$\int_{-\infty}^{\infty}\mathrm{d}t\,\frac{\mathrm{d}\varphi(t)}{\mathrm{d}t} = 0. \tag{2.81}$$

J_1 for the one-sided exponential waveform If we use the one-sided waveform with finite fall time $\varphi(t) = \exp(-t/\tau_\mathrm{d})H_1(t/\tau_\mathrm{d})$, we get

$$\begin{aligned}\vartheta(t) &= \tau_\mathrm{d}\frac{\mathrm{d}\varphi(t)}{\mathrm{d}t}\\ &= \tau_\mathrm{d}\left[-\frac{1}{\tau_\mathrm{d}}\exp\left(-\frac{t}{\tau_\mathrm{d}}\right)H_1\left(\frac{t}{\tau_\mathrm{d}}\right) + \exp\left(-\frac{t}{\tau_\mathrm{d}}\right)\delta\left(\frac{t}{\tau_\mathrm{d}}\right)\right]\\ &= \exp\left(-\frac{t}{\tau_\mathrm{d}}\right)\left[\delta\left(\frac{t}{\tau_\mathrm{d}}\right) - H_1\left(\frac{t}{\tau_\mathrm{d}}\right)\right],\end{aligned}$$

where $\delta(t) = \mathrm{d}H_a(t)/\mathrm{d}t$ is the Dirac Delta. Integrating this is straightforward, and gives

$$J_1 = \frac{1}{\tau_\mathrm{d}}\left[\tau_\mathrm{d}\exp\left(-\frac{0}{\tau_\mathrm{d}}\right) - \tau_\mathrm{d}\right] = 0, \tag{2.82}$$

as required. Note, however, that because of the Dirac delta function in $\vartheta(t)$, we cannot evaluate J_n for $n > 1$, as $[\delta(t)]^n$ and $H_1(t)\delta(t)$ are not defined. Neither can we use the second part of Campbell's theorem (section 2.1.3), as this requires convolving the waveform with itself. We can also not simply ignore the delta-function, since without it we violate the condtition in Eq. (2.81). Thus we cannot say anything about the PDF of $\Theta(t)$ for a one-sided exponential pulse shape.

J_1 for the double-sided exponential waveform Let us now use the full waveform

$$\varphi(t) = \exp\left(\frac{t}{\tau_\mathrm{r}}\right) H_{1/2}\left(-\frac{t}{\tau_\mathrm{d}}\right) + \exp\left(-\frac{t}{\tau_\mathrm{f}}\right) H_{1/2}\left(\frac{t}{\tau_\mathrm{d}}\right).$$

The normalized and differentiated waveform is then

$$\begin{aligned}\vartheta(t) = \frac{\tau_\mathrm{d}}{\tau_\mathrm{r}} \exp\left(\frac{t}{\tau_\mathrm{r}}\right) H_{1/2}\left(-\frac{t}{\tau_\mathrm{d}}\right) - \frac{\tau_\mathrm{d}}{\tau_\mathrm{f}} \exp\left(-\frac{t}{\tau_\mathrm{f}}\right) H_{1/2}\left(\frac{t}{\tau_\mathrm{d}}\right) \\ + \left[\exp\left(-\frac{t}{\tau_\mathrm{f}}\right) - \exp\left(-\frac{t}{\tau_\mathrm{r}}\right)\right] \delta\left(\frac{t}{\tau_\mathrm{d}}\right). \quad (2.83)\end{aligned}$$

There is a small difference between this waveform and the waveform from the one-sided function: Here we have a Dirac delta multiplied by two exponentials which cancel at $t = 0$. We may therefore discard the Dirac delta entirely, meaning that we get the waveform

$$\vartheta(t) = \frac{\tau_\mathrm{d}}{\tau_\mathrm{r}} \exp\left(\frac{t}{\tau_\mathrm{r}}\right) H_{1/2}\left(-\frac{t}{\tau_\mathrm{d}}\right) - \frac{\tau_\mathrm{d}}{\tau_\mathrm{f}} \exp\left(-\frac{t}{\tau_\mathrm{f}}\right) H_{1/2}\left(\frac{t}{\tau_\mathrm{d}}\right). \quad (2.84)$$

Discarding the Dirac delta is desireable, as it means we will be able to compute both the second part of Campbell's theorem and compute J_n for $n > 1$. It is not, however, obvious that the effects of the delta function are negliable. We will for now assume that it is possible, and later justify this assumption.

Using the waveform from Eq. (2.84), we find that the requirement in Eq. (2.81) is indeed fullfilled:

$$\int_{-\infty}^{\infty} \mathrm{d}t\, \vartheta(t) = -\frac{\tau_\mathrm{d}}{\tau_\mathrm{f}} \cdot \tau_\mathrm{f} + \frac{\tau_\mathrm{d}}{\tau_\mathrm{r}} \cdot \tau_\mathrm{r} = 0.$$

Note that the result would be the same if we used the waveform from Eq. (2.83), since the last term integrates to 0. Also note that when making the transition from Eq. (2.83) to Eq. (2.84), the limits $\lim_{\tau_\mathrm{r}\to 0} \vartheta(t)$ and $\lim_{\tau_\mathrm{r}\to 0} \vartheta(t)$ are no longer well defined; in effect we are removing the possibility of going from the double-sided pulse shape to one of the one-sided pulse shapes.

J_n for the double exponential waveform The integral J_n of the waveform in Eq. (2.84) becomes

$$J_n = \frac{1}{n}\left[\frac{\tau_\mathrm{r}}{\tau_\mathrm{d}}\left(\frac{\tau_\mathrm{d}}{\tau_\mathrm{r}}\right)^n + \frac{\tau_\mathrm{f}}{\tau_\mathrm{d}}\left(-\frac{\tau_\mathrm{d}}{\tau_\mathrm{f}}\right)^n\right]. \tag{2.85}$$

This is a more complicated result than the one found for the signal itself, Eq. (2.9). Also, it does not have well defined limits for $\tau_\mathrm{r} \to 0$ or $\tau_\mathrm{f} \to 0$, as discussed above.

Convolution of the double exponential waveform Applying the convolution in Eq. (2.4) to the normalized derivative of the double exponential waveform given by Eq. (2.84) gives

$$R_\vartheta(\tau) = \frac{1}{\tau_\mathrm{d}}\int_{-\infty}^{\infty} \mathrm{d}t\, \vartheta(t)\vartheta(t-\tau) = \frac{\tau_\mathrm{d}^2}{2\tau_\mathrm{r}(\tau_\mathrm{f}-\tau_\mathrm{r})}\exp\left(-\frac{|\tau|}{\tau_\mathrm{r}}\right) - \frac{\tau_\mathrm{d}^2}{2\tau_\mathrm{f}(\tau_\mathrm{f}-\tau_\mathrm{r})}\exp\left(-\frac{|\tau|}{\tau_\mathrm{f}}\right). \tag{2.86}$$

In particular, $R_\vartheta(0) = \tau_\mathrm{d}^2/(2\tau_\mathrm{f}\tau_\mathrm{r})$. Comparing this convolution to the convolution of the waveform itself from Eq. (2.10), they both have the same rate of exponential decay, only differentiated by the factors in front of the exponential functions.

2.2.1 Variance of the time derivative of a shot noise process

To find the variance of $\Theta(t)$, we will use Campbell's theorem. We have from Section 2.1.3 that:

$$\begin{aligned}\left\langle\Theta^2\right\rangle &= \frac{\left\langle A^2\right\rangle}{\tau_\mathrm{w}} R_\vartheta(0) \\ &+2\frac{\left\langle A^2\right\rangle}{\tau_\mathrm{w}}\left[\int_0^\infty \mathrm{d}\tau\, P_\tau(\tau)R_\vartheta(\tau) + \int_0^\infty \mathrm{d}\tau_1 \int_0^\infty \mathrm{d}\tau_2\, P_\tau(\tau_1)P_\tau(\tau_2)R_\vartheta(\tau_1+\tau_2) + \cdots\right].\end{aligned} \tag{2.87}$$

Proceeding exactly as in Section 2.1.3 and remembering that the mean of Θ is zero, we find

$$\Theta_\mathrm{rms}^2 = \gamma\left\langle A^2\right\rangle\left(\frac{\tau_\mathrm{d}^2}{\tau_\mathrm{r}\tau_\mathrm{f}} + \frac{\tau_\mathrm{d}}{\tau_\mathrm{f}-\tau_\mathrm{r}}\left[\frac{q_\mathrm{r}}{\tau_\mathrm{r}(1-q_\mathrm{r})} - \frac{q_\mathrm{f}}{\tau_\mathrm{f}(1-q_\mathrm{f})}\right]\right), \tag{2.88}$$

where

$$q_\mathrm{r} = \int_0^\infty \mathrm{d}\tau\, P_\tau(\tau)\exp(-\tau/\tau_\mathrm{r})$$

and

$$q_{\mathrm{f}} = \int_0^\infty \mathrm{d}\tau\, P_\tau(\tau) \exp(-\tau/\tau_{\mathrm{f}}).$$

If we assume Poisson distribution of events, we have exponentially distributed waiting times and this gives $q_{\mathrm{r}} = \tau_{\mathrm{r}}/(\tau_{\mathrm{w}} + \tau_{\mathrm{r}})$, $q_{\mathrm{f}} = \tau_{\mathrm{f}}/(\tau_{\mathrm{w}} + \tau_{\mathrm{f}})$ and

$$\Theta_{\mathrm{rms}}^2 = \frac{\gamma\left\langle A^2\right\rangle}{2}\frac{\tau_{\mathrm{d}}^2}{\tau_{\mathrm{f}}\tau_{\mathrm{r}}} = \Phi_{\mathrm{rms}}^2\frac{\tau_{\mathrm{d}}^2}{\tau_{\mathrm{f}}\tau_{\mathrm{r}}}. \tag{2.89}$$

In this case, we have not assumed anything about the distribution of the pulse amplitudes A, except that its first two moments exist. Note that also here, the impossibility of taking the limits $\tau_{\mathrm{r}} \to 0$ and $\tau_{\mathrm{f}} \to 0$ arises, and that in the case of a symmetric waveform $\tau_{\mathrm{f}} = \tau_{\mathrm{r}} = \tau_{\mathrm{d}}/2$, we have $\Theta_{\mathrm{rms}} = \Phi_{\mathrm{rms}}/2$.

2.2.2 Moments of the time derivative of a shot noise process

Since all assumptions about the main signal also hold for the normalized derivative of the signal, only I_n changes to J_n in the derivation of the characteristic function of $\Theta(t)$. Therefore, Eq. (2.56) holds for $\Theta(t)$ as well, and have the same cumulants (up to the difference from J_n):

$$\kappa_n = \gamma\langle A^n\rangle J_n. \tag{2.90}$$

Following the calculations in Section 2.1.4, we have when calculating the integrals:

$$\begin{aligned}
\langle\Theta\rangle &= 0,\\
\Theta_{\mathrm{rms}}^2 &= \frac{\gamma\left\langle A^2\right\rangle}{2}\frac{\tau_{\mathrm{d}}^2}{\tau_{\mathrm{r}}\tau_{\mathrm{f}}},\\
S_\Theta &= \left(\frac{8}{9\gamma}\right)^{1/2}\frac{\left\langle A^3\right\rangle}{\langle A^2\rangle^{3/2}}\frac{\tau_{\mathrm{f}}-\tau_{\mathrm{r}}}{(\tau_{\mathrm{f}}\tau_{\mathrm{r}})^{1/2}},\\
F_\Theta &= 3 + \gamma^{-1}\frac{\left\langle A^4\right\rangle}{\langle A^2\rangle^2}\frac{(\tau_{\mathrm{f}}-\tau_{\mathrm{r}})^2 + \tau_{\mathrm{r}}\tau_{\mathrm{f}}}{\tau_{\mathrm{r}}\tau_{\mathrm{f}}}.
\end{aligned}$$

Note that the expression for Θ_{rms} here is the same as when applying Campbell's theorem, given above in Eq. (2.88). We see that the skewness vanishes for $\tau_{\mathrm{r}} = \tau_{\mathrm{f}}$, implying the expected result that a symmetric pulse waveform gives a symmetric PDF. Also, $\tau_{\mathrm{r}} > \tau_{\mathrm{f}}$ gives negative skewness while $\tau_{\mathrm{f}} > \tau_{\mathrm{r}}$ gives positive skewness. Thus, when $\tau_{\mathrm{f}} > \tau_{\mathrm{r}}$, the negative ϑ-values contribute longer, pushing the signal as a whole towards negative values and thus positive skewness. This

does not imply that the mean value of Θ becomes different from 0. While the negative ϑ-values may contribute more over time, the positive values have higher base values (due to the $1/\tau_r$-factor in front of the exponential function), keeping the requirement $\langle\Theta\rangle = 0$.

When assuming exponentially distributed amplitudes we have:

$$\langle\Theta\rangle = 0, \tag{2.91}$$

$$\Theta_{\text{rms}}^2 = \gamma\langle A\rangle^2 \frac{\tau_d^2}{\tau_r\tau_f}, \tag{2.92}$$

$$S_\Theta = 2\gamma^{-1/2}\frac{\tau_f - \tau_r}{(\tau_f\tau_r)^{1/2}}, \tag{2.93}$$

$$F_\Theta = 3 + \frac{6}{\gamma}\frac{(\tau_f - \tau_r)^2 + \tau_f\tau_r}{\tau_r\tau_f}. \tag{2.94}$$

and we have the parabolic relation between F_Θ and S_Θ given by:

$$\begin{aligned} F_\Theta(S_\Theta) &= 3 + \frac{I_2 I_4}{I_3^2}\frac{\langle A^2\rangle\langle A^4\rangle}{\langle A^3\rangle^2}S_\Theta^2 \\ &= 3 + \frac{3}{2}\frac{(\tau_f - \tau_r)^2 + \tau_f\tau_r}{(\tau_f - \tau_r)^2}S_\Theta^2. \end{aligned} \tag{2.95}$$

wile this relation appears to diverge for $\tau_r = \tau_r$, it must be recalled that the PDF is symmetric in this case and thus S_Θ vanishes. Note also that this relation appears to have well-defined limits for $\tau_r \to 0$ and $\tau_f \to 0$. For both of these, the last fraction goes to 1, and we end up with $F_\Theta(S) = 3 + 3S_\Theta^2/2$, which is the same relation that is found for the signal itself. However, S_Θ approaches infinity for both these cases.

2.2.3 The PDF of the time derivative of a shot noise process for the double exponential waveform

In the following, Poisson distribution of pulse events are assumed, and the pulse amplitudes are assumed to be exponentially distributed. From this, we can start from Eq. (2.56) and get that the logarithm of the characteristic function of $P_\Theta(\Theta)$ is

$$\ln\langle\exp(i\Theta u)\rangle = \sum_{n=1}^{\infty}\frac{\tau_r}{\tau_w}\frac{(iu\langle A\rangle\tau_d/\tau_r)^n}{n} + \sum_{n=1}^{\infty}\frac{\tau_f}{\tau_w}\frac{(-iu\langle A\rangle\tau_d/\tau_f)^n}{n}, \tag{2.96}$$

with the corresponding characteristic function

$$\langle i\Theta u\rangle = \left(1 - iu\langle A\rangle\frac{\tau_d}{\tau_r}\right)^{-\tau_r/\tau_w}\left(1 - iu(-\langle A\rangle)\frac{\tau_d}{\tau_f}\right)^{-\tau_f/\tau_w}. \tag{2.97}$$

This is the multiplication of two characteristic functions for gamma distributions; one distribution over the positive Θ-values with shape parameter τ_r/τ_w and scale parameter $\langle A\rangle\tau_d/\tau_r$, and one mirrored distribution over the negative Θ-values with shape parameter τ_f/τ_w and scale parameter $-\langle A\rangle\tau_d/\tau_f$. The former distribution is called $P_{\Theta_+}(\Theta;\langle A\rangle\tau_d/\tau_r,\tau_r/\tau_w)$ and the latter distribution is called $P_{\Theta_\div}(\Theta;-\langle A\rangle\tau_d/\tau_f,\tau_f/\tau_w)$ Multiplying characteristic functions corresponds to convolving the PDFs (see appendix, Section B.4):

$$\langle i\Theta u\rangle = \langle i\Theta_+ u\rangle\langle i\Theta_\div u\rangle = \left(1 - iu\langle A\rangle\frac{\tau_d}{\tau_r}\right)^{-\frac{\tau_r}{\tau_w}}\left(1 - iu(-\langle A\rangle)\frac{\tau_d}{\tau_f}\right)^{-\frac{\tau_f}{\tau_w}},$$

which implies that the PDF is given by

$$P_\Theta(\Theta) = P_{\Theta_+}\left(\Theta;\langle A\rangle\frac{\tau_d}{\tau_r},\frac{\tau_r}{\tau_w}\right) * P_{\Theta_\div}\left(\Theta;-\langle A\rangle\frac{\tau_d}{\tau_f},\frac{\tau_f}{\tau_w}\right) = \int_{-\infty}^{\infty} \mathrm{d}x\, P_{\Theta_+}(x)P_{\Theta_\div}(\Theta - x). \tag{2.98}$$

In order to simplify the notation, we introduce the dimensionless parameter $\lambda = \tau_r/\tau_d$ which signifies the asymmetry of the waveform. We have $0 \le \lambda \le 1$. Using this and $\gamma = \tau_d/\tau_w$, we find that $\tau_r/\tau_w = \gamma\lambda$, $\tau_f/\tau_d = 1 - \lambda$ and $\tau_f/\tau_w = \gamma(1-\lambda)$. Then the PDF of the positive values becomes

$$P_{\Theta_+}(\Theta) = \frac{\Theta^{\tau_r/\tau_w - 1}\exp(-\Theta\tau_r/\langle A\rangle\tau_d)}{(\langle A\rangle\tau_d/\tau_r)^{\tau_r/\tau_w}\Gamma(\tau_r/\tau_w)}H_0(\Theta) = \frac{\Theta^{\gamma\lambda-1}\exp(-\lambda\Theta/\langle A\rangle)}{(\langle A\rangle/\lambda)^{\gamma\lambda}\Gamma(\gamma\lambda)}H_0(\Theta),$$

and the PDF for the negative values is

$$\begin{aligned} P_{\Theta_\div}(\Theta) &= -\frac{\Theta^{\tau_f/\tau_w - 1}\exp(-\Theta\tau_f/-\langle A\rangle\tau_d)}{(-\langle A\rangle\tau_d/\tau_f)^{\tau_f/\tau_w}\Gamma(\tau_f/\tau_w)}H_0(-\Theta) \\ &= -\frac{\Theta^{\gamma(1-\lambda)-1}\exp((1-\lambda)\Theta/\langle A\rangle)}{[-\langle A\rangle/(1-\lambda)]^{\gamma(1-\lambda)}\Gamma(\gamma(1-\lambda))}H_0(-\Theta). \end{aligned}$$

Thus, the PDF for the time derivative of the signal $\Phi(t)$ becomes

$$\begin{aligned} P_\Theta(\Theta) &= \int_{-\infty}^{\infty}\mathrm{d}\Theta'\, P_{\Theta_+}(\Theta')P_{\Theta_\div}(\Theta-\Theta') \\ &= -\frac{(\langle A\rangle/\lambda)^{1-\gamma\lambda}[-\langle A\rangle/(1-\lambda)]^{1-\gamma(1-\lambda)}}{\Gamma(\gamma\lambda)\Gamma(\gamma(1-\lambda))}\int_{-\infty}^{\infty}\mathrm{d}\Theta'\Bigg[\Theta'^{\gamma\lambda-1}(\Theta-\Theta')^{\gamma(1-\lambda)-1} \\ &\quad\times\exp\left(-\frac{\lambda\Theta'}{\langle A\rangle}\right)\exp\left(\frac{(1-\lambda)(\Theta-\Theta')}{\langle A\rangle}\right)H_0(\Theta')H_0(\Theta'-\Theta)\Bigg]. \end{aligned} \tag{2.99}$$

Some manipulations lead to the somewhat simpler expression:

$$P_\Theta(\Theta) = \frac{(1-\lambda)^{\gamma(1-\lambda)}\lambda^{\gamma\lambda}\langle A\rangle^{-\gamma}}{\Gamma(\gamma\lambda)\Gamma(\gamma(1-\lambda))}\exp\left(-\lambda\frac{\Theta}{\langle A\rangle}\right) \times \int_{\max(0,-\Theta)}^{\infty} \mathrm{d}\Theta'(\Theta+\Theta')^{\gamma\lambda-1}(\Theta')^{\gamma(1-\lambda)-1}\exp\left(-\frac{\Theta'}{\langle A\rangle}\right). \quad (2.100)$$

For further simplification, we define $\widehat{\Theta} = \Theta/\langle A\rangle$, giving $\widehat{\Theta}' = \Theta'/\langle A\rangle$. This gives the rescaled PDF:

$$\langle A\rangle P_\Theta(\widehat{\Theta}) = \frac{(1-\lambda)^{\gamma(1-\lambda)}\lambda^{\gamma\lambda}}{\Gamma(\gamma\lambda)\Gamma(\gamma(1-\lambda))}\exp\left(-\lambda\widehat{\Theta}\right) \times \int_{\max\left(0,-\widehat{\Theta}\right)}^{\infty} \mathrm{d}\widehat{\Theta}'\left(\widehat{\Theta}+\widehat{\Theta}'\right)^{\gamma\lambda-1}\left(\widehat{\Theta}'\right)^{\gamma(1-\lambda)-1}\exp\left(-\widehat{\Theta}'\right). \quad (2.101)$$

We could also express Eq. (2.100) with Θ scaled by $\langle\Phi\rangle$ through Campbell's theorem $\langle\Phi\rangle = \gamma\langle A\rangle$. This is sometimes advantageous, as $\langle\Phi\rangle$ is easy to calculate and γ is already a parameter in the function.

The PDF in Eq. (2.100) does not have a simpler form, and taking the limits of $\lambda \to 0$ and $\lambda \to 1$ is not possible since $\lim_{\lambda\to 0} \lambda^{\gamma\lambda}/\Gamma(\gamma\lambda) = \infty$. It is however possible to evaluate the PDF numerically. Some examples are presented in figure 2.8. Above, $\gamma\langle A\rangle P_\Theta(\Theta/\langle A\rangle)$ is plotted as a function of $\Theta/\langle A\rangle$ for $\lambda = 1/2$ and various γ. Below, $\langle A\rangle P_\Theta(\Theta/\langle A\rangle)$ is plotted as a function of $\Theta/\langle A\rangle$ for $\gamma = 2$ and various λ. For all cases in the figure, the mean of the distribution is zero. In the figure below, the skewed distributions have a peak on one side of 0, but the tail extends far to the other side, making the integral the same over both sides. The sharp peak in the uppermost figure for $\gamma = 1$ is due to the singularity at $\Theta = 0$.

Note that for the the special case $\gamma = 2$, $\lambda = 1/2$, the integral can be calculated, and the result is

$$P_\Theta(\Theta) = \frac{1}{2\langle\Phi\rangle}\exp\left(-\frac{|\Theta|}{\langle\Phi\rangle}\right), \quad (2.102)$$

which is the so-called Laplace distribution (see appendix, Section B.5.5) with

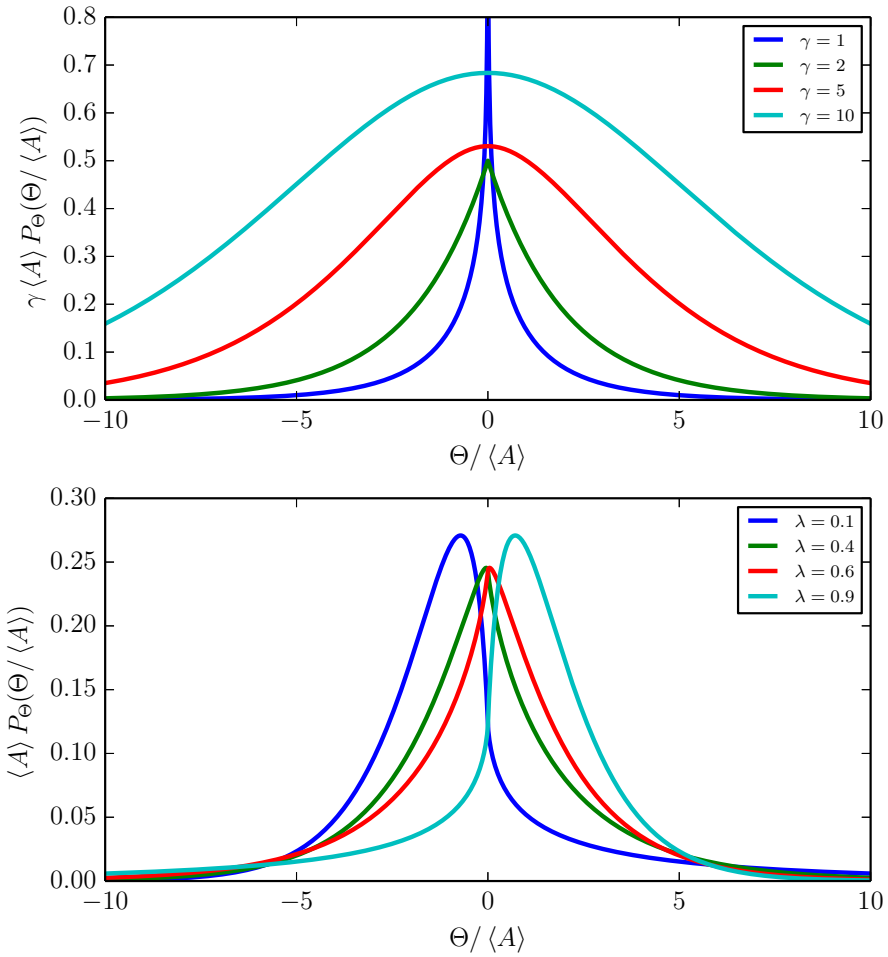

Figure 2.8: The PDF of the time derivative of a shot noise process, from equation (2.100). Above, $\lambda = 1/2$ for various γ. Below,$\gamma = 2$ for various λ.

location parameter 0 and scale parameter $\langle \Phi \rangle$. It has the moments

$$\begin{aligned} \langle \Theta \rangle &= 0, \\ \Theta_{\text{rms}}^2 &= 2\langle \Phi \rangle, \\ S_\Theta &= 0, \\ F_\Theta &= 6, \end{aligned}$$

which is consistent with setting $\gamma = 2$ and $\lambda = 1/2$ in Eqns. 2.91-2.94. $S_\Theta = 0$ for $\tau_r = \tau_f$ is also seen in Figure 2.8, where the symmetry of the PDF around $\lambda = 1/2$ is evident. These are consisitent, as a symmetric PDF has vanishing skewness.

Moments of $\Theta(t)$ from the PDF

The PDF of $\Theta(t)$ is given in Eq. (2.100), and in principle we can calulate the moments of $P_\Theta(\Theta)$ by

$$\begin{aligned}\langle\Theta^n\rangle &= \int_{-\infty}^{\infty} \mathrm{d}\Theta\, \Theta^n P_\Theta(\Theta) \\ &= \langle A\rangle^{n+1} \int_{-\infty}^{\infty} \mathrm{d}\widehat{\Theta}\, \widehat{\Theta}^n P_\Theta\left(\widehat{\Theta}\right) \\ &= \frac{\langle A\rangle^n (1-\lambda)^{\gamma(1-\lambda)}\lambda^{\gamma\lambda}}{\Gamma(\gamma\lambda)\Gamma(\gamma(1-\lambda))} \\ &\times \int_{-\infty}^{\infty} \mathrm{d}\widehat{\Theta} \int_{\max(0,-\widehat{\Theta})}^{\infty} \mathrm{d}x\, \widehat{\Theta}^n \left(\widehat{\Theta}+x\right)^{\gamma\lambda-1} x^{\gamma(1-\lambda)-1} \exp[-(x+\lambda\Theta)], \quad (2.103)\end{aligned}$$

where we have written x instead of Θ' for readability. This double integral can be split in two, one over $-\infty < \widehat{\Theta} < 0$ and one over $0 < \widehat{\Theta} < \infty$, giving

$$\begin{aligned}\langle\Theta^n\rangle &= \frac{\langle A\rangle^n (1-\lambda)^{\gamma(1-\lambda)}\lambda^{\gamma\lambda}}{\Gamma(\gamma\lambda)\Gamma(\gamma(1-\lambda))} \\ &\times \left\{ \int_{-\infty}^{0} \mathrm{d}\widehat{\Theta} \int_{-\widehat{\Theta}}^{\infty} \mathrm{d}x\, \widehat{\Theta}^n \left(\widehat{\Theta}+x\right)^{\gamma\lambda-1} x^{\gamma(1-\lambda)-1} \exp[-(x+\lambda\Theta)] \right. \\ &+ \left. \int_{0}^{\infty} \mathrm{d}\widehat{\Theta} \int_{0}^{\infty} \mathrm{d}x\, \widehat{\Theta}^n \left(\widehat{\Theta}+x\right)^{\gamma\lambda-1} x^{\gamma(1-\lambda)-1} \exp[-(x+\lambda\Theta)] \right\}.\end{aligned}$$

This equation can be solved by Mathematica for the first four moments, and it gives the same result as calculating them from the characteristic function of Θ.

2.3 The joint PDF $P_{\Phi\Theta}(\Phi,\Theta)$

By generalizing expression (9.22) in Pécseli [2000], Rowland [1936], and assuming Poisson distributed pulses and exponentially distributed pulse amplitudes, we have that the joint PDF between $\Phi(t)$ and $\Theta(t)$ is

$$P_{\Phi\Theta}(\Phi,\Theta) = \frac{1}{(2\pi)^2}\int_{-\infty}^{\infty} \mathrm{d}u \int_{-\infty}^{\infty} \mathrm{d}v \, \exp(-i\Phi u - i\Theta v) \\ \exp\left\{\frac{1}{\tau_\mathrm{w}}\int_{-\infty}^{\infty} \mathrm{d}A\, P_A(A) \int_{-\infty}^{\infty} \mathrm{d}t \, \exp[iuA\varphi(t) + ivA\vartheta(t)] - 1\right\}. \tag{2.104}$$

2.3.1 The characteristic function of $P_{\Phi\Theta}(\Phi,\Theta)$

Let us for now concentrate on the integral inside the second exponential. Changing order of integration and remembering that $\int_{-\infty}^{\infty} \mathrm{d}A\, P_A(A) = 1$, we get

$$\begin{aligned}
&\frac{1}{\tau_\mathrm{w}}\int_{-\infty}^{\infty} \mathrm{d}A\, P_A(A) \int_{-\infty}^{\infty} \mathrm{d}t \, \{\exp[iuA\varphi(t) + ivA\vartheta(t)] - 1\} \\
&= \frac{1}{\tau_\mathrm{w}}\int_{-\infty}^{\infty} \mathrm{d}t \left\{-1 + \int_{-\infty}^{\infty} \mathrm{d}A\, \frac{1}{\langle A\rangle} \exp\left(-\frac{A}{\langle A\rangle}\right) \exp(-[-iu\varphi(t) - iv\vartheta(t)]A)\right\} \\
&= \frac{1}{\tau_\mathrm{w}}\int_{-\infty}^{\infty} \mathrm{d}t \left[\frac{1}{1 - iu\langle A\rangle\varphi(t) - iv\langle A\rangle\vartheta(t)} - 1\right].
\end{aligned} \tag{2.105}$$

Instead of using the Heaviside function in the waveforms, we here prefer to write them as

$$\varphi(t) = \begin{cases} \exp(t/\tau_\mathrm{r}) & t < 0 \\ \exp(-t/\tau_\mathrm{f}) & t > 0 \end{cases}, \quad \vartheta(t) = \begin{cases} \dfrac{1}{\lambda}\exp(t/\tau_\mathrm{r}) & t < 0 \\ \dfrac{1}{1-\lambda}\exp(-t/\tau_\mathrm{f}) & t > 0 \end{cases},$$

and split the integral in Eq. (2.105) into integrals over the positive line and the negative line:

$$\begin{aligned}
&\frac{1}{\tau_w}\int_{-\infty}^{\infty} dt\left[\frac{1}{1-iu\langle A\rangle\varphi(t)-iv\langle A\rangle\vartheta(t)}-1\right]\\
&=\frac{1}{\tau_w}\int_{-\infty}^{0} dt\left[\frac{1}{1-i\langle A\rangle(u+v/\lambda)\exp(t/\tau_r)}-1\right]\\
&+\frac{1}{\tau_w}\int_{0}^{\infty} dt\left[\frac{1}{1-i\langle A\rangle(u-v/(1-\lambda))\exp(-t/\tau_f)}-1\right]\\
&=-\frac{\tau_r}{\tau_w}\ln\left[1-i\langle A\rangle\left(u+\frac{v}{\lambda}\right)\right]-\frac{\tau_f}{\tau_w}\ln\left[1-i\langle A\rangle\left(u-\frac{v}{1-\lambda}\right)\right], \qquad (2.106)
\end{aligned}$$

where we have used Mathematica to perform the last integration. Taking the exponential of this gives the characteristic function of $P_{\Phi,\Theta}(\Phi,\Theta)$ [where $\tau_r/\tau_w=\gamma\lambda$ and $\tau_f/\tau_w=\gamma(1-\lambda)$]:

$$\langle iu\Phi+iv\Theta\rangle=\left[1-i\langle A\rangle\left(u+\frac{v}{\lambda}\right)\right]^{-\gamma\lambda}\left[1-i\langle A\rangle\left(u-\frac{v}{1-\lambda}\right)\right]^{-\gamma(1-\lambda)}. \qquad (2.107)$$

It is clear that this function is not separable into one function of u multiplied by another function of v, which means that $\Phi(t)$ and $\Theta(t)$ are not independent. As a consistency check, we note that setting $v=0$ gives

$$\langle\exp(iu\Phi)\rangle=(1-i\langle A\rangle u)^{-\gamma},$$

which is the characteristic function for $P_\Phi(\Phi)$ given in Eq. (2.59), while setting $u=0$ gives

$$\langle\exp(iv\Theta)\rangle=\left(1-i\langle A\rangle\frac{v}{\lambda}\right)^{-\gamma\lambda}\left(1+i\langle A\rangle\frac{v}{1-\lambda}\right)^{-\gamma(1-\lambda)},$$

which is the characteristic function of $P_\Theta(\Theta)$ found in Eq. (2.97).

2.3.2 The full joint PDF $P_{\Phi\Theta}(\Phi,\Theta)$

We now have an expression for the joint PDF between $\Phi(t)$ and $\Theta(t)$:

$$\begin{aligned}
P_{\Phi\Theta}(\Phi,\Theta)=\frac{1}{(2\pi)^2}\int_{-\infty}^{\infty}du\int_{-\infty}^{\infty}dv\Bigg\{&\exp(-iu\Phi-iv\Theta)\\
&\times\left[1-i\langle A\rangle\left(u+\frac{v}{\lambda}\right)\right]^{-\gamma\lambda}\left[1-i\langle A\rangle\left(u-\frac{v}{1-\lambda}\right)\right]^{-\gamma(1-\lambda)}\Bigg\}. \qquad (2.108)
\end{aligned}$$

Doing the change of varialbes $x = u + v/\lambda$, $y = u - v/(1-\lambda)$ and using the shorthand

$$\alpha = \frac{\lambda}{\langle A\rangle}[\Phi + (1-\lambda)\Theta],$$
$$\beta = \frac{1-\lambda}{\langle A\rangle}(\Phi - \lambda\Theta),$$

we can write the joint PDF as

$$P_{\Phi\Theta}(\Phi,\Theta) = \frac{\lambda(1-\lambda)}{(2\pi\langle A\rangle)^2}\int_{-\infty}^{\infty} \mathrm{d}x\,[1-ix]^{-\gamma\lambda}\exp(-i\alpha x)\int_{-\infty}^{\infty}\mathrm{d}y\,[1-ix]^{-\gamma(1-\lambda)}\exp(-i\beta y). \tag{2.109}$$

We now have two separate integrals over x and y. Mathematica can perform these, and the result is

$$P_{\Phi\Theta}(\Phi,\Theta) = \frac{\lambda(1-\lambda)}{(2\pi\langle A\rangle)^2}\frac{2\pi\exp(-\alpha)\alpha^{\gamma\lambda-1}H_{1/2}(\alpha)}{\Gamma(\gamma\lambda)}\frac{2\pi\exp(-\beta)\beta^{\gamma(1-\lambda)-1}H_{1/2}(\beta)}{\Gamma(\gamma(1-\lambda))}, \tag{2.110}$$

replacing α and β and doing the calulations possible, we end up with a general expression for the joint PDF of $\Phi(t)$ and $\Theta(t)$:

$$P_{\Phi\Theta}(\Phi,\Theta) = \frac{\lambda^{\gamma\lambda}(1-\lambda)^{\gamma(1-\lambda)}\exp(-\Phi/\langle A\rangle)}{\langle A\rangle^{\gamma}\Gamma(\gamma\lambda)\Gamma(\gamma(1-\lambda))}$$
$$\times[\Phi+(1-\lambda)\Theta]^{\gamma\lambda-1}(\Phi-\lambda\Theta)^{\gamma(1-\lambda)-1}H[\Phi+(1-\lambda)\Theta]H[\Phi-\lambda\Theta]. \tag{2.111}$$

The dependency between Φ and Θ is evident in this equation for the joint PDF, they are not at all separable. It will be shown in Section 2.3.4 that this PDF indeed can be reduced to the marginal PDFs of Φ and Θ [Equations (2.60) and (2.100) respectively]. Note that only Φ falls off exponentially in the joint PDF, even though there are exponential functions in the PDF of Θ. This is due to the lack of independence, and how the exponential function in $P_\Theta(\Theta)$ appears is seen in Section 2.3.4. Before discussing this function in depth, we will make some remarks regarding correlations and dependencies in the joint PDF and show that it is reducible to the marginal PDFs.

2.3.3 Correlation and dependencies in the joint PDF

From Eq. (2.111), it is clear that under the common assumptions, $\Phi(t)$ and $\Theta(t)$ are not independent. We do however know that as long as $\Phi(t)$ is a stationary process, they are always uncorrelated:

$$\langle(\Phi-\langle\Phi\rangle)(\Theta-\langle\Theta\rangle)\rangle = \langle(\Phi-\langle\Phi\rangle)\Theta\rangle = \langle\Phi\Theta\rangle = \frac{\tau_\mathrm{d}}{2}\left\langle\frac{\mathrm{d}\Phi^2}{\mathrm{d}t}\right\rangle = \frac{\tau_\mathrm{d}}{2}\frac{\mathrm{d}}{\mathrm{d}t}\left\langle\Phi^2\right\rangle = 0. \tag{2.112}$$

The derivation operator can be moved through the averaging, since it is a linear operator [Stark and Woods, 2012], and $\left\langle \Phi^2 \right\rangle$ is independent of time since Φ is a stationary process.

We also see from Section 2.1.4 and Section 2.2.2 that in the limit of large γ, the skewness and flatness of both Φ and Θ disappear, and it can be shown (Section 2.1.4) that $P_\Phi(\Phi)$ approaches a normal distribution in this limit. By using the same arguments, Θ also approaches a normal distribution.

Thus, in the limit of large γ, both marginal PDFs of Φ and Θ are normally distributed and uncorrelated. This does not mean that they are independent, however. They need to be *jointly* normally distributed to be independent, which has not been shown. Therefore, the assumption of inependence that will be made in Section 3.3 is still an assumption.

2.3.4 Reduction of the joint PDF to the marginal PDFs

$P_{\Phi\Theta}(\Phi\Theta)$ to $P_\Phi(\Phi)$ First, we will get the PDF of Φ. To save space, the heaviside functions are evaluated directly in the second line below:

$$
\begin{aligned}
P_\Phi(\Phi) &= \int_{-\infty}^{\infty} \mathrm{d}\Theta\, P_{\Phi\Theta}(\Phi\Theta) \\
&= \frac{\lambda^{\gamma\lambda}(1-\lambda)^{\gamma(1-\lambda)}\exp(-\Phi/\langle A\rangle)}{\langle A\rangle^{\gamma}\Gamma[\gamma\lambda]\Gamma[\gamma(1-\lambda)]} \int_{-\frac{\Phi}{1-\lambda}}^{\frac{\Phi}{\lambda}} \mathrm{d}\Theta\,[\Phi+(1-\lambda)\Theta]^{\gamma\lambda-1}(\Phi-\lambda\Theta)^{\gamma(1-\lambda)-1}.
\end{aligned}
$$

Concentrating on just the integral and substituting $x(\Theta) = \Phi + (1-\lambda)\Theta$ gives

$$
\begin{aligned}
&\int_{-\frac{\Phi}{1-\lambda}}^{\frac{\Phi}{\lambda}} \mathrm{d}\Theta\,[\Phi+(1-\lambda)\Theta]^{\gamma\lambda-1}(\Phi-\lambda\Theta)^{\gamma(1-\lambda)-1} \\
&= (1-\lambda)^{-\gamma(1-\lambda)} \int_0^{\Phi/\lambda} \mathrm{d}x\, x^{\gamma\lambda-1}(\Phi-\lambda x)^{\gamma(1-\lambda)-1},
\end{aligned}
$$

and substituting $y(x) = \Phi - \lambda x$ gives

$$(1-\lambda)^{-\gamma(1-\lambda)} \int_0^{\Phi/\lambda} \mathrm{d}x\, x^{\gamma\lambda-1}(\Phi-\lambda x)^{\gamma(1-\lambda)-1}$$
$$= (1-\lambda)^{-\gamma(1-\lambda)}\lambda^{-\gamma\lambda} \int_0^{\Phi} \mathrm{d}y\, (\Phi-y)^{\gamma\lambda-1} y^{\gamma(1-\lambda)-1}.$$

Mathematica can perform this integral, and the result is

$$\begin{aligned} P_\Phi(\Phi) &= \frac{\exp(-\Phi/\langle A\rangle)}{\langle A\rangle^\gamma \Gamma[\gamma\lambda]\Gamma[\gamma(1-\lambda)]} \int_0^{\Phi} \mathrm{d}y\, (\Phi-y)^{\gamma\lambda-1} y^{\gamma(1-\lambda)-1} \\ &= \frac{\exp(-\Phi/\langle A\rangle)}{\langle A\rangle^\gamma \Gamma[\gamma\lambda]\Gamma[\gamma(1-\lambda)]} \frac{\Phi^{\gamma-1}\Gamma[\gamma\lambda]\Gamma[\gamma(1-\lambda)]}{\Gamma[\gamma]} \\ &= \frac{\Phi^{\gamma-1}}{\langle A\rangle^\gamma \Gamma[\gamma]} \exp\left[-\frac{\Phi}{\langle A\rangle}\right]. \end{aligned} \tag{2.113}$$

which is equal to the expression for $P_\Phi(\Phi)$ in Eq. (2.60).

$P_{\Phi\Theta}(\Phi\Theta)$ to $P_\Theta(\Theta)$ Leaving the Heaviside functions alone for now and directly substituting $x(\Phi) = \Phi + (1-\lambda)\Theta$ gives

$$\begin{aligned} P_\Theta(\Theta) &= \int_{-\infty}^{\infty} \mathrm{d}\Phi\, P_{\Phi\Theta}(\Phi\Theta) \\ &= \frac{\lambda^{\gamma\lambda}(1-\lambda)^{\gamma(1-\lambda)}}{\langle A\rangle^\gamma \Gamma[\gamma\lambda]\Gamma[\gamma(1-\lambda)]} \\ &\cdot \int_{-\infty}^{\infty} \mathrm{d}\Phi\, \exp(-\Phi/\langle A\rangle)[\Phi+(1-\lambda)\Theta]^{\gamma\lambda-1}(\Phi-\lambda\Theta)^{\gamma(1-\lambda)-1} H(\Phi+(1-\lambda)\Theta) H(\Phi-\lambda\Theta) \\ &= \frac{\lambda^{\gamma\lambda}(1-\lambda)^{\gamma(1-\lambda)}}{\langle A\rangle^\gamma \Gamma[\gamma\lambda]\Gamma[\gamma(1-\lambda)]} \int_0^{\infty} \mathrm{d}x\, \exp\left(-\frac{x-(1-\lambda)\Theta}{\langle A\rangle}\right) x^{\gamma\lambda-1}(x-\Theta)^{\gamma(1-\lambda)-1} H(x-\Theta). \end{aligned}$$

Now, substituting $y(x) = x - \Theta$ gives

$$\begin{aligned} &\frac{\lambda^{\gamma\lambda}(1-\lambda)^{\gamma(1-\lambda)}}{\langle A\rangle^\gamma \Gamma[\gamma\lambda]\Gamma[\gamma(1-\lambda)]} \int_0^{\infty} \mathrm{d}x\, \exp\left(-\frac{x-(1-\lambda)\Theta}{\langle A\rangle}\right) x^{\gamma\lambda-1}(x-\Theta)^{\gamma(1-\lambda)-1} H(x-\Theta) \\ &= \frac{\lambda^{\gamma\lambda}(1-\lambda)^{\gamma(1-\lambda)}}{\langle A\rangle^\gamma \Gamma[\gamma\lambda]\Gamma[\gamma(1-\lambda)]} \int_{\max(0,-\Theta)}^{\infty} \mathrm{d}y\, \exp\left(-\frac{y+\lambda\Theta}{\langle A\rangle}\right)(y+\Theta)^{\gamma\lambda-1} y^{\gamma(1-\lambda)-1}, \end{aligned} \tag{2.114}$$

which is the same as the expression in Eq. (2.100) with $\Theta' = y$.

2.3.5 Discussion

In Figure 2.10, $P_{\Phi\Theta}(\Phi,\Theta)$ and $P_\Phi(\Phi)P_\Theta(\Theta)$ are plotted as functions of $\widehat{\Phi}$ and $\widehat{\Theta}$, with $\widehat{\Phi} = (\Phi - \langle\Phi\rangle)/\Phi$ and $\widehat{\Theta} = (\Theta - \langle\Theta\rangle)/\Theta_{\text{rms}}$. The two uppermost plots have linear scaling while the two plots below have logarithmic scaling of the joint PDF. In Figure 2.9, the joint PDF is presented for $\gamma = 5$ and various values of λ. The white spaces in all figures are the values outside the domain where the Heaviside functions in Eq. (2.111) are positively valued.

With $\gamma = 100$ in Figure 2.10a, the joint PDF and the product of the two marginal PDFs are quite close to each other, resembling a normal distribution. The left side of the joint PDF is still triangular, although it is far removed from the domain where the Heaviside functions matter. This domain is seen in Figure 2.10a, where differences between the joint PDF and the product of the marginal PDFs are evident. In Figure 2.10c and Figure 2.10d, neither function is unimodal, both have a singularity at $(\widehat{\Theta} = 0, \widehat{\Phi} = -\langle\Phi\rangle)$. In these two Figures, the joint PDF and the product of the two marginal PDFs no longer resemble each other, signifying the importance of the dependency between Φ and Θ for small values of γ.

In Figure 2.9, the effect of changing λ is seen. For $\lambda = 0.5$, the joint PDF is symmetric around $\Theta = 0$, as expected, since the PDF of Θ is symmetric for $\lambda = 0$. As λ decreases, the distribution does not change shape as in Figure 2.10. Instead, the haviside functions seems to truncate the joint PDF.

We have discussed the cutoff in the joint PDF in terms of the Heaviside functions in Eq. (2.111), which limits the non-zero values of the join PDF to the range $-\Phi/(1-\lambda) < \Theta < \Phi/\lambda$. The interpretation is the following: consider a point in time t' in the shot noise process where every contributing pulse is growing (that is, t' is before the arrival time of all contributing pulses). At this point, the derivative is a scaling of the shot noise process, specifically $\Theta(t') = \tau_{\text{d}}\Phi(t')/\tau_{\text{r}} = \Phi(t')/\lambda$. This is the highest possible value for Θ as a function of Φ, since any contributing falling pulses reduces the value of the derivative. On the other hand, at a point t'' where only decaying pulses contribute, the value of the derivative becomes $\Theta(t'') = -\tau_{\text{d}}\Phi(t'')\tau_{\text{f}} = -\Phi(t'')/(1-\lambda)$. In he same way as above, any growing pulses contributing increases the value of Θ as a function of Φ. Thus the range $-\Phi/(1-\lambda) < \Theta < \Phi/\lambda$ is the range of all posible values of Θ as a function of Φ.

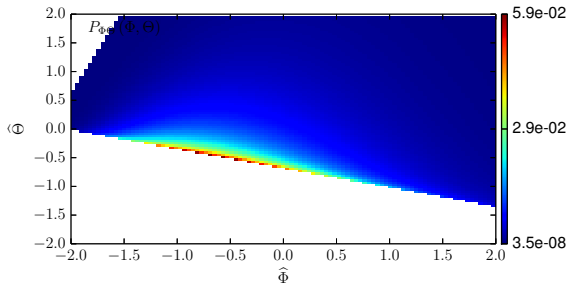

(a) $\lambda = 0.1$

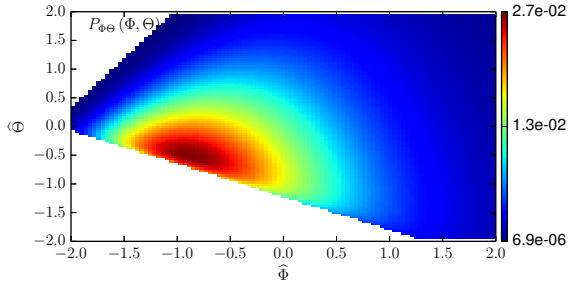

(b) $\lambda = 0.25$

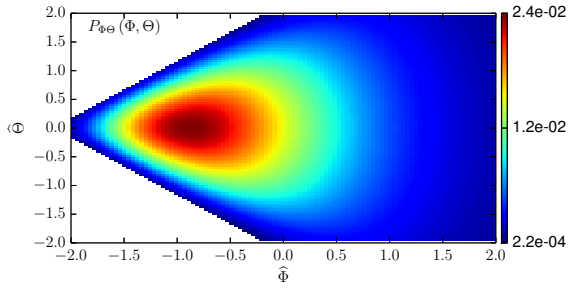

(c) $\lambda = 0.5$

Figure 2.9: Joint PDF between Φ and Θ for $\gamma = 5$ with changing λ.

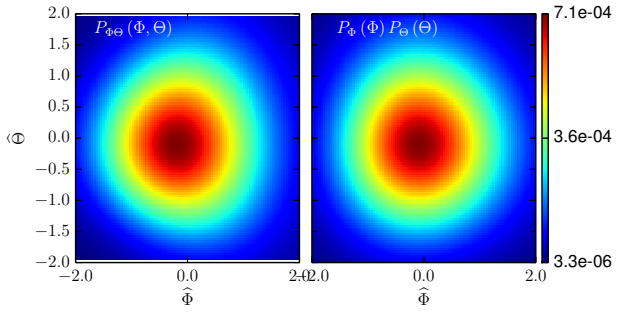

(a) $\gamma = 100$

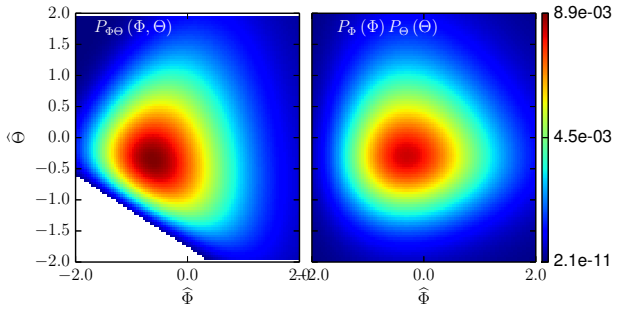

(b) $\gamma = 10$

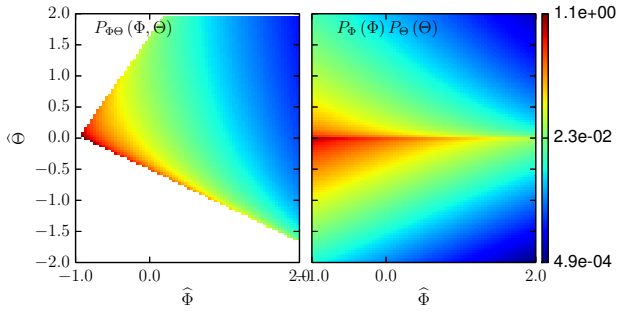

(c) $\gamma = 1$, logarithmic scale.

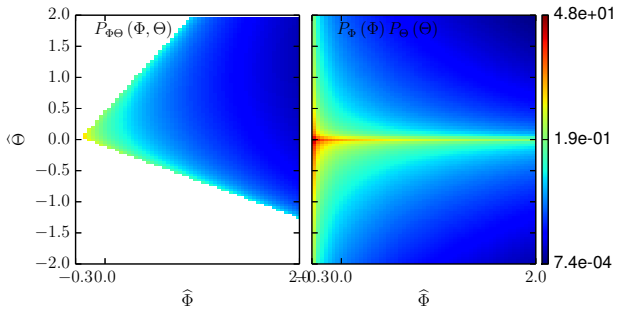

(d) $\gamma = 0.1$, logarithmic scale.

Figure 2.10: Joint pdf (left) and product of the marginal pdfs (right) between Φ and Θ for $\lambda = 0.25$ and various γ.

3

Excess time statistics

It is often of interest to know how long a process $\Phi(t)$ spends above a certain threshold value C, how often it passes this value and how long, on average, the signal spends above the threshold value for each up crossing. This endeavour is frequently referred to as *excess time statistics*, and has been considered by e.g Rice [1944], Israel and Nemirovsky [1972], Fattorini et al. [2012], Sato et al. [2012], Kristensen et al. [1991] and Biermé and Desolneux [2012].

The time the n'th burst *above the threshold* spends above the threshold value C is denoted $\mathcal{T}_n(C)$. We do not consider the bursts below the threshold. The total number of upcrossings above the threshold is $\mathscr{N}(C)$ such that the total time the signal spends above the threshold value is $\mathscr{T}(C) = \sum_{n=1}^{\mathscr{N}(C)} \mathcal{T}_n(C)$. The average time the signal spends above the threshold for each upcrossing is approximated by

$$\langle \mathcal{T} \rangle(C) \approx \frac{\sum_{n=1}^{\mathscr{N}(C)} \mathcal{T}_n(C)}{\mathscr{N}(C)} = \frac{\mathscr{T}(C)}{\mathscr{N}(C)}. \tag{3.1}$$

Note that normalli, the number of upcrossings over C is considered instead of the total number of crossings, since for a stationary process, the number of upcrossings is the same as the number of downcrossings. An example of excess times is presented in Figure 3.1. In this figure, the blue line gives the signal amplitude $\Phi(t)$, the green dotted line gives the threshold C and the red lines give the time duration above the threshold for each burst, $\mathcal{T}_n$. We have excess times $\mathcal{T}_n$ with $n = 1 \ldots 6$, so $\mathscr{N} = 6$, $\mathscr{T} = \sum_{n=1}^{6} \mathcal{T}_n$ and $\langle \mathcal{T} \rangle = \mathscr{T}/\mathscr{N} = \sum_{n=1}^{6} \mathcal{T}_n/6$.

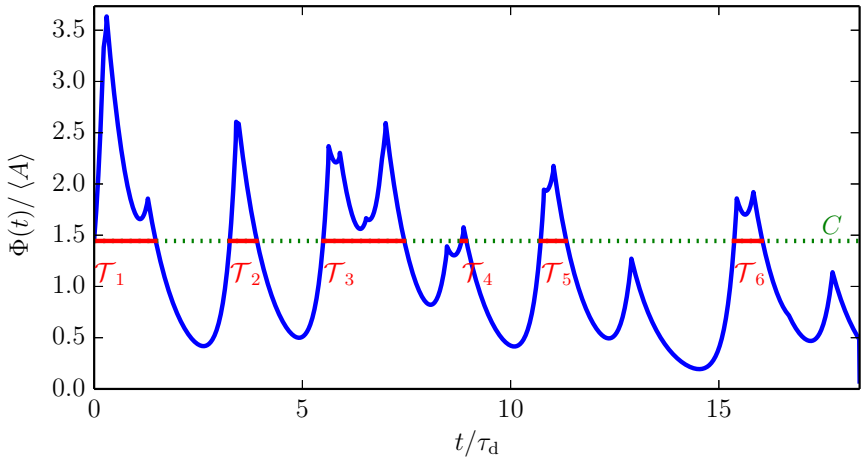

Figure 3.1: Example of excess times over the threshold $\zeta = \widehat{\Phi}/2$ for a synthetic signal with $\gamma = 1$ and $\lambda = 0.25$.

3.1 Definition of total time above threshold, number of upcrossings and average time above threshold

We have a shot noise process $\Phi(t)$ with time duration T, the time derivative $\dot{\Phi}(t) = \mathrm{d}\Phi(t)/\mathrm{d}t$ and well defined PDFs $P_\Phi(\Phi)$ and $P_{\Phi\dot{\Phi}}(\Phi,\dot{\Phi})$. We assume that both the signal and its derivative are stationary, so the joint PDF and $\langle\Phi\rangle$ are independent of time and accordingly $\langle\dot{\Phi}\rangle = 0$. The complementary CDF of Φ, $\mathrm{CDF}_\Phi(C)$ gives the probability that the signal value is above C. Multiplied by the total duration of the signal, T, this gives the total time the signal spends above C:

$$\mathscr{T}(C) = T\int_C^\infty \mathrm{d}\Phi\, P_\Phi(\Phi) = T[1 - \mathrm{CDF}_\Phi(C)]. \tag{3.2}$$

The probability that the signal amplitude is somewhere in the interval $[\Phi, \Phi + \mathrm{d}\Phi]$ and at the same time the value of $\dot{\Phi}$ is somewhere in $[\dot{\Phi}, \dot{\Phi}+\mathrm{d}\dot{\Phi}]$ is $\mathrm{d}\Phi\,\mathrm{d}\dot{\Phi}\,P_{\Phi\dot{\Phi}}(\Phi,\dot{\Phi})$. Since the time the signal takes to cross $\mathrm{d}\Phi$ is $\mathrm{d}t = \mathrm{d}\Phi/\dot{\Phi}$, and we don't care how fast the signal crosses the threshold, only that $\dot{\Phi} > 0$, we then have that the total number of upwards crossings is

$$\mathscr{N}(C) = \int_0^T \mathrm{d}t \int_0^\infty \mathrm{d}\dot{\Phi}\,\dot{\Phi} P_{\Phi\dot{\Phi}}(C,\dot{\Phi}) = T\int_0^\infty \mathrm{d}\dot{\Phi}\,\dot{\Phi} P_{\Phi\dot{\Phi}}(C,\dot{\Phi}), \tag{3.3}$$

since the joint PDF is independent of time. In the following, we will use the nor-

malized derivative $\Theta = \tau_d \dot{\Phi}$, so we substitute and use $P_{\Phi\dot{\Phi}}(\Phi, \dot{\Phi}) = (1/\tau_d) P_{\Phi\Theta}(\Phi, \Theta)$ to get the integral:

$$\mathcal{N}(C) = \frac{T}{\tau_d} \int_0^\infty \mathrm{d}\Theta \, \Theta P_{\Phi\Theta}(C, \Theta). \tag{3.4}$$

This is the celebrated Rice's formula [Rice, 1945, Leadbetter and Spaniolo, 2004] for level crossings. It is also found formulated in the normal limit (Eq. (3.26)).

Then, from Eq. (3.1) we have an estimate for the average time spent above C:

$$\int_0^\infty \mathrm{d}\mathcal{T} \, \mathcal{T} P_{\mathcal{T}}(\mathcal{T}|C) = \langle \mathcal{T} \rangle(C) \approx \frac{\mathscr{T}}{\mathscr{N}} = \frac{\int_C^\infty \mathrm{d}\Phi \, P_\Phi(\Phi)}{\int_0^\infty \mathrm{d}\Theta \, \Theta P_{\Phi\,\Theta}(C, \Theta)}, \tag{3.5}$$

where $P_{\mathcal{T}}(\mathcal{T}|C)$ is the PDF of time intervals above C.

In general, since we only consider signals with positive pulse waveforms and pulse amplitudes, we have $\Phi(t) > 0$, giving a sharp cutoff at $C = 0$. Intuitively we expect $\mathscr{T}(0) = T$ and $\mathscr{N}(0) = 0$, giving $\langle \mathcal{T} \rangle(0) = \infty$, since at $C = 0$, the entire signal is above the threshold, and there are no upwards crossings over the threshold. As C increases, we expect both $\mathscr{T}(C)$ and $\mathscr{N}(C)$ to converge towards 0, since fewer and fewer bursts pass above the threshold. $\lim_{C \to \infty} \langle \mathcal{T} \rangle(C)$ is not as clear, as it depends on how fast $\mathscr{T}$ and $\mathscr{N}$ go towards 0. This implies that $\mathscr{T}(C)$ is a monotonically decreasing function (which it is, since it is a complementary CDF) and that $\mathscr{N}(C)$ has a maxima at some finite value of C.

3.1.1 The models

The expressions above for total time above threshold ,Eq. (3.2), total number of upwards threshold crossings, Eq. (3.4), and average time above threshold, Eq. (3.5), will be investigated for a general model with two asymptotic limits, $\gamma \to 0$ and $\gamma \to \infty$.

First, under the assumptions that the pulse waiting times and pulse amplitudes are exponentially distributed and that we have the double exponential pulse waveforms, we are able to calculate the expressions above from the joint PDF in Section 2.3. This will be referred to as the 'general model'.

Then, we will use the non-intermittent limit $\gamma \to \infty$ where $\Phi(t)$ and $\Theta(t)$ are assumed to have a joint normal distribution. This model is common in the literature, and we will follow Fattorini et al. [2012] in this discussion.

Lastly, we investigate the strong intermittency limit for $\gamma \to 0$ which uses the same assumptions as the general model. In addition, we assume that there is no pulse overlap, so each pulse is one burst in the resulting signal.

Note that since $\Phi(t)$ and $\Theta(t)$ are both shot noise processes, they are both normally distributed in the non-intermittent limit. However, we must still assume that they are independent in order for them to have a joint normal distribution in the non-intermittent limit (see Section 2.3.3). A remaining question, which is not explored in this thesis, is what the lowest order deviation from $P_{\Phi\Theta}(\Phi,\Theta) = P_\Phi(\Phi)P_\Theta(\Theta)$ is in the non-intermittent limit.

3.1.2 The normalized threshold

The threshold values are values in the main signal. When we are comparing multiple signals, these threshold values will vary much, making comparisons difficult. Therefore, we introduce the normalized threshold ζ over the normalized threshold $\widehat{\Phi} = (\Phi - \langle\Phi\rangle)/\Phi_{\text{rms}}$. The normalized threshold gives the lowest value we register in the normalized signal:

$$\begin{aligned} \widehat{\Phi} &> \zeta \\ \frac{\Phi - \langle\Phi\rangle}{\Phi_{\text{rms}}} &> \zeta \\ \Phi &> \zeta\Phi_{\text{rms}} + \langle\Phi\rangle. \end{aligned}$$

Thus the normalized threshold is related to the threshold by

$$C = \zeta\Phi_{\text{rms}} + \langle\Phi\rangle. \tag{3.6}$$

In general, we only consider signals with positive values $\Phi(t) > 0$, so the threshold C has a sharp cutoff at $C = 0$. This corresponds to a cutoff for the normalized threshold at $\zeta = -\langle\Phi\rangle/\Phi_{\text{rms}} = -\sqrt{\gamma}$.

The limit $\zeta \gg 1$

We will wish to investigate the case of very large threshold, and to see if the models have some common behaviour. To ensure we take the same limit in all cases, we will use ζ for all, and let $\zeta \to \infty$.

3.1.3 Another way to the number of upwards crossings

The previous discussion presupposes that $P_{\Phi\Theta}(\Phi,\Theta)$ exists, which is not the case for arbitrary pulse amplitude and waiting time distributions and pulse waveform [an example is the pulse waveform $\varphi(t) = \exp(-t/\tau_d)H_1(t)$, for which $P_\Theta(\Theta)$ does not exist]. A different approach is suggested by Biermé and Desolneux [2012], where a shot noise process with Poisson distribution of pulse events is considered. There, the Fourier transform of $\langle\mathcal{N}\rangle(C)$ is found to exist as long as:

- $\langle A\rangle < \infty$,
- $\varphi(t)$ and $\vartheta(t)$ are piecewise continuous functions with a finite amount of discontinuous points,
- $\int_{-\infty}^{\infty} \mathrm{d}t\,|f(t)| < \infty$ where $f(t) = \varphi(t)$, $\dot{\varphi}(t)$ and $\ddot{\varphi}(t)$ with the points of discontinuity removed.

This condition is fulfilled for both the double exponential pulse waveform and the one-sided exponential pulse waveforms.

In the case of one-sided exponential waveforms (where the points of discontinuity, and thus the delta functions in the derivative, have been removed), the average value of $\mathcal{N}(C)$ in a time interval of length τ_d is found. The total number of upwards crossings is this average value times T/τ_d, and we have

$$\frac{\tau_d}{T}\mathcal{N}(C) = \frac{\gamma}{\Gamma(\gamma+1)}\left(\frac{C}{\langle A\rangle}\right)^\gamma \exp\left(-\frac{C}{\langle A\rangle}\right). \tag{3.7}$$

Note that in Biermé and Desolneux [2012], the total number of threshold crossings is considered, so we divide their result by 2 in order to get the number of upcrossings of the threshold for a stationary process.

In the case of exponentially distributed pulse amplitudes and either the double exponential pulse waveform (which is continuous) or the one-sided exponential pulse waveform [which has one jump discontinuity from $\varphi(t<0) = 0$ to $\varphi(t=0) = 1$], the normal limit $\gamma \to \infty$ of the average value of $\mathcal{N}(\zeta)$ in a time interval of length τ_d has also been found in Biermé and Desolneux [2012]:

$$\frac{\tau_d}{T}\mathcal{N}(\zeta) = \begin{cases} \dfrac{1}{2\pi\sqrt{\lambda(1-\lambda)}}\exp\left(-\zeta^2/2\right) & 0<\lambda<1 \\ \sqrt{\dfrac{\gamma}{2\pi}}\exp\left(-\zeta^2/2\right) & \lambda = 0 \text{ or } \lambda = 1 \end{cases}, \tag{3.8}$$

although they did not consider the double-sided exponential waveform, which follows from Rice's formula.

Some comments are in order. First, we will later see that all these results can be obtained from the general model, and that the second part of Eq. (3.8) can be obtained from Eq. (3.7) by taking the limit $\gamma \to \infty$. Second, note that there is a qualitative difference between $\lambda = 0$ and $\lambda > 0$; the first case has a factor $\sqrt{\gamma}$ not found in the second. Thus, for large γ, a definite difference should be seen between these cases.

3.2 The general model

If we assume that we have the double-sided waveform, Poisson distribution of events and exponentially distributed pulse amplitudes, we have from previous sections that

$$P_\Phi(\Phi) = \frac{\gamma}{\langle\Phi\rangle\Gamma(\gamma)}\left(\frac{\gamma\Phi}{\langle\Phi\rangle}\right)^{\gamma-1}\exp\left(-\frac{\gamma\Phi}{\langle\Phi\rangle}\right)H_0(\Phi), \tag{3.9}$$

and

$$\begin{aligned} P_{\Phi\Theta}(\Phi,\Theta) = {} & \frac{\lambda^{\gamma\lambda}(1-\lambda)^{\gamma(1-\lambda)}\exp(-\Phi/\langle A\rangle)}{\langle A\rangle^\gamma\Gamma(\gamma\lambda)\Gamma(\gamma(1-\lambda))} \\ & \times[\Phi+(1-\lambda)\Theta]^{\gamma\lambda-1}(\Phi-\lambda\Theta)^{\gamma(1-\lambda)-1}H_{1/2}(\Phi+(1-\lambda)\Theta)H_{1/2}(\Phi-\lambda\Theta). \end{aligned}$$

For the threshold, we also note that $\langle\Phi\rangle = \gamma\langle A\rangle$ and that $\Phi_{\text{rms}} = \gamma^{1/2}\langle A\rangle$, meaning that we can write

$$\frac{C}{\langle\Phi\rangle} = \frac{C}{\gamma\langle A\rangle} = \frac{\zeta}{\gamma^{1/2}} + 1. \tag{3.10}$$

3.2.1 Total time above threshold

The total time the signal spends above the threshold is given by the CDF of Φ. For a Gamma distributed process, this is known:

$$\mathscr{T}(C) = T[1 - CDF_\Phi(C)] = T\left(1 - \frac{\Gamma_{\text{L}}(\gamma,\gamma C/\langle\Phi\rangle)}{\Gamma(\gamma)}\right) = T\frac{\Gamma_{\text{U}}(\gamma,\gamma C/\langle\Phi\rangle)}{\Gamma(\gamma)} = TQ\left(\gamma,\gamma\frac{C}{\langle\Phi\rangle}\right). \tag{3.11}$$

We can remove the explicit appearance of $\langle\Phi\rangle$ from this expression by using the normalized threshold from Eq. (3.10):

$$\mathscr{T}(\zeta) = TQ(\gamma,\sqrt{\gamma}\zeta + \gamma). \tag{3.12}$$

The regularized gamma function $Q(\gamma, C/\langle A\rangle)$ behaves as expected; for large ζ, this function approaches zero and $Q(\gamma, 0) = 1$, to give $\mathscr{T}(0) = T$. For $\zeta = 0$, we have $C = \langle\Phi\rangle$ and $\mathscr{T}$ approaches $1/2$ as γ increases, since a Gaussian process is above the mean value half the time.

3.2.2 The total number of upwards threshold crossings

The total number of upward crossings is given by integrating the joint PDF as given by Eq. (3.4):

$$\begin{aligned}\frac{\tau_\mathrm{d}}{T}\mathscr{N}(C) &= \int_0^\infty \mathrm{d}\Theta\,\Theta P_{\Phi\Theta}(C,\Theta)\\ &= \frac{\lambda^{\gamma\lambda}(1-\lambda)^{\gamma(1-\lambda)}\exp(-C/\langle A\rangle)}{\langle A\rangle^\gamma\Gamma(\gamma\lambda)\Gamma(\gamma(1-\lambda))}\\ &\times\int_0^\infty \mathrm{d}\Theta\,\Theta\frac{(C+(1-\lambda)\Theta)^{\gamma\lambda-1}}{(C-\lambda\Theta)^{1-\gamma(1-\lambda)}}H_{1/2}(C+(1-\lambda)\Theta)H_{1/2}(C-\lambda\Theta)\\ &= \frac{\lambda^{\gamma\lambda}(1-\lambda)^{\gamma(1-\lambda)}\exp(-C/\langle A\rangle)}{\langle A\rangle^\gamma\Gamma(\gamma\lambda)\Gamma(\gamma(1-\lambda))}\frac{C^\gamma}{\gamma\lambda(1-\lambda)}\\ &= \frac{\lambda^{\gamma\lambda-1}(1-\lambda)^{\gamma(1-\lambda)-1}}{\gamma\Gamma(\gamma\lambda)\Gamma(\gamma(1-\lambda))}\left(\frac{C}{\langle A\rangle}\right)^\gamma\exp\left(-\frac{C}{\langle A\rangle}\right).\end{aligned} \tag{3.13}$$

The integral is done by Mathematica.

Using the normalized threshold If we substitute the normalized threshold into $\mathscr{N}(C)$, we get

$$\mathscr{N}(\zeta) = \frac{T}{\tau_\mathrm{d}}\frac{\lambda^{\gamma\lambda-1}(1-\lambda)^{\gamma(1-\lambda)-1}}{\gamma\Gamma(\gamma\lambda)\Gamma(\gamma(1-\lambda))}\big(\sqrt{\gamma}\zeta+\gamma\big)^\gamma\exp\big(-\sqrt{\gamma}\zeta+\gamma\big). \tag{3.14}$$

Again, the result fits the intuition as we see that $\mathscr{N}(0) = 0$ and $\mathscr{N}(\zeta)$ approaches zero as C increases.

3.2.3 The average time above the threshold

The average time above the threshold C is estimated by the total time divided by the number of upwards crossings:

$$\langle\mathcal{T}\rangle(C) = \frac{\mathscr{T}}{\mathscr{N}}(C) = \tau_\mathrm{d}\frac{\gamma\Gamma(\gamma\lambda)\Gamma(\gamma(1-\lambda))}{\lambda^{\gamma\lambda-1}(1-\lambda)^{\gamma(1-\lambda)-1}}Q\left(\gamma,\frac{\gamma C}{\langle\Phi\rangle}\right)\left(\frac{\gamma C}{\langle\Phi\rangle}\right)^{-\gamma}\exp\left(\frac{\gamma C}{\langle\Phi\rangle}\right). \tag{3.15}$$

For $C = 0$, this equation is simple; $\langle \mathcal{T} \rangle(0) = 0$. The limit of $\zeta \to \infty$ is more complicated, and is covered in Section 3.2.6. The result is that in this limit, $\langle \mathcal{T} \rangle(\zeta) = 0$.

3.2.4 The limit of large γ

In the limit of large γ, the regularized gamma function in $\mathcal{T}(C)$ has no simpler form but still has values between 0 and 1, so it will not be investigated further. $\mathcal{N}(C)$ and $\langle \mathcal{T} \rangle(C)$, on the other hand, can be simplified. First, we use Stirling's approximation for the gamma functions in these expressions:

$$\begin{aligned}\lim_{\gamma\to\infty} \Gamma(\gamma\lambda)\Gamma(\gamma(1-\lambda)) &= \frac{1}{\gamma\lambda}\sqrt{2\pi\gamma\lambda}(\gamma\lambda)^{\gamma\lambda}\exp(-\gamma\lambda) \\ &\quad\times \frac{1}{\gamma(1-\lambda)}\sqrt{2\pi\gamma(1-\lambda)}(\gamma(1-\lambda))^{\gamma(1-\lambda)}\exp(-\gamma(1-\lambda)) \\ &= 2\pi\gamma^{\gamma-1}\lambda^{\gamma\lambda-1/2}(1-\lambda)^{\gamma(1-\lambda)-1/2}\exp(-\gamma)\end{aligned}$$

This result inserted into Eq. (3.13) and Eq. (3.15), and expressed by the normalized threshold ζ, gives:

$$\lim_{\gamma\to\infty} \mathcal{N}(\zeta) = \frac{T}{\tau_\mathrm{d}} \frac{1}{2\pi\sqrt{\lambda(1-\lambda)}} \left(\frac{\zeta}{\gamma^{1/2}} + 1\right)^{\gamma} \exp\left(-\gamma^{1/2}\zeta\right) \tag{3.16}$$

and

$$\lim_{\gamma\to\infty} \langle \mathcal{T} \rangle(\zeta) = 2\pi\tau_\mathrm{d}\sqrt{\lambda(1-\lambda)}\, Q\left(\gamma, \frac{\gamma C}{\langle \Phi \rangle}\right)\left(\frac{\zeta}{\gamma^{1/2}} + 1\right)^{-\gamma} \exp\left(\gamma^{1/2}\zeta\right). \tag{3.17}$$

With the result in Section A.4, we have that $\lim_{\gamma\to\infty}\left(\zeta/\gamma^{1/2}+1\right)^{\gamma}\exp\left(-\gamma^{1/2}\zeta\right) = \exp\left(-\zeta^2/2\right)$, and we see that Eq. (3.16) is equivalent to the first expression in Eq. (3.8).

3.2.5 The limit of the one-sided waveform

Surprisingly, although it is not possible to take the limits $\lambda \to 0$ or $\lambda \to 1$ in any previous results, such as for $P_\Theta(\Theta)$ or $P_{\Phi\Theta}(\Phi, \Theta)$, it is possible to take these limits for $\mathcal{N}(C)$ and $\langle \mathcal{T} \rangle(C)$. This is because

$$\begin{aligned}\lim_{\lambda\to 0} \frac{\gamma\Gamma(\gamma\lambda)\Gamma(\gamma(1-\lambda))}{\lambda^{\gamma\lambda-1}(1-\lambda)^{\gamma(1-\lambda)-1}} &= \lim_{\lambda\to 0} \frac{\gamma(\gamma\lambda)^{-1}\Gamma(\gamma)}{\lambda^{\gamma\lambda-1}} \\ &= \lim_{\lambda\to 0} \lambda^{-\gamma\lambda}\Gamma(\gamma) \\ &= \Gamma(\gamma),\end{aligned}$$

and the result of taking $\lambda \to 1$ is the same. This gives

$$\mathcal{N}(C) = \frac{T}{\tau_\mathrm{d}\Gamma(\gamma)}\left(\frac{C}{\langle A\rangle}\right)^\gamma \exp\left(-\frac{C}{\langle A\rangle}\right), \tag{3.18}$$

$$\langle \mathcal{T}\rangle(C) = \tau_\mathrm{d}\Gamma(\gamma)Q\left(\gamma, \frac{C}{\langle A\rangle}\right)\left(\frac{C}{\langle A\rangle}\right)^{-\gamma} \exp\left(\frac{C}{\langle A\rangle}\right). \tag{3.19}$$

Note that Eq. (3.18) is equivalent to Eq. (3.7). For these equations, we can also take the limit $\gamma \to \infty$, as above. The result is

$$\mathcal{N}(C) = \frac{T}{\tau_\mathrm{d}}\sqrt{\frac{\gamma}{2\pi}}\left(\frac{C}{\gamma\langle A\rangle}\right)^\gamma \exp\left(\gamma - \frac{C}{\langle A\rangle}\right), \tag{3.20}$$

$$\langle \mathcal{T}\rangle(C) = \tau_\mathrm{d}\sqrt{\frac{2\pi}{\gamma}}Q\left(\gamma, \frac{C}{\langle A\rangle}\right)\left(\frac{C}{\gamma\langle A\rangle}\right)^{-\gamma} \exp\left(\frac{C}{\langle A\rangle} - \gamma\right). \tag{3.21}$$

It is not possible to get to this equation from the equations in Section 3.2.4, but comparing equations tells us that for $\gamma \to \infty$, there is a qualitative difference between a continuous pulse waveform ($0 < \lambda < 1$) and a discontinuous pulse waveform ($\lambda = 0$ or $\lambda = 1$), which is in agreement with the careful analysis by Biermé and Desolneux [2012]. The main part of this difference is the $\gamma^{1/2}$-behaviour in Eq. (3.20). Comparing Eq. (3.20) to the second part of Eq. (3.8), and using the result from Section A.4, we find that

$$\begin{aligned}\lim_{\gamma\to\infty}&\left(\frac{C}{\gamma\langle A\rangle}\right)^\gamma \exp\left(\gamma - \frac{C}{\langle A\rangle}\right)\\ &= \lim_{\gamma\to\infty}\left(\frac{\zeta}{\gamma^{1/2}} + 1\right)^\gamma \exp\left(-\gamma^{1/2}\zeta\right)\\ &= \exp\left(-\frac{\zeta^2}{2}\right).\end{aligned}$$

and the equations are equivalent.

3.2.6 The limit of $\zeta \gg 1$

For large threshold values, we have from the appendix (Section A.2) that $\lim_{x\to\infty} \Gamma_U(s,x) = x^{s-1}\exp(-x)$, giving $\langle \mathcal{T} \rangle(C)$ in the limit of large ζ:

$$\begin{aligned}
\lim_{\zeta\to\infty} \langle \mathcal{T} \rangle(C) &= \lim_{\zeta\to\infty} \frac{\gamma\Gamma(\gamma\lambda)\Gamma(\gamma(1-\lambda))}{\lambda^{\gamma\lambda-1}(1-\lambda)^{\gamma(1-\lambda)-1}} \frac{\Gamma_U\big(\gamma, \sqrt{\gamma}\zeta+\gamma\big)}{\Gamma(\gamma)} \big(\sqrt{\gamma}\zeta+\gamma\big)^{-\gamma} \exp\big(\sqrt{\gamma}\zeta+\gamma\big) \\
&= \lim_{\zeta\to\infty} \frac{\gamma\Gamma(\gamma\lambda)\Gamma(\gamma(1-\lambda))}{\lambda^{\gamma\lambda-1}(1-\lambda)^{\gamma(1-\lambda)-1}} \\
&\quad \times \frac{\big(\sqrt{\gamma}\zeta+\gamma\big)^{\gamma-1}\exp\big(-\sqrt{\gamma}\zeta-\gamma\big)}{\Gamma(\gamma)} \big(\sqrt{\gamma}\zeta+\gamma\big)^{-\gamma} \exp\big(\sqrt{\gamma}\zeta+\gamma\big) \\
&= \lim_{\zeta\to\infty} \frac{\sqrt{\gamma}\Gamma[\gamma\lambda]\Gamma[\gamma(1-\lambda)]}{\lambda^{\gamma\lambda-1}(1-\lambda)^{\gamma(1-\lambda)-1}\Gamma(\gamma)} \big(\zeta+\sqrt{\gamma}\big)^{-1} \\
&\propto \frac{1}{\zeta+\sqrt{\gamma}}. \qquad (3.22)
\end{aligned}$$

This result will be discussed together with the results from the normal and the strongly intermittent model in Section 3.5.1.

3.3 The normal limit $\gamma \gg 1$

Following the argumentation by Fattorini et al. [2012] and Kristensen et al. [1991], we can analytically obtain a simple expression for $\langle \mathcal{T} \rangle$ in the non-intermittent Gaussian limit. We assume that $P_\Phi(\Phi)$ and $P_\Theta(\Theta)$ are normally distributed, with means $\langle\Phi\rangle$ and $\langle\Theta\rangle = 0$ and standard deviations Φ_{rms} and Θ_{rms}:

$$\lim_{\gamma\to\infty} P_\Phi(\Phi) = \frac{1}{\sqrt{2\pi}\Phi_{\text{rms}}} \exp\left[-\frac{(\Phi-\langle\Phi\rangle)^2}{2\Phi_{\text{rms}}^2}\right], \qquad (3.23)$$

$$\lim_{\gamma\to\infty} P_\Theta(\Theta) = \frac{1}{\sqrt{2\pi}\Theta_{\text{rms}}} \exp\left(-\frac{\Theta^2}{2\Theta_{\text{rms}}^2}\right). \qquad (3.24)$$

We also assume that Φ and Θ are statistically independent (see Section 2.3.3), so $P_{\Phi\Theta}(\Phi,\Theta) = P_\Phi(\Phi)P_\Theta(\Theta)$.

3.3.1 The total time above threshold

We find that Eq. (3.2) simplifies to:

$$\begin{aligned}\lim_{\gamma\to\infty}\frac{1}{T}\mathscr{T}(C) &= 1 - CDF_\Phi(C) = 1 - \frac{1}{2}\left[1 + \operatorname{erf}\left(\frac{C-\langle\Phi\rangle}{\sqrt{2}\Phi_{\text{rms}}}\right)\right] \\ &= \frac{1}{2}\left[1 - \operatorname{erf}\left(\frac{C-\langle\Phi\rangle}{\sqrt{2}\Phi_{\text{rms}}}\right)\right] \\ &= \frac{1}{2}\operatorname{erfc}\left(\frac{C-\langle\Phi\rangle}{\sqrt{2}\Phi_{\text{rms}}}\right) \\ &= \frac{1}{2}\operatorname{erfc}\left(\frac{\zeta}{\sqrt{2}}\right)\end{aligned} \tag{3.25}$$

where we in the last equation have used the normalized threshold. Note that for this $\mathscr{T}(\zeta)$, there is no minimal accepted ζ-value; $\mathscr{T}(\zeta)$ approaches T for $\zeta \to -\infty$ and it approaches 0 for $\zeta \to \infty$. At the mean value, we have as expected $\mathscr{T}(\zeta = 0) = T/2$.

3.3.2 The total number of upwards crossings

Using the assumptions in this section, Eq. (3.3) becomes:

$$\begin{aligned}\lim_{\gamma\to\infty}\frac{\tau_{\text{d}}}{T}\mathscr{N}(C) &= \int_0^\infty \mathrm{d}\Theta\,\Theta P_{\Phi\Theta}(C,\Theta) = P_\Phi(C)\int_0^\infty \mathrm{d}\Theta\,\Theta P_\Theta(\Theta) \\ &= \frac{1}{\sqrt{2\pi}\Phi_{\text{rms}}}\exp\left[-\frac{(C-\langle\Phi\rangle)^2}{2{\Phi_{\text{rms}}}^2}\right]\int_0^\infty \mathrm{d}\Theta\,\frac{1}{\sqrt{2\pi}\Theta_{\text{rms}}}\Theta\exp\left[-\left(\frac{\Theta}{\sqrt{2}\Theta_{\text{rms}}}\right)^2\right].\end{aligned}$$

Substituting $u = \Theta^2/\left(2{\Theta_{\text{rms}}}^2\right)$ and integrating, we get that:

$$\begin{aligned}\lim_{\gamma\to\infty}\frac{\tau_{\text{d}}}{T}\mathscr{N}(C) &= \frac{1}{\sqrt{2\pi}\Phi_{\text{rms}}}\exp\left[-\frac{(C-\langle\Phi\rangle)^2}{2{\Phi_{\text{rms}}}^2}\right]\frac{\Theta_{\text{rms}}}{\sqrt{2\pi}} \\ &= \frac{\Theta_{\text{rms}}}{2\pi\Phi_{\text{rms}}}\exp\left[-\frac{(C-\langle\Phi\rangle)^2}{2{\Phi_{\text{rms}}}^2}\right] \\ &= \frac{\Theta_{\text{rms}}}{2\pi\Phi_{\text{rms}}}\exp\left[-\frac{\zeta^2}{2}\right].\end{aligned} \tag{3.26}$$

This equation has a maximal value at $C = \langle\Phi\rangle$ (or $\zeta = 0$), $\mathscr{N}(\zeta = 0) = T\Theta_{\text{rms}}/(2\pi\tau_{\text{d}}\Phi_{\text{rms}})$, and it goes towards 0 for $\zeta \to \pm\infty$.

3.3.3 The average time above threshold

The Gaussian limit of $\langle \mathcal{T} \rangle$ becomes:

$$\begin{aligned}\lim_{\gamma \to \infty} \langle \mathcal{T} \rangle(C) &= \frac{\mathscr{T}(C)}{\mathscr{N}(C)} \\ &= \pi \tau_{\mathrm{d}} \frac{\Phi_{\mathrm{rms}}}{\Theta_{\mathrm{rms}}} \operatorname{erfc}\left(\frac{C - \langle \Phi \rangle}{\sqrt{2} \Phi_{\mathrm{rms}}} \right) \exp\left(\frac{(C - \langle \Phi \rangle)^2}{2 {\Phi_{\mathrm{rms}}}^2} \right) \\ &= \pi \tau_{\mathrm{d}} \frac{\Phi_{\mathrm{rms}}}{\Theta_{\mathrm{rms}}} \operatorname{erfc}\left(\frac{\zeta}{\sqrt{2}} \right) \exp\left(\frac{\zeta^2}{2} \right).\end{aligned} \tag{3.27}$$

For $\zeta \to -\infty$, $\operatorname{erfc}\left(\zeta / \sqrt{2}\right) \to 2$ and $\exp\left(\zeta^2/2\right) \to \infty$, so $\langle \mathcal{T} \rangle(\zeta \to -\infty) \to \infty$, as expected. The other limit, $\zeta \to \infty$ is more complicated and is covered below. Also note that $\langle \mathcal{T} \rangle(\zeta = 0) = \pi \tau_{\mathrm{d}} \Phi_{\mathrm{rms}} / \Theta_{\mathrm{rms}}$.

The average time above threshold for $\zeta \gg 1$

For large threshold values ζ, we can make the approximation (see appendix, Section A.3)

$$\lim_{x \to \infty} \operatorname{erfc}(x) = \frac{\exp\left(-x^2\right)}{\sqrt{\pi} x} \sum_{n=0}^{\infty} (-1)^n \frac{(2n-1)!!}{\left(2x^2\right)^n} = \frac{\exp\left(-x^2\right)}{\sqrt{\pi} x} + \mathcal{O}\left(x^{-2}\right)$$

thus, we write $\langle \mathcal{T} \rangle(C)$ in the non-intermittent limit as

$$\begin{aligned}\lim_{\zeta \to \infty} \zeta \langle \mathcal{T} \rangle(C) &= \lim_{\zeta \to \infty} \pi \tau_{\mathrm{d}} \frac{\Phi_{\mathrm{rms}}}{\Theta_{\mathrm{rms}}} \zeta \operatorname{erfc}\left(\frac{\zeta}{\sqrt{2}} \right) \exp\left(\frac{\zeta^2}{2} \right) \\ &= \pi \tau_{\mathrm{d}} \frac{\Phi_{\mathrm{rms}}}{\Theta_{\mathrm{rms}}} \frac{\sqrt{2}}{\sqrt{\pi}} \\ &= \sqrt{2\pi} \tau_{\mathrm{d}} \frac{\Phi_{\mathrm{rms}}}{\Theta_{\mathrm{rms}}} \\ &= \sqrt{2\pi \lambda (1 - \lambda)} \tau_{\mathrm{d}}\end{aligned} \tag{3.28}$$

where we in the last expression have used $\Phi_{\mathrm{rms}} = \sqrt{\gamma} \langle A \rangle$ and $\Theta_{\mathrm{rms}} = \sqrt{\gamma / [\lambda(1-\lambda)]} \langle A \rangle$. Thus, for very large ζ, $\langle \mathcal{T} \rangle(\zeta) \propto 1/\zeta$, meaning that it approaches 0, and the $\mathscr{T}(\zeta)$-tendency towards 0 is stronger than the $\mathscr{N}(\zeta)$-tendency towards 0.

3.4 The strong intermittency limit $\gamma \ll 1$

We will now investigate the limit of $\gamma \to 0$, where the assumption of independence between $\Phi(t)$ and $\Theta(t)$ evidently breaks down and we replace this

with an assumption that the pulses do not overlap at all, such that each pulse appears as a burst in the resulting signal. In this limit, we can find the total time above threshold, the number of upwards crossings, the average time above threshold and even the distribution of time above threshold for each upcrossing without going through the joint PDF of $\Phi(t)$ and $\Theta(t)$.

3.4.1 The total time above threshold

Here, we use the CDF directly. If $\Phi(t)$ is gamma distributed, the expression for $\mathscr{T}(C)$ becomes

$$\mathscr{T}(C) = T[1 - CDF_{\Phi}(C))] = T\frac{\Gamma_U(\gamma, C/\langle A\rangle)}{\Gamma(\gamma)}, \tag{3.29}$$

which obviously is equal to Eq. (3.11). When $\gamma \to 0$, the upper incomplete gamma function is still well defined, and $\lim_{\gamma\to 0}\Gamma(\gamma) = 1/\gamma$. Thus, Eq. (3.29) becomes:

$$\lim_{\gamma\to 0}\mathscr{T}(C) = T\gamma\Gamma_U(0, C/\langle A\rangle). \tag{3.30}$$

Using the property given by Eq. (A.20) from the appendix (Section A.3), we can express $\mathscr{T}(C)$ for the non-intermittent limit as a gamma function:

$$\lim_{\gamma\to\infty}\mathscr{T}(C) = \frac{1}{2}\operatorname{erfc}\left(\frac{C - \langle\Phi\rangle}{\sqrt{2}\Phi_{\text{rms}}}\right) = \frac{1}{2\sqrt{\pi}}\Gamma_{\text{U}}\left[\frac{1}{2}, \frac{1}{\gamma}\left(\frac{C}{\langle A\rangle} - \sqrt{\gamma}\right)^2\right],$$

where we also have assumed that $\langle\Phi\rangle = \gamma\langle A\rangle$ and $\Phi_{\text{rms}}^2 = \gamma\langle A\rangle^2$ hold. The difference in the first argument (o for strong intermittency limit, 1/2 for the non-intermittent limit) causes $\mathscr{T}_{\gamma\to\infty}(C)$ to have higher values for small threshold values, but the fact that this function depends on the square of C ensures it falls off much quicker than $\mathscr{T}(C)$ in the strong intermittency limit. This difference with increasing threshold is seen in the uppermost part of Figure 3.5 (although here, the rapid fall is also caused by the $1/\gamma$-dependency of $\mathscr{T}_{\gamma\to\infty}(C)$, which is significant for $\gamma = 100$).

3.4.2 The total number of upwards crossings

When the pulses are completely separated, the total number of upwards crossings above the threshold must be the same as the total number of pulses with amplitude higher than the threshold value. Therefore, the total umber of up-

wards crossings can be written as

$$\lim_{\gamma\to 0}\mathscr{N}(C) = K\int_C^\infty \mathrm{d}A\, P_A(A) = K\int_C^\infty \mathrm{d}A\,\frac{1}{\langle A\rangle}\exp\left(-\frac{A}{\langle A\rangle}\right)$$
$$= K\exp\left(-\frac{C}{\langle A\rangle}\right) = \frac{T}{\tau_\mathrm{d}}\gamma\exp\left(-\frac{C}{\langle A\rangle}\right), \quad (3.31)$$

where K is the total number of pulses, $\tau_\mathrm{w} = T/K$ and $\tau_\mathrm{d}/\tau_\mathrm{w} = \gamma$. This is a purely exponential function, and thus falls off much slower with increasing C than $\mathscr{N}(C)$ does in the Gaussian limit, given by Eq. (3.26), which falls off exponentially with C^2.

Equivalence with Section 3.2.2 To see that Eq. (3.31) is equivalent to Eq. (3.14), we start from Eq. (3.31) and take the limit $\gamma \to 0$, using that $\lim_{s\to 0}\Gamma(s) = s$:

$$\begin{aligned}\mathscr{N}(C) &= \frac{T}{\tau_\mathrm{d}}\frac{\lambda^{\gamma\lambda-1}(1-\lambda)^{\gamma(1-\lambda)-1}}{\gamma\Gamma(\gamma\lambda)\Gamma(\gamma(1-\lambda))}\left(\frac{C}{\langle A\rangle}\right)^\gamma\exp\left(-\frac{C}{\langle A\rangle}\right)\\ &= \frac{T}{\tau_\mathrm{d}}\lambda^{\gamma\lambda}(1-\lambda)^{\gamma(1-\lambda)}\gamma\left(\frac{C}{\langle A\rangle}\right)^\gamma\exp\left(-\frac{C}{\langle A\rangle}\right)\\ &= \frac{T}{\tau_\mathrm{d}}\gamma\exp\left(-\frac{C}{\langle A\rangle}\right).\end{aligned}$$

3.4.3 The average time above threshold

Estimating $\langle\mathcal{T}\rangle(C)$ by $\mathscr{T}(C)/\mathscr{N}(C)$, given by Eq. (3.30) and Eq. (3.31), we find that the average time above threshold is given by:

$$\lim_{\gamma\to 0}\langle\mathcal{T}\rangle(C) = \frac{\mathscr{T}}{\mathscr{N}}(C) = \tau_\mathrm{d}\exp\left(\frac{C}{\langle A\rangle}\right)\Gamma_U\left(0,\frac{C}{\langle A\rangle}\right). \quad (3.32)$$

The proportionality with τ_d is obvious; longer pulses means that the ones that do reach above the threshold stay above the threshold for a longer time. This expression has no dependency on τ_w, which is due to the assumption that we have no pulse overlap.

3.4.4 The PDF of $\mathcal{T}$ and another way to $\langle\mathcal{T}\rangle(C)$

In Figure 3.2, an example of excess times in the strong intermittency limit is presented. $\Phi(t)$ is given by the blue line, the threshold C is given by the green dotted line. Here, the pulses are almost completely separated, so each pulse

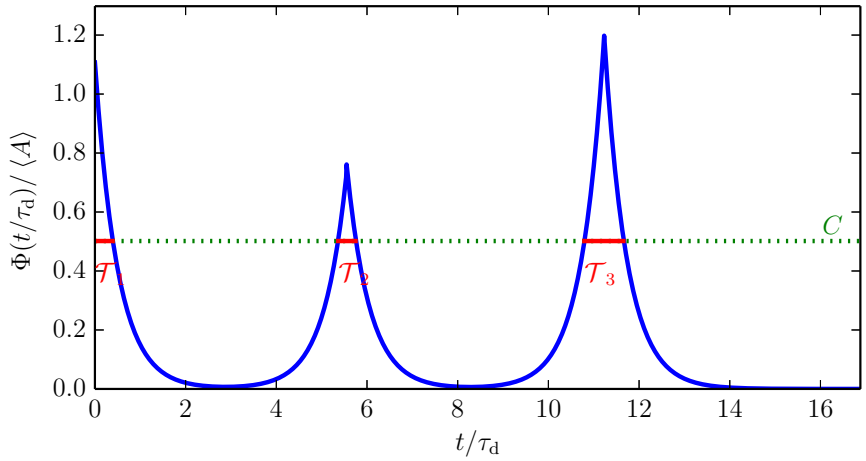

Figure 3.2: Excess times for a shot noise process with $\gamma = 0.1$ and $\lambda = 0.5$

corresponds to one burst. We see that for pulses with amplitude $A_n > C$ (which for the example in Figure 3.2, are all three), the signal spends a time $\mathcal{T}_n$ above the threshold. With the double exponential waveform, $\mathcal{T}_n$ can be divided into a time before the peak, $\mathcal{T}_{rn}$, and a time after the peak, $\mathcal{T}_{fn}$. The time before the peak is given by

$$C = A_n \exp\left(\frac{\mathcal{T}_{rn}}{\tau_r}\right)$$
$$\mathcal{T}_{rn} = -\tau_r \ln\left(\frac{A_n}{C}\right),$$

and the time after the peak is given by

$$C = A_n \exp\left(-\frac{\mathcal{T}_{fn}}{\tau_f}\right)$$
$$\mathcal{T}_{fn} = \tau_f \ln\left(\frac{A_n}{C}\right).$$

Thus, the total time that the n'th pulse spends above the threshold is

$$\mathcal{T}_n = \mathcal{T}_{fn} - \mathcal{T}_{rn} = \tau_d \ln\left(\frac{A_n}{C}\right). \tag{3.33}$$

This value is always positive, since $A_n > C$ for all the relevant amplitudes. We know that A_n are exponentially distributed, and can therefore find the distribution of $\mathcal{T}_n$. However, since we are not using all the amplitudes, only the ones above C, we must use the truncated exponential distribution (see Appendix, Section B.8:

$$P_A(A|A > C) = \frac{1}{\langle A\rangle} \exp\left(-\frac{A - C}{\langle A\rangle}\right) H(A - C). \tag{3.34}$$

To find the PDF of $\mathcal{T}$, we use the transformation of variables [Stark and Woods, 2012]:

$$P_{\mathcal{T}}(\mathcal{T}) = P_A(a_1)\left|\frac{\mathrm{d}a_1}{\mathrm{d}\mathcal{T}}\right|, \tag{3.35}$$

where a_1 is the root of A_n in Eq. (3.33). This root is

$$\mathcal{T}_n = \tau_\mathrm{d} \ln\left(\frac{a_1}{C}\right)$$
$$a_1 = C \exp\left(\frac{\mathcal{T}}{\tau_\mathrm{d}}\right),$$

and the derivative gives

$$\left|\frac{\mathrm{d}a_1}{\mathrm{d}\mathcal{T}}\right| = \frac{C}{\tau_\mathrm{d}} \exp\left(\frac{\mathcal{T}}{\tau_\mathrm{d}}\right).$$

Inserting these results into Eq. (3.35) gives

$$\lim_{\gamma\to 0} P_{\mathcal{T}}(\mathcal{T}) = \frac{C}{\tau_\mathrm{d}\langle A\rangle} \exp\left(\frac{\mathcal{T}}{\tau_\mathrm{d}} + \frac{C}{\langle A\rangle}\left[1 - \exp\left(\frac{\mathcal{T}}{\tau_\mathrm{d}}\right)\right]\right) H_1\left(C\left[\exp\left(\frac{\mathcal{T}}{\tau_\mathrm{d}}\right) - 1\right]\right).$$

A positive constant does not change a Heaviside function, and $\exp(\mathcal{T}/\tau_\mathrm{d}) > 1$ in the same ranges as $\mathcal{T} > 0$. Therefore, the PDF of $\mathcal{T}$ becomes:

$$\lim_{\gamma\to 0} P_{\mathcal{T}}(\mathcal{T}) = \frac{1}{\tau_\mathrm{d}} \frac{C}{\langle A\rangle} \exp\left(\frac{C}{\langle A\rangle}\right) \exp\left[\frac{\mathcal{T}}{\tau_\mathrm{d}} - \frac{C}{\langle A\rangle} \exp\left(\frac{\mathcal{T}}{\tau_\mathrm{d}}\right)\right] H_1(\mathcal{T}). \tag{3.36}$$

This is the so-called Gompertz distribution (see the appendix, Section B.5.5) with shape parameter $C/\langle A\rangle$ and scale parameter $1/\tau_\mathrm{d}$. Some examples of this distribution are plotted in figure 3.3 for various threshold values. As the excess time increases, the probability falls as a double exponential, since the excess times are exponentially related to the pulse amplitudes, and the available pulses which can give such large times fall off exponentially as the excess time increases. Note that this function is independent of $\lambda = \tau_\mathrm{r}/\tau_\mathrm{d}$. This dependency disappeared in Eq. (3.33), where the whole pulse contributes to the excess time regardless of the exact shape. Also note that for $C/\langle A\rangle < 1$, the Gompertz distribution has a peak at a positive value instead of decreasing monotonically from o, as is the case for $C/\langle A\rangle \geq 1$. When the threshold is below the mean amplitude value, this mean value will generate excess times, and thus the most likely excess time to be generated is [from Eq. (3.33)] $\mathcal{T}_\mathrm{peak} = \tau_\mathrm{d} \ln(\langle A\rangle/C)$.

Since $P_{\mathcal{T}}(\mathcal{T})$ is a well known distribution, the mean is also known and this is given by

$$\lim_{\gamma\to 0}\langle\mathcal{T}\rangle(C) = \tau_\mathrm{d} \exp\left(\frac{C}{\langle A\rangle}\right)\Gamma_U\left(0, \frac{C}{\langle A\rangle}\right), \tag{3.37}$$

which is exactly the same as the estimate given by Eq. (3.32). A graphical presentation is given in figure 3.4 with error bars of $\pm\mathcal{T}_\mathrm{rms}$. The function is monotonically decreasing, although the decay is slow for large threshold values. While there is an analytic expression for the rms-value of $\mathcal{T}$, the formula is complicated and not discussed here.

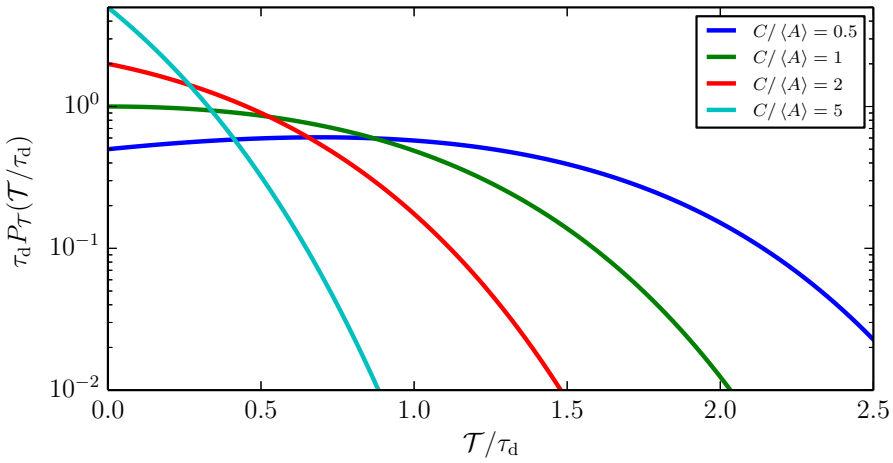

Figure 3.3: The PDF of time above threshold in the strong intermittency limit where pulse overlap can be neglected, for various threshold values.

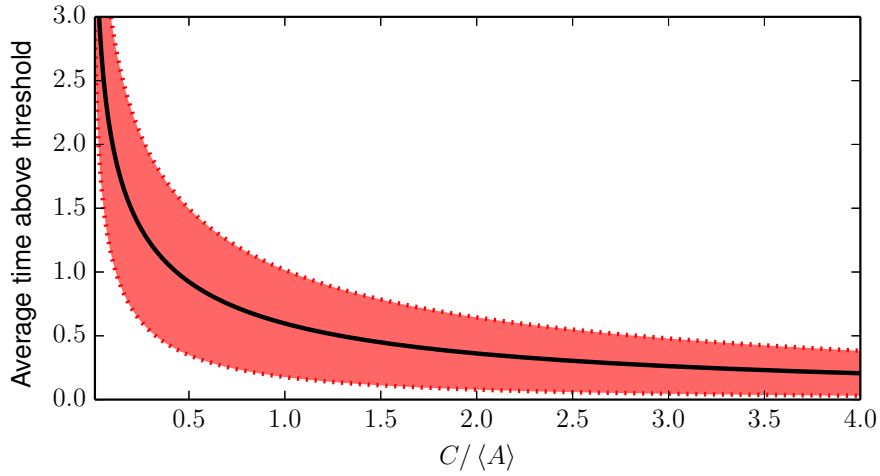

Figure 3.4: The average time above threshold in the strong intermittency limit where pulse overlap can be neglected, with bounds of rms-value of time above threshold.

The average time above threshold for $\zeta \gg 1$

If we let $\zeta \gg 1$ for the normal limit $\gamma \gg 1$, we find that $\langle \mathcal{T} \rangle(\zeta) \sim 1/\zeta$. If we are in the strong intermittency limit $\gamma \ll 1$, and let $\zeta \to \infty$, we find that:

$$\begin{aligned}\lim_{\zeta\to\infty} \langle \mathcal{T} \rangle(\zeta) &= \lim_{\zeta\to\infty} \tau_{\mathrm{d}} \exp\left(\gamma^{1/2}\zeta + \gamma\right) \Gamma_U\left(0, \gamma^{1/2}\zeta + \gamma\right) \\ &= \tau_{\mathrm{d}} \exp\left(\gamma^{1/2}\zeta + \gamma\right)\left(\gamma^{1/2}\zeta + \gamma\right)^{-1} \exp\left(-\gamma^{1/2}\zeta + \gamma\right) \\ &= \frac{\tau_{\mathrm{d}}}{\sqrt{\gamma}} \frac{1}{\zeta + \sqrt{\gamma}}, \end{aligned} \tag{3.38}$$

where we have used that $\lim_{x\to\infty} \Gamma_U(s,x) = x^{s-1}\exp(-x)$. Since in the strong intermittency limit, $\gamma \ll 1$, such that $1/\left(\zeta + \gamma^{1/2}\right) \approx 1/\zeta$, and $\langle \mathcal{T} \rangle(\zeta)$ has the same ζ-dependency for large thresholds in the strong intermittency limit as in the normal limit.

3.5 Comparisons

We now have expressions for $\mathcal{T}(C)$, $\mathcal{N}(C)$ and $\langle \mathcal{T} \rangle(C)$ for the general case (Section 3.2) (under assumptions of exponentially distributed pulse amplitudes, pulse arrivals according to a Poisson process and a double-sided exponential waveform), the strong intermittency limit (Section 3.4) (under the same assumptions) and the non-intermittent limit (Section 3.3) (under the assumption that $P_{\Phi\Theta}(\Phi,\Theta)$ is jointly normally distributed). We have in Section 3.4.2 shown that strong intermittency limit is consistent with taking $\gamma \to 0$ in the general case.

In Figure 3.5, we present the fraction of time above threshold $\mathcal{T}(C/\langle\Phi\rangle)/T$ (above), rate of threshold crossings $(\tau_{\mathrm{d}}/T)\mathcal{N}(C/\langle\Phi\rangle)$ (middle) and average time above threshold $\tau_{\mathrm{d}}\langle \mathcal{T} \rangle(C/\langle\Phi\rangle)$ as a function of $C/\langle\Phi\rangle$ for various values of γ. The general model is computed for all γ-values, the strong intermittency limit is computed for $\gamma = 0.01$ and the normal limit is computed for $\gamma = 100$ (for the normalized threshold $C/\langle\Phi\rangle$, we need a γ-value for both asymptotic limits). In all three cases, it is evident that the general case converges to the asymptotic cases for $\gamma \to 0$ and $\gamma \to \infty$.

In the uppermost part of Figure 3.5 for very small γ, the fraction of time above threshold falls very slowly with increasing threshold. This is because very few bursts fall below the threshold as the threshold increases, so the time above threshold only decreases with the pulse decay. That few bursts fall below the threshold is seen in the middle part of Figure 3.5, where the decay of the rate of upwards threshold crossings is very slow for $\gamma = 0.01$.

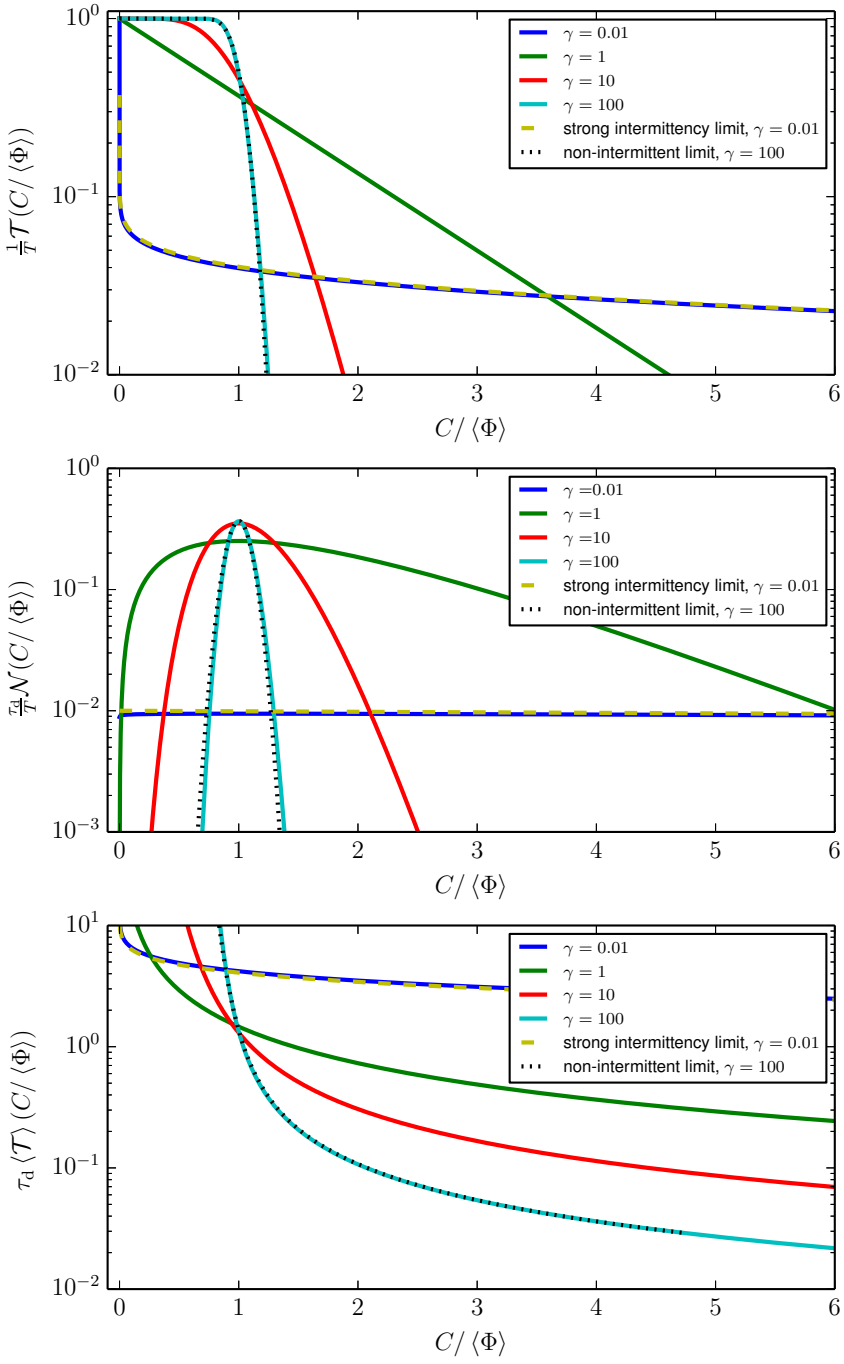

Figure 3.5: Comparison of analytic expressions for excess times for $\lambda = 0.25$ and various intermittency parameters.

As γ increases, the signal value varies less and less around $\langle\Phi\rangle$. Thus, the fraction of time above threshold decays much more quickly with increasing threshold as γ increases. For low threshold values, the fraction of time above threshold approaches 1 as the entire signal ends up above the threshold. The rate of threshold crossings is greatest around the mean value. As the threshold moves away from the mean value of the signal, fewer bursts cross the threshold and the rate of upcrossings decreases. This decay is amplified with increasing γ.

In the lowest part of Figure 3.5, the average time above threshold is seen. Despite the qualitative differences seen in the fraction of time above threshold and in the rate of upcrossings above the threshold, the average time above threshold does not change qualitatively for changing γ, in all cases it is a monotonically decreasing function with fast decay for small threshold values followed by slow decay for large threshold values. The value of γ changes when this transition occurs, but not the qualitative behaviour of $\langle\mathcal{T}\rangle(C/\langle\Phi\rangle)$.

3.5.1 Comparisons of expressions for $\zeta \gg 1$

In both the strong intermittency limit and the non-intermittent limit, $\langle\mathcal{T}\rangle(\zeta)$ has the same dependency on ζ for $\zeta \gg 1$, $\langle\mathcal{T}\rangle(\zeta) \propto 1/\zeta$. For γ on the order of unity, we have $\langle\mathcal{T}\rangle(\zeta) \propto 1/\left(\zeta + \sqrt{\gamma}\right)$. Going from γ on the order of unity to the strong intermittency limit is simple, since here, $\zeta \gg \sqrt{\gamma}$ is fulfilled. Going to the non-intermittent limit is not as evident, and here $\zeta \gg \sqrt{\gamma}$ becomes a real restriction. For instance, for $\gamma = 10$, we require $\zeta \gg 10^{1/2} \approx 3.2$, so we require $(C - \langle\Phi\rangle) > 3.2\Phi_{\text{rms}}$, which has a probability of less than 10^{-3} for a Gaussian process. Thus, we will not likely see this behaviour in real data sets for large γ.

3.6 Excess time statistics of synthetic data

Before applying excess time statistics to experimental data, some questions need to be investigated. The expression for $\mathcal{N}(C)$ should be verified, especially the differences found in Eq. (3.8) for $0 < \lambda < 1$ vs. $\lambda = 0$ and $\lambda = 1$. The estimate in Eq. (3.5) needs to be verified. While both the strong intermittency limit and the normal limit follow analytically from the general model, the rate of convergence is not known, and should be investigated. In addition, we have no knowledge of $P_{\mathcal{T}}(\mathcal{T}|C)$ or $\langle\mathcal{T}^2\rangle$ for γ of order unity, and should investigate the behaviour of these values. In the following, these investigations are erformed through analysis of synthetic data.

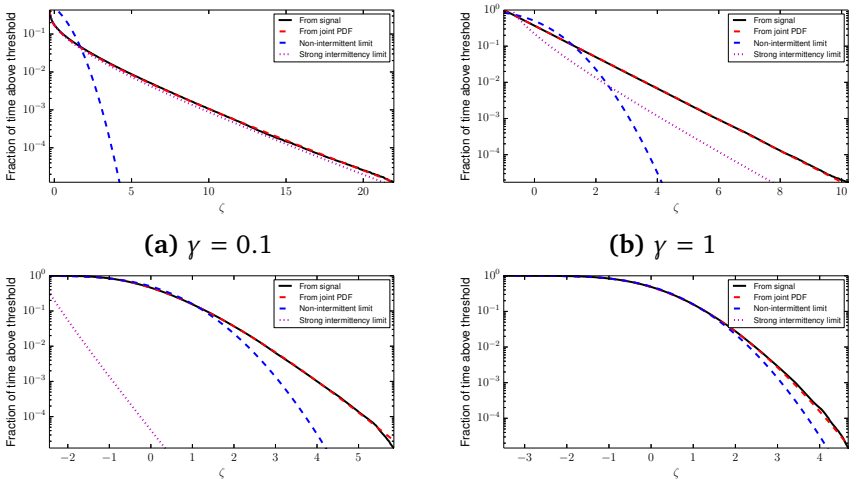

(a) $\gamma = 0.1$ **(b)** $\gamma = 1$

(c) $\gamma = 10$ **(d)** $\gamma = 100$

Figure 3.6: Fraction of time above threshold for $\lambda = 0.25$ and varying γ.

3.6.1 Method

$\mathscr{T}(C)$, $\mathscr{N}(C)$ and $\langle\mathcal{T}\rangle(C)$ are all computed directly from synthetically generated time series. These time series are generated with exponentially distributed pulse waiting times and pulse amplitudes and double exponential waveforms. $\tau_d = 1$, $\langle A\rangle = 1$ and, in the first sections, $\lambda = 0.25$. We set $K = 10^5\gamma$, since this ensures the time series are about the same length for each γ, $N \approx 10^7$. The threshold is $C = \Phi_{\text{rms}}\zeta + \langle\Phi\rangle$, and ζ is plotted along the x-axis of the figures. Generation of time series and calculation of excess time statistics are found in the appendix, Chapter C.

3.6.2 Total time above threshold from synthetic data

Figure 3.6 shows logarithmic plots of $\mathscr{T}(\zeta)/T$ computed from the synthetic signal for varying γ, along with the three analytic expressions given by Eqns. (3.11), (3.25) and (3.30). It is clear that the general expression obtained from the joint PDF of Φ and Θ holds in all cases presented. The expression for the strong intermittency limit holds well in Figure 3.6a when $\gamma = 0.1$, but quickly becomes irrelevant as γ increases. The non-intermittent Gaussian limit has a too strongly curved tail to make a good fit, although for $\gamma = 100$ it fits well for $\zeta < 1$. While $P_\Phi(\Phi)$ is well described by a Gaussian at $\gamma = 100$ (see for instance Figure B.1), the true PDF of Φ evidently still has a weaker right tail than a Gaussian. Thus, the normal limit is a slowly convergent limit, not fitting for $\zeta > 2$ for the total time above threshold with $\gamma = 10^2$.

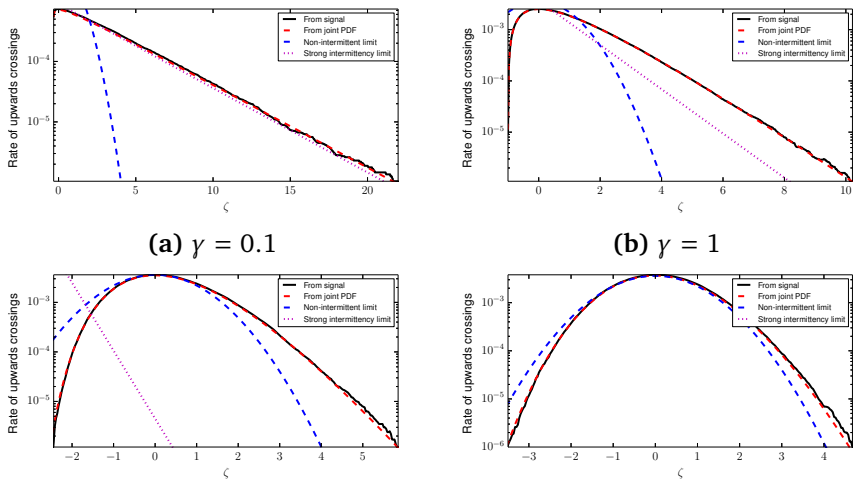

(a) $\gamma = 0.1$ **(b)** $\gamma = 1$

(c) $\gamma = 10$ **(d)** $\gamma = 100$

Figure 3.7: Rate of upwards crossings over threshold for $\lambda = 0.25$ and varying γ.

3.6.3 Number of upwards crossings from synthetic data

Figure 3.7 shows logarithmic plots of $\mathcal{N}(\zeta)/N$, where N is the total number of data points in the time series, computed from the synthetic signal for varying γ, along with the three analytic expressions given by Eqns. (3.13), (3.26) and (3.31). The results are the same as in the previous section; the expression from the joint PDF holds well for all cases shown, the expression for the strong intermittency limit holds for $\gamma = 0.1$ and the expression for the non-intermittent limit holds in an area around $\zeta = 0$ ($C = \langle\Phi\rangle$) which increases as γ increases. The interpretation is the same as above: the joint PDF of Φ and Θ has weaker tails than a joint Gaussian distribution, and therefore the number of upwards crossings falls slower. The normal limit is also here slowly convergent, not fitting the signal with $\gamma = 10^2$ for ζ-values > 2 and < -2.

3.6.4 Average time above threshold from synthetic data

Figure 3.8 shows logarithmic plots of $\langle\mathcal{T}\rangle(C)$ computed from the synthetic signal for various γ, along with the three analytic expressions given by Eqns. (3.15), (3.27) and (3.32). Note that while the conclusion for the expressions from the joint PDF and the strong intermittency limit is the same as in the cases above, the expression for the non-intermittent limit with $\zeta > 0$ is a very good fit for $\gamma \geq 1$; only in Figure 3.8a is there an appreciable difference. Note, however, that the non-intermittent limit is not a good fit for low and negative ζ-values. Apparently, where the right tails of $\mathcal{T}(C)$ and $\mathcal{N}(C)$ from the non-intermittent limit fall off too quickly, this effect is cancelled for $\langle\mathcal{T}\rangle(C) = \mathcal{T}(C)/\mathcal{N}(C)$ and

the Gaussian analytic expression ends up being better for $\zeta > 0$. For $\zeta < 0$, the expression for the total time above threshold in the non-intermittent limit is good, while the expression for the number of upwards crossings does not fit well, meaning that the non-intermittent expression for the average time above threshold does not fit well for thresholds close to the minimal signal value.

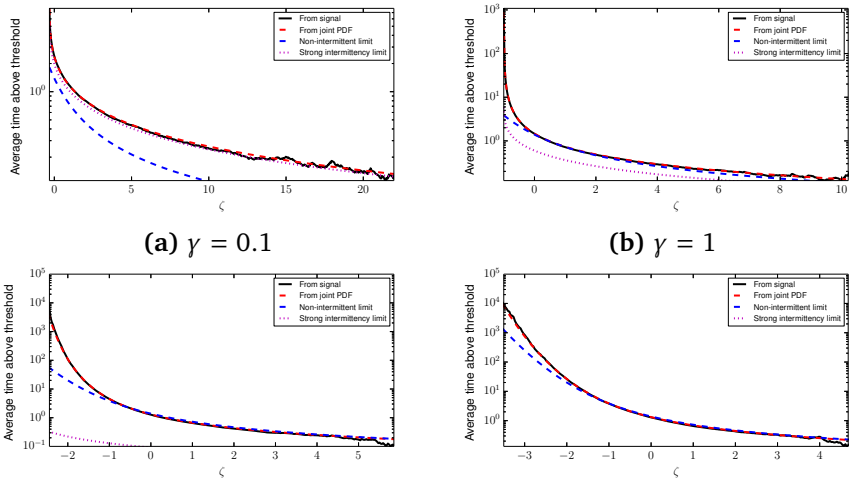

(a) $\gamma = 0.1$ **(b)** $\gamma = 1$

(c) $\gamma = 10$ **(d)** $\gamma = 100$

Figure 3.8: Average time above threshold for $\lambda = 0.25$ and varying γ.

Effects of changing λ

In Section 3.1.3, it was shown that there should be a qualitative difference between $\lambda = 0$ and $\lambda > 0$ in the expressions for the total number of upwards crossings (and therefore, also for the average time above threshold). In Figure 3.9, the average time above threshold as a function of the normalized threshold ζ is presented for various γ. From Eq. (3.8), we have that $\langle \mathcal{T} \rangle(\zeta)$ for $\lambda = 0$ should be smaller than $\langle \mathcal{T} \rangle(\zeta)$ for $\lambda > 0$ by a factor $[2\pi\gamma\lambda(1-\lambda)]^{-1/2}$, so this difference should be small for small intermittency parameters and increase as γ increases. This is exactly the behaviour seen in Figure 3.9. The reason for this difference is discussed in depth in Section 3.6.5, where we also have $\langle \mathcal{T}^2 \rangle$ for synthetic data.

Behaviour of the average time above threshold for large threshold values

In this section we will test the prediction that for $\zeta \gg 1$ the average time above threshold $\langle \mathcal{T} \rangle(\zeta) \propto 1/\zeta$ in both the strongly intermittent limit and in

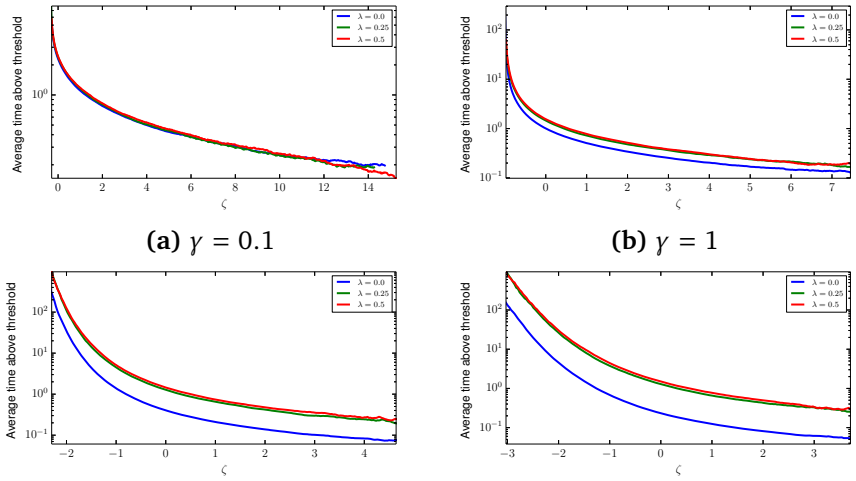

(a) $\gamma = 0.1$ **(b)** $\gamma = 1$

(c) $\gamma = 10$ **(d)** $\gamma = 100$

Figure 3.9: Comparison of average time above threshold for $\lambda = 0$ and $\lambda > 0$ calculated from synthetic data.

the non-intermittent limit, while $\langle \mathcal{T} \rangle(\zeta) \propto 1/(\zeta + \sqrt{\gamma})$ for γ-values of order unity. Figure 3.10 presents the average time above threshold (blue line), the average time above threshold in the limit of large ζ given by Eq. (3.22) (red dotted line) and power law fit to the largest values (green line) as a function of ζ for different intermittency parameters. Concentrating on the expression for the limit of large ζ (Eq. (3.22)), this is approximately correct for $\gamma = 1$ (Figure 3.10c). For lower γ, this value is too high, although in Figure 3.10b, $\langle \mathcal{T} \rangle$ from the synthetic data converges towards the analytic expression. In the same way, in the figures for $\gamma > 1$, the analytic expression is too small, although the synthetic data in Figure 3.10d also seems to converge towards the analytic expression.

Looking at the power law fit, this is the fit $\langle T \rangle_{\text{fit}} = \alpha \zeta^{\beta}$, where α and β are fit parameters. The fit range is the same as the plot range for the fits, from $\zeta = 1$ until (at most) $\zeta = 10^2$, although this decreases with increasing γ. While the power law fits are acceptable for all figures except Figure 3.10a, the exponent is around -0.75 in all cases, not consistent with the asymptotic scaling $\langle \mathcal{T} \rangle(\zeta) \propto \zeta^{-1}$. Thus, while it seems possible to find a power law fit to the synthetic data for large ζ, the expression from the general model seems to indicate that these synthetic data sets are not long enough to reach large enough ζ-values for $\langle \mathcal{T} \rangle(\zeta) \propto \zeta^{-1}$ to be fulfilled.

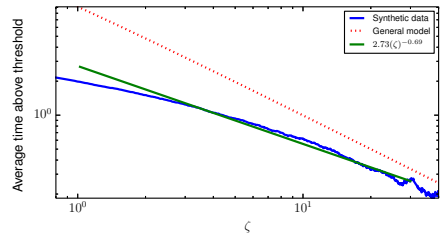

(a) $\gamma = 0.01$

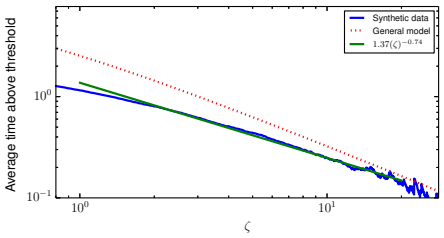

(b) $\gamma = 0.1$

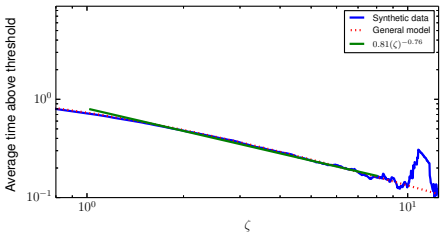

(c) $\gamma = 1$

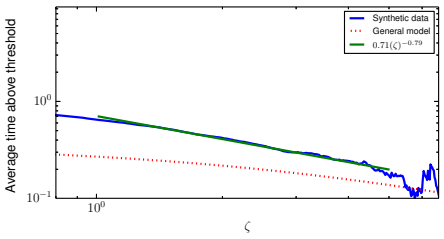

(d) $\gamma = 10$

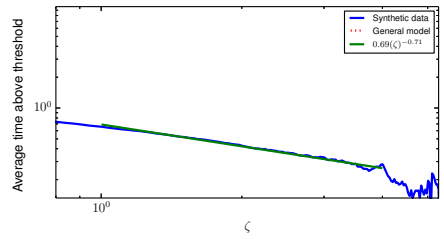

(e) $\gamma = 100$

Figure 3.10: Average time above threshold for large threshold. $\lambda = 0.25$ and γ varies.

3.6.5 The rms-value of the time above threshold

While we have no theoretical expression for $\mathcal{T}_{\text{rms}}$, it can still be found numerically from synthetic data. Figure 3.11 presents the second raw moment of $\mathcal{T}$ as a function of ζ comparing different λ for four given values of γ. Similarly, Figure 3.12 presents $\langle \mathcal{T}^2 \rangle$ as a function of ζ for two values of λ, comparing different values of γ. In all cases, $\langle \mathcal{T}^2 \rangle(\zeta)$ is a monotonically decreasing function which has a singularity at a threshold corresponding to $\Phi = 0$.

In Figure 3.11, the same difference between $\lambda = 0$ and $\lambda > 0$ can be seen as for the average time above threshold, the $\langle \mathcal{T}^2 \rangle$-value for $\lambda = 0$ becomes smaller with increasing γ compared to the $\langle \mathcal{T}^2 \rangle$-value for $\lambda > 0$. The lack of a finite rise time for $\lambda = 0$ gives less possibilities for pulse build up, any steps over the threshold happens suddenly and after the threshold is crossed upwards, new pulses are needed to keep the signal above the threshold. For $\lambda > 0$, any crossing over the threshold is caused by a rising pulse, allowing for build up above the threshold even in the absence of other pulses. Although the time above threshold is the same for any pulse of the same amplitude, independent of λ, the fact that for $\lambda = 0$, the pulses are only falling decreases both the time above threshold for the bursts and the variation possible in the length of the bursts. As γ increases, this difference increases since closer pulses means there are more ways pulses with $\lambda > 0$ can interact to form bursts than pulses with $\lambda = 0$, leading to both larger $\langle \mathcal{T} \rangle$ and larger $\langle \mathcal{T}^2 \rangle$ for $\lambda > 0$ than for $\lambda = 0$.

In Figure 3.12, it can be seen how, for increasing γ, the $\langle \mathcal{T}^2 \rangle$-value decreases for all ζ. This is due to pulse overlap becoming more significant, decreasing the ratio of $\Phi_{\text{rms}}/\langle \Phi \rangle$ and thus decreasing the variation in excess times for any given ζ. The increase towards ∞ for $C \to 0$ is due to the large variation in time above threshold seen for thresholds below $\langle \Phi \rangle$. As the threshold decreases, it begins catching the bursts that essentially make up the baseline mean value, so it gets both very long bursts and extremely short bursts, leading to a sharp increase in the variation of time above threshold for small threshold values.

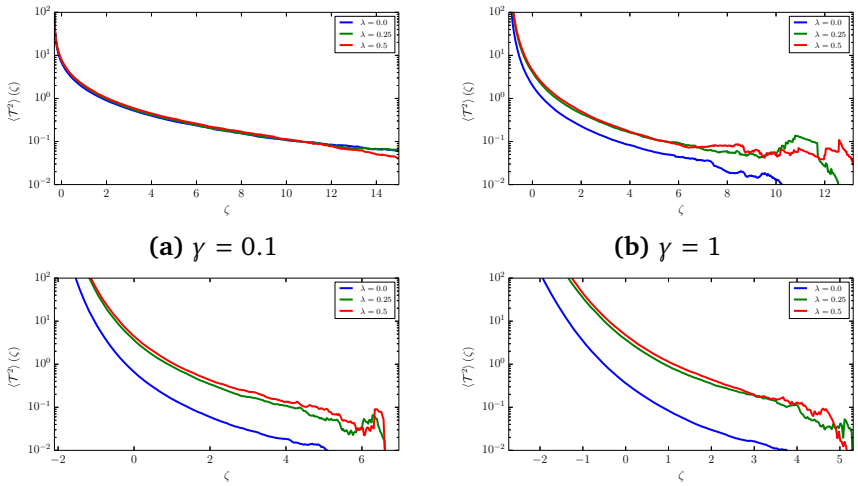

(a) $\gamma = 0.1$ **(b)** $\gamma = 1$

(c) $\gamma = 10$ **(d)** $\gamma = 100$

Figure 3.11: The second raw moment of time above threshold for changing γ

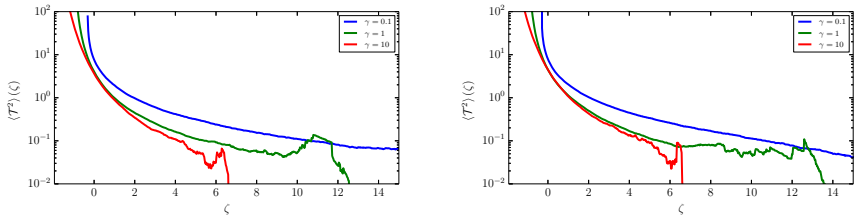

(a) $\lambda = 0.25$ **(b)** $\lambda = 0.5$

Figure 3.12: The second raw moment of time above threshold for changing λ

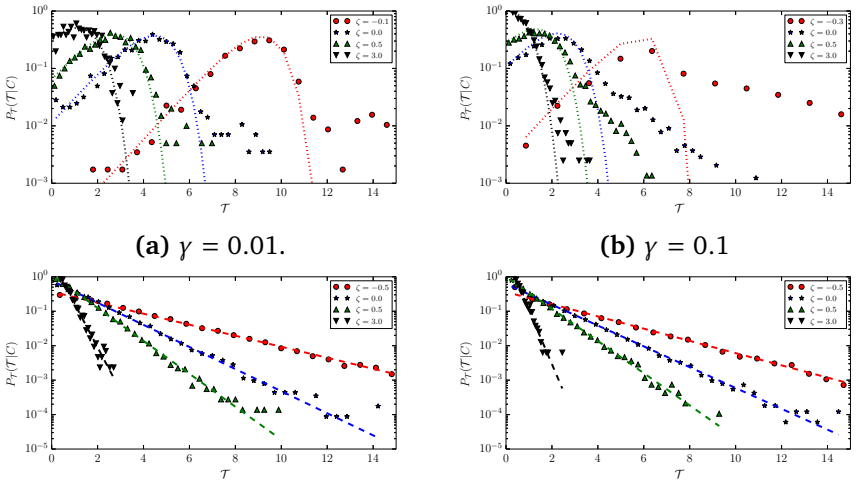

(a) $\gamma = 0.01$. **(b)** $\gamma = 0.1$

(c) $\gamma = 1$ **(d)** $\gamma = 10$

Figure 3.13: The PDF of time above threshold for $\lambda = 0.25$ and changing γ

3.6.6 The PDF of the time above threshold

In Figure 3.13, $P_{\mathcal{T}}\left(\mathcal{T}|\widehat{\Phi} > \zeta\right)$ is plotted against $\mathcal{T}$ for changing thresholds ζ and various values of γ. In Figure 3.13a and Figure 3.13b, the dots refer to the PDF calculated from the signal, while the dotted lines is the analytic expression for the PDF of $\mathcal{T}$ in the strong intermittency limit, given by Eq. (3.36). In Figure 3.13b and Figure 3.13d, the dots refer to the PDF calculated from the signal, while the dotted lines is an exponential fit to the synthetic data.

For $\gamma = 0.01$, the analytic expression fits the data very well, the points outside the fits are most likely due to binning issues and lack of data points for large $\mathcal{T}$. In contrast, for $\gamma = 0.1$, the fits are acceptable for low $\mathcal{T}$-values, but have a much weaker tail than the analytic expression for the strong intermittency limit predicts. Evidently, the strong intermittency limit is not a good fit for $\gamma \geq 0.1$.

Considering the Figures for $\gamma = 1$ and $\gamma = 10$, they are in all cases well approximated by an exponential. In addition, going from $\gamma = 1$ to $\gamma = 10$ appears to have little effect on the PDF of $\mathcal{T}$.

4

Conditional averaging

4.1 Theory and methods

The conditional average is a method for picking out large-amplitude structures in noisy signals; examples of previous applications include fusion plasma devices [Antar et al., 2005, Boedo et al., 2001, Rudakov et al., 2002, Garcia, 2009], magnetized tori [Øynes et al., 1998, Fredriksen et al., 2008, Block et al., 2006] and linear devices [Grulke et al., 1999, Huld et al., 1991, Nielsen et al., 1996]. We intend to use the same methods to discuss the statistics of large-amplitude fluctuations in a shot noise signal, the distribution of pulse amplitudes and waiting times and the preservation of the signal pulse shape.

Note that there is a discrepancy between the assumptions we use and the assumptions in the works referenced above; these works assume the signal consists of non-overlapping coherent structures with overlapping noise, and a central problem is whether the condition is fulfilled by a coherent structure or randomly due to noise. We, on the other hand, assume that the signal consists completely of overlapping, coherent structures. Thus, the question for us becomes whether the condition is fulfilled by a single, large structure or a superposition of many, smaller structures.

Given a time series $\Phi(t)$, we use a condition C to pick out certain subintervals from the main signal. This can for instance simply be the condition that the signal value reaches a certain threshold. The conditionally averaged signal is

then the ensemble average of all subintervals

$$\Phi_C = \langle \Phi | C \rangle. \tag{4.1}$$

We will use the following condition: First, we find all the maxima of Φ above a *threshold value* α. Then, we pick out the subintervals $(t_\mathrm{m} - \Delta, t_\mathrm{m} + \Delta)$ where t_m is the time of the maxima and 2Δ is the length of a subinterval. To ensure statistical independence between the subintervals, they are not allowed to overlap. In cases where overlap happens, the larger maxima is preferred. An example of this method is shown in Figure 4.1. Note especially how, in the first subinterval, a lower peak has been picked. This is to ensure independence between the subintervals, since picking the higher peak would cause overlap with the third subinterval. The waiting time distribution is constructed from the time between the red stars and the amplitude distribution is constructed from the signal value of the subsequent maxima, indicated by the red stars in Figure 4.1. The conditionally averaged signal is then constructed as

$$\Phi_C = \frac{1}{M} \sum_{m=1}^{M} \Phi(t - t_m) \text{ for } t - t_m \in (-\Delta, \Delta) \tag{4.2}$$

In addition to finding the subintervals, we also note the time and amplitude of their peaks, and construct waiting time and amplitude distributions of the peaks of the signal.

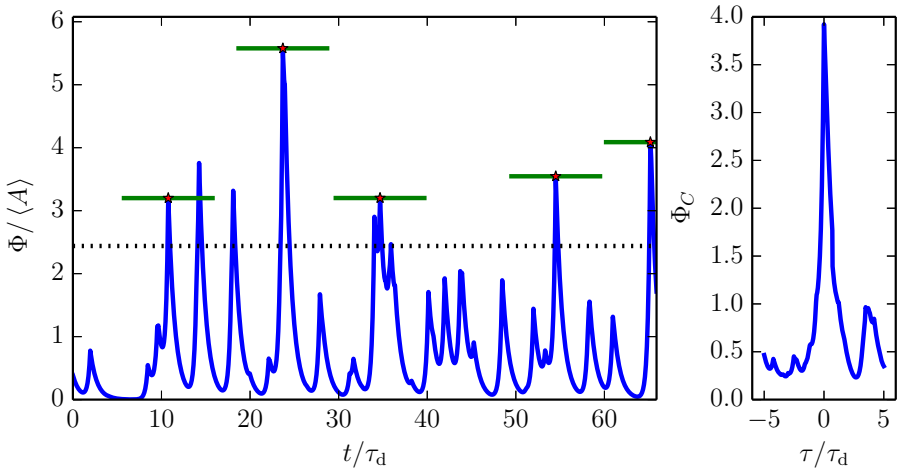

Figure 4.1: Left: A synthetically generated shot noise process with $\lambda = 0.25$ and $\gamma = 1$ (blue lime), threshold (black dotted line), found peak values (red stars) and corresponding subintervals (green horizontal bars). Right: The average from all subintervals.

4.1.1 Problems and prospects

It has been demonstrated elsewhere Block et al. [2006] that conditional averaging does not preserve signal amplitude or the size of the waveforms. For us, this means that and estimate of $\langle A \rangle$ and τ_{d}, which we would like to get for $P_A(A)$ and $P_\tau(\tau)$ are out of reach by conditional averaging methods. Neither can we find τ_{w}, since only waiting times larger than 2Δ are found. We are instead focusing on the following questions:

- Is the pulse amplitude distribution $P_A(A)$ preserved by conditional averaging?
- Is the pulse waiting time distribution $P_\tau(\tau)$ preserved?
- Is the waveform of the pulses preserved?
- Is λ preserved?

Looking at figure 4.1, we see that for the peaks to be registered as such, they must have an amplitude higher than the threshold value, and must be further away from each other than the length of a subinterval. Lower peaks and waiting times are not recorded. Thus when we are fitting distributions to the data we get from the conditional average, we cannot simply compare the result to the original PDFs $P_A(A)$ or $P_\tau(\tau)$, we must compare them to $P_A(A|A > \alpha)$ and $P_\tau(\tau|\tau > \Delta)$, where α is the threshold value and Δ is the subinterval length. (At least for highly intermittent signals it is this clear cut. When the intermittency becomes lower, bursts will overlap and for instance two bursts which individually were not large enough to satisfy the condition $\Phi > C$ will give one large peak if they are close enough together, that is, for significant pulse overlap. But the main point, that the distributions we get are truncated, still holds). Thus all comparisons to analytic distributions will be comparisons to *truncated* distributions, covered in Section B.8.

4.1.2 Choice of threshold

There are two main ways to set the threshold value α. One way is to say that

$$\frac{\Phi - \langle \Phi \rangle}{\Phi_{\mathrm{rms}}} > \alpha, \tag{4.3}$$

while another way is to use

$$\frac{\Phi - \langle \Phi \rangle}{\langle \Phi \rangle} > \beta, \tag{4.4}$$

which can also be formulated as

$$\frac{\Phi - \langle\Phi\rangle}{\Phi_{\text{rms}}} > \beta\frac{\langle\Phi\rangle}{\Phi_{\text{rms}}} = \alpha.$$

From Section 2.1.3 we know that for degenerate, uniform, Rayleigh and exponential pulse amplitude distributions and pulse waiting time distributions, $\langle\Phi\rangle/\Phi_{\text{rms}} \approx \gamma^{1/2}$, so the two conditions are not qualitatively different. Eq. (4.4) has the advantage that it is not dependent on γ. Therefore, it can be useful for comparing signals with different intermittency parameter. Sometimes, however, it is necessary to remove the mean value of the signal before starting analysis. Then we have to use Eq. (4.3). In the following analysis of synthetic data, we have used the threshold Eq. (4.3) since it is the most commonly used method for analyzing experimental data. In addition, it will in the next section turn out that when using the threshold in Eq. (4.3), the number of conditional bursts remains roughly equal for all generated processes when the number of of pulses in the process is proportional to γ.

4.2 Conditional averaging of synthetic data

Here, we present results from conditional averaging of synthetically generated shot noise data. The data is generated with a sampling time $\Delta t = 0.01$ and we have set $\tau_{\text{d}} = 1$ and $\langle A\rangle = 1$. The number of data points in the signal varies, and we have used $K = 10^5\gamma$ pulses, giving $N \approx 10^7$ data points. Thus the synthetic signals have an end time of $T/\tau_{\text{d}} \approx 10^5$. Conditional averaging has been performed as described in the previous chapter, with the threshold in Eq. (4.3) and $\alpha = 2.5$. This threshold, together with $K \propto \gamma$ kept the number of stored events after conditional averaging in the same ballpark, at around $2000 - 5000$ stored events.

When testing the preservation of amplitude and waiting time distributions, λ is set to 0.2 and γ varies, deciding τ_{w} through $\tau_{\text{w}} = \tau_{\text{d}}/\gamma = 1/\gamma$. Amplitudes and waiting times for the pulses in the shot noise process are degenerately, exponentially, uniformly and Rayleigh distributed. These distributions have all been defined through their mean value as described in the appendix, Section B.5.

When testing pulse waveform preservation, we have used fewer ($K = 10^4\gamma$) pulses and λ has been allowed to vary. Pulse amplitudes and waiting times are only exponentially distributed.

Distributions are calculated using a histogram method, so we will present the complementary CDF in the results instead of the PDF to minimize binning

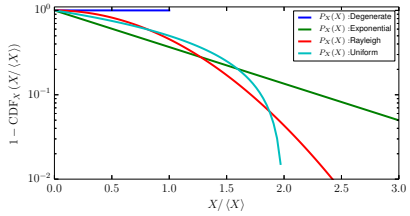

(a) Comparison of complementary CDFs with a logarithmic scale.

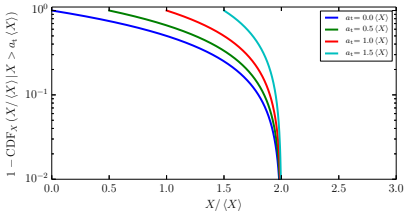

(b) Complementary CDF of the uniform distribution with changing truncation parameter.

Figure 4.2: Graphical representation of complementary CDFs

issues. We fit the cCDF to truncated distributions, see Section B.8 with the distribution parameter and the truncation threshold are parameters to be fitted. We will call the distribution parameter l and the truncation parameter a for universality.

We will be comparing the complementary CDF of the distributions in log-lin-plots, and a graphical presentation of these distributions is given in Figure 4.2a. In all cases, the complementary CDF has a maximal value of 1 at $X = 0$ and decays monotonically with increasing X. All distributions have the same mean value, $\langle X\rangle = 1$. The distributions we present in the following Sections will also be truncated, as described in Section 4.1.1. An example of the effect of truncation on the CDF of the uniform distribution can be seen in Figure 4.2b. Truncation effectively causes the complementary CDF to start at the truncation parameter a_t with a maximal value of 1. In addition, truncation rescales the signal such that $\int_{-\infty}^{\infty} \mathrm{d}x\, P_X(x|x > a_t) = 1$.

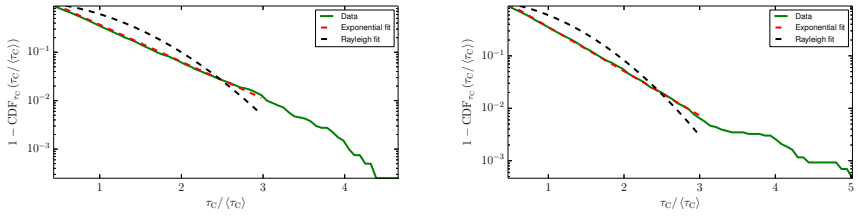

(a) Exponentially distributed pulse waiting times and amplitudes.

(b) Rayleigh distributed pulse waiting times and amplitudes.

Figure 4.3: Waiting time distributions of conditionally averaged signals with $\gamma = 1$, with fitted exponential and Rayleigh distributions.

4.2.1 Preservation of waiting time distribution

In Figure 4.3, complementary CDFs of waiting time distributions of conditionally averaged signals with $\gamma = 1$ are presented together with fitted truncated exponential and Rayleigh distributions. In all cases, the fits are made between the truncation parameter a_t and $\tau_C/\langle\tau_C\rangle = 3$. In Figure 4.6a, the truncation parameter is $a_t = 0.47$ and the exponential distribution parameter is 1.94. In Figure 4.6b, the truncation parameter is $a_t = 0.44$ while the exponential distribution parameter is 1.76. It is evident that in both cases, despite differences in both pulse waiting time distribution and pulse amplitude distribution, the resulting waiting time distributions of the conditionally averaged signals are remarkably similar.

In Figure 4.4, we present waiting time distributions between large-amplitude events from a variety of pulse waiting time distributions, pulse amplitude distributions and intermittency parameters. In all cases, the resulting waiting times are clearly exponentially distributed for more than two orders of magnitude on the ordinate.

It should be noted that not all cases are clearly exponentially distributed; two examples are shown in Figure 4.5. In both cases, the intermittency is significant ($\gamma = 0.1$), so there is little pulse overlap. In Figure 4.5a, we see that for degenerately distributed pulse amplitudes, the conditionally averaged waiting times follow a Rayleigh distribution, which is the same as the pulse waiting time distribution. For all other pulse amplitude distributions, the conditionally averaged waiting times are exponentially distributed. In Figure 4.5b, we see that for a low intermittency parameter and degenerately distributed pulse amplitudes, the waiting time distribution follows the underlying pulse waiting time distribution.

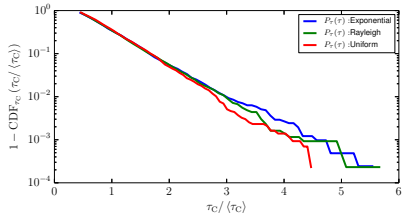

(a) $\gamma = 0.5$ and the pulse amplitudes are exponentially distributed for various pulse waiting time distributions.

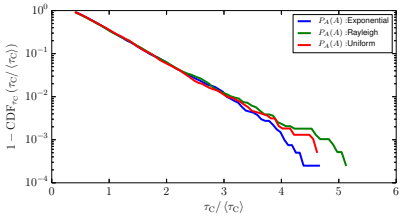

(b) $\gamma = 1.0$ and the pulse waiting times are exponentially distributed for various pulse amplitude distributions.

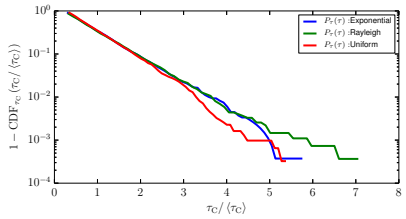

(c) $\gamma = 5.0$ and the pulse amplitudes are Rayleigh distributed for various pulse waiting time distributions.

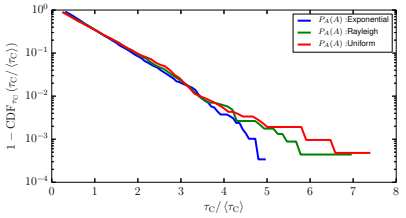

(d) $\gamma = 10.0$ and the pulse waiting times are Rayleigh distributed for various pulse amplitude distributions.

Figure 4.4: Comparisons of waiting time distributions for large-amplitude events.

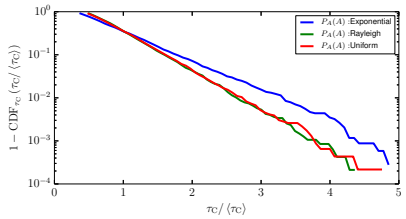

(a) Varying pulse amplitude distributions and Rayleigh distributed pulse waiting times.

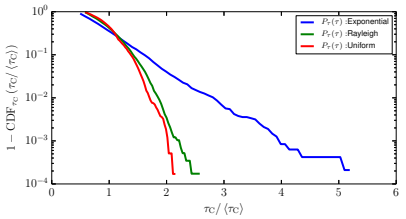

(b) Varying pulse waiting time distributions and degenerately distributed pulse amplitudes.

Figure 4.5: Comparison of conditionally averaged waiting times with intermittency parameter $\gamma = 0.1$.

Conclusion and interpretation

In conclusion, the waiting time distribution of a conditionally averaged shot noise process is exponentially distributed for almost all pulse waiting time- and amplitude distributions and all but the most intermittent signals. Of the cases investigated here, only for $\gamma = 0.1$ and degenerately distributed pulse amplitudes does the conditionally averaged waiting times follow the same distribution type as the pulse waiting times. Therefore, conditional averaging does not seem equipped to determine the waiting time distribution of the pulses of a shot noise process.

A possible interpretation of the uniformity of the exponentially distributed waiting times is the following: For a shot noise process with pulse overlap, the position of the largest bursts is determined by a combination of the degree of pulse overlap (γ), increasing with the distribution of large pulse amplitudes and the distribution of waiting times (many short waiting times after one another may lead to a single, large burst). Thus, any information about where the original pulses are is lost. This may mean that we also lose any dependencies in the signal, such that even if the number of pulses in a certain time interval did depend on the number of pulses in a previous interval, the bursts display no such dependency. We already know that two large bursts cannot occur at the same time for a conditionally averaged process, and since the shot noise process is stationary, it is reasonable to expect the conditionally averaged process to be stationary as well. If all this is true, then the number of bursts in a conditionally averaged shot noise process is a Poisson process, and the waiting time between bursts must have an exponential distribution.

4.2.2 Preservation of amplitude distribution

The amplitude distribution of the conditionally averaged bursts exhibits the same type of information loss as the waiting time distribution, although instead of a pure exponential distribution, the amplitudes taper off, sharper with increasing intermittency parameter. Two examples of this, with exponential and Rayleigh fits, are seen in Figure 4.6. Here, both processes end up with conditionally averaged amplitudes closer to a Rayleigh distribution than to an exponential distribution.

While a degenerate pulse waiting time distribution ensures that we retain the pulse amplitude distribution, even in the case of significant pulse overlap, (Figure 4.7), any other pulse waiting time distribution leads to information loss (Figure 4.8). Note how the burst amplitude distribution in Figure 4.8a remains an exponential while the burst amplitude distribution in Figure 4.8b tapers off.

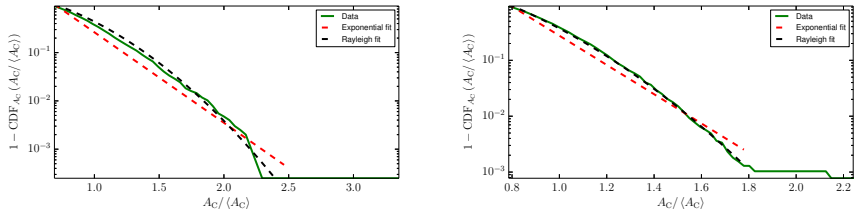

(a) Pulse amplitudes are exponentially distributed.

(b) Pulse amplitudes are Rayleigh distributed.

Figure 4.6: Conditionally averaged amplitude distributions with fitted exponential and Rayleigh distributions. $\gamma = 1$ and the pulse waiting times are exponentially distributed.

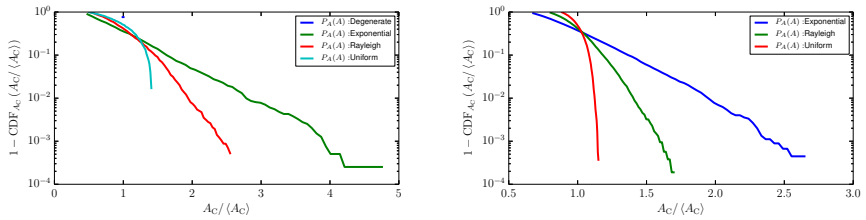

(a) $\gamma = 0.1$.

(b) $\gamma = 1$.

Figure 4.7: Comparison of conditionally averaged amplitude distributions. The pulse waiting times are degenerately distributed.

As a final note before discussing these results, we point to the influence of the pulse waiting time distribution on the conditionally averaged amplitude distribution, Figure 4.9. Here we again see that the degenerate pulse waiting time distribution preserves the pulse amplitude distribution, at least for highly intermittent signals (Figure 4.9a). This is less pronounced for less intermittent signals, (Figure 4.9b). Note that while there is a clear difference between the plots for the exponentially and Rayleigh distributed pulse waiting times in Figure 4.9a, Figure 4.10 reveals that this is not a difference in distribution, only in parameters; the Rayleigh distribution parameter in Figure 4.10a is 0.51, while the distribution parameter in Figure 4.10b is 0.42.

Conclusion

The pulse waiting time distribution has a greater effect on the conditionally averaged amplitudes than the pulse amplitude distribution has on the conditionally averaged waiting times. In addition, we see that if the conditionally averaged amplitudes go towards a common distribution, it is rather the Rayleigh distribution than the exponential distribution, and here they display a greater range of fit parameter discrepancy than the conditionally averaged waiting

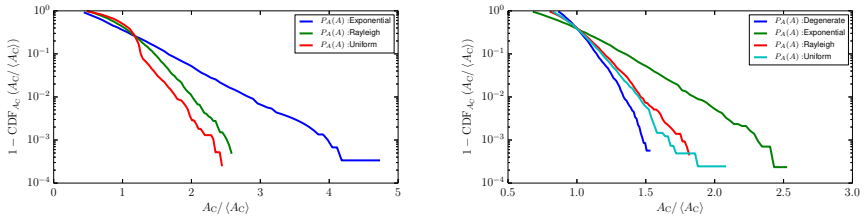

(a) $\gamma = 0.1$ and exponentially distributed pulse waiting times.

(b) $\gamma = 1$ and Rayleigh distributed pulse waiting times.

Figure 4.8: Comparison of conditionally averaged amplitude distributions with non-degenerate pulse waiting time distributions.

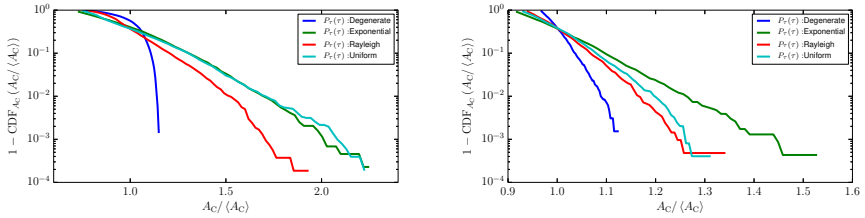

(a) $\gamma = 0.5$.

(b) $\gamma = 10$.

Figure 4.9: Comparison of conditionally averaged amplitude distributions with uniformly distributed pulse amplitudes and varying pulse waiting time distribution.

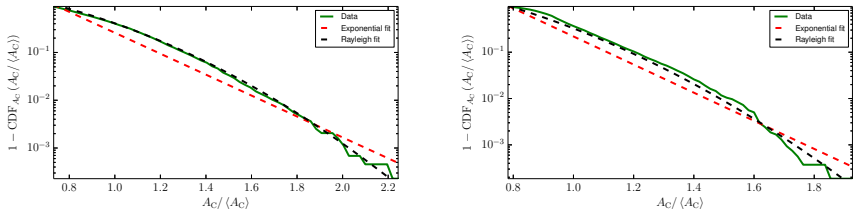

(a) Exponentially distributed pulse waiting times.

(b) Rayleigh distributed pulse waiting times.

Figure 4.10: Conditionally averaged amplitude distributions fitted to exponential and Rayleigh distributions. $\gamma = 0.5$ and pulse amplitude distribution is uniform.

times. This is termed *tapering off* of the distribution tail, and may be due to the pulse overlap; the signal amplitude increases due to short waiting times and we get a greater range of amplitudes in the resulting signal than in the individual pulses. In the case of the waiting times, the pulse overlap leads to increased likelihood of peaks over the entire range of waiting times, and the tapering off does not occur.

4.2.3 Preservation of the pulse waveform

Preservation of the waveform shape

To reveal the extent of waveform preservation, we have analyzed the same shot noise process with four different waveforms: a double exponential waveform, given in Eq. (2.5) with $\tau_r = \tau_f = \tau_d/2$, the derivative of this waveform, given in Eq. (2.84), a box waveform:

$$\varphi_{box}(t) = \begin{cases} 1, & \text{if } -\frac{\tau_d}{2} \leq t \leq \frac{\tau_d}{2} \\ 0, & \text{else} \end{cases}, \tag{4.5}$$

and a Gaussian waveform

$$\varphi_{Gauss}(t) = \exp\left[-\pi\left(\frac{t}{\tau_d}\right)^2\right]. \tag{4.6}$$

All of these waveforms have the maximal value $\varphi(0) = 1$ and all have $I_1 = 1$.

In Figure 4.11, an example of a conditionaly averaged signal is presented. The original signal had exponentially distributed pulse amplitudes and waiting times, $\gamma = 10$ and $\tau_r = \tau_f$. This is the average of 200 recorded bursts, from 10^5 pulses. In order to get from this signal to the (assumed) pulse shape, it must be centered and scaled to have a maximal value of 1 at $\tau = 0$ and to fall off towards 0 as the absolute value of τ increases. It is centered by subtracting the average value of Φ_C for the parts where $|\tau| \gg 0$. Then we divide by the maximal value of the resulting signal to get the desired shape.

The results of this process are presented in Figure 4.12. Here, the same shot noise process with four different pulse shapes has been conditionally averaged and fitted to an exponential function. It is quite clear that only the originally exponential waveform can be well fitted to an exponential. It is also interesting to note that only the originally exponential and Gaussian waveforms have been preserved. The derivative of the double exponential should fall below 0 as far as it rises above, since with $\tau_r = \tau_f$, this waveform is symmetric. The box waveform has been distorted as well, most likely since the largest peaks arise from layers

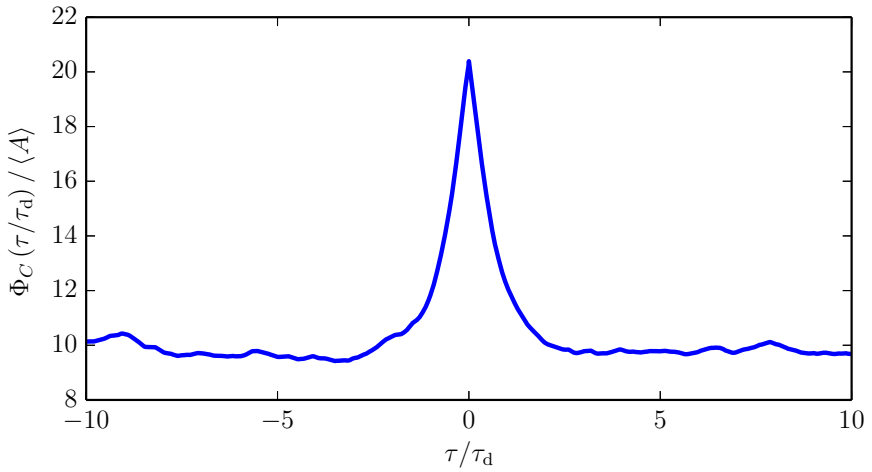

Figure 4.11: An example of a conditionally averaged signal with threshold $\alpha = 2.5$.

of box waveforms arriving after one another, creating a pyramidal shape. Note that the exponential pulse shape, while being well preserved, did not conserve τ_d. For the exponential pulse shape, the fitted τ_d was 1.45, for the derivative of the exponential pulse shape, it was 0.36, the box shape gave $\tau_d = 0.89$ and the Gaussian waveform gave $\tau_d = 1.13$. In all cases, the decay time of the original signal was $\tau_d = 1$.

Even if the fit is not perfect to the signal with double exponential, these results seem to indicate that if the conditionally averaged signal has an exponential shape, then the pulse waveform is exponential as well.

Preservation of τ_r/τ_d and τ_f/τ_d

We have previously stated that conditional averaging does not preserve τ_d. It is, however, possible that it preserves the relationship between τ_r and τ_f (that is, it preserves the parameter λ, where $\tau_r/\tau_d = \lambda$ and $\tau_f/\tau_d = 1 - \lambda$). The results presented here only use exponential pulse amplitude- and waiting time distributions.

In Figure 4.13a, normalized, conditionally averaged signals with various values of γ have been fitted to the function $\varphi(t) = \exp(t\tau_d/\lambda)H(-t)+\exp(-t\tau_d/(1-\lambda))$ where τ_d and λ are fit parameters. Estimated standard deviation error is $< 10^{-2}$ in all cases, and does not exceed the plot points. Setting τ_d to its true value does not increase accuracy of λ. In this figure, the loss of accuracy with increasing γ is clear; for $\gamma = 0.1$, the results can be trusted, but for $\gamma \geq 1$, they can only be used as an indicator of which way the waveform is skewed. Note, however, that

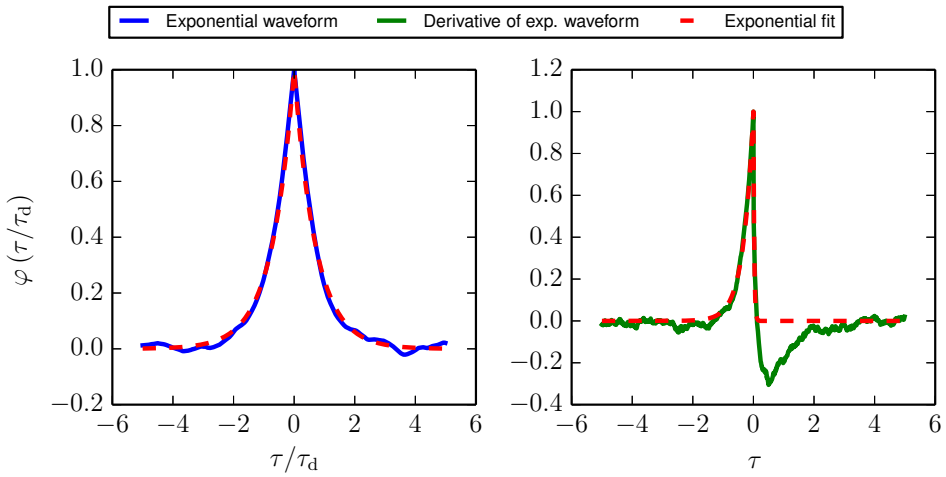

(a) Pulse waveforms are double exponential (left) and the derivative of the double exponential (right).

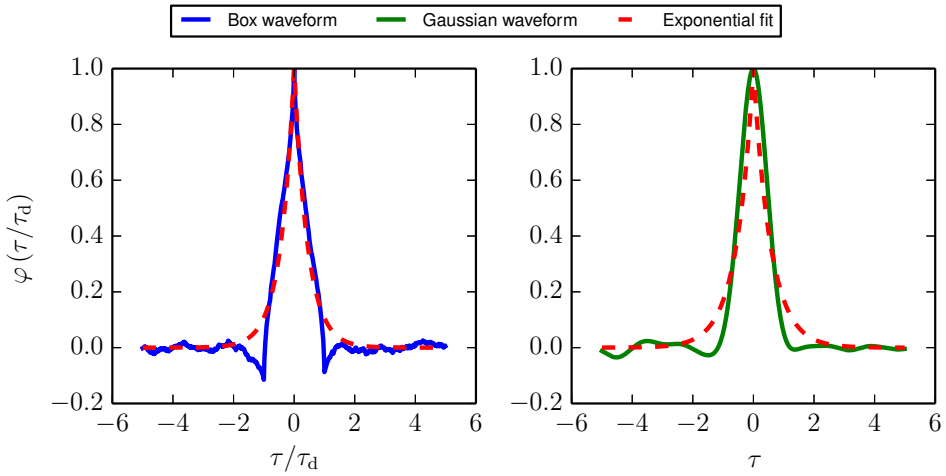

(b) Pulse waveforms are box (left) and gaussian (right).

Figure 4.12: Conditionally averaged signals with $K = 10^5$ and $\gamma = 10$. Pulse amplitudes and waiting times are exponentially distributed. The conditionally averaged signal has been normalized to fall off towards 0 and to have a peak at 1

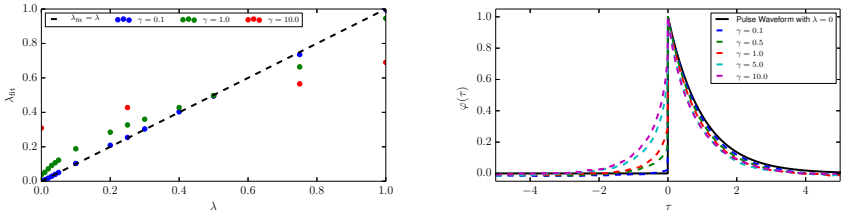

(a) Result of fitting normalized, conditionally averaged shot noise processes to a double-sided exponential function.

(b) Normalized, conditionally averaged signals with different γ superimposed on the original pulse waveform of the signal.

Figure 4.13: Comparisons of λ and waveforms after conditional averaging and normalization.

the error decreases as $\lambda \to 0.5$, implying that a very symmetric conditionally averaged signal indeed has symmetric underlying pulse waveforms, at least for signals with mid-range intermittency parameters.

Figure 4.13b presents waveforms from conditional averaging with $\lambda = 0.0$ for increasing γ, and it is clear how the discontinuous jump is gradually lost. This is due to the fact that for weakly intermittent signals, the largest peaks are not necessarily due to only large pulse amplitudes, but also to pockets of lower amplitude pulses forming one large burst.

4.2.4 Conclusion

Returning to the questions in Section 4.1.1, only the third question can be answered positively; when we have exponential pulse waveforms, they are well preserved. The other questions cannot in general be answered positively for $\gamma \geq 1$, although if the ratio between τ_{r} and τ_{f} is close to 1, then this will show up in conditional averaging as well.

Conditional averaging may also point to a loss of information about the underlying pulse amplitude and waiting time distributions. In the case of pulse waiting times, this loss leads to exponentially distributed waiting times between the peaks of the signal, which may be interpreted as pulse overlap pushing the number of large scale events in the shot noise process towards a Poisson distribution. In the case of pulse amplitudes, pulse overlap seems to create a lessening of large values, pushing the distribution of large scale events towards a Rayleigh distribution.

Thus, conditional averaging will reveal the structure of the waveforms, but little else of interest to us. It does however present an interesting thought: if the

pulse amplitude distribution and pulse waiting time distribution is irrevocably lost in the creation of the signal, then the assumptions about them may be very flexible; that is effects that could be due to changes in waiting time and amplitude distribution will instead be ascribed to changes in (for instance) the intermittency parameter.

5

Results from TCV

In the introduction, we presented the TCV tokamak and the results from a particular experimental run of the machine, discharge 26701. We used conditional averaging of the experimental data to motivate the investigation of the statistical properties of a shot noise process, and to place particular weight on shot noise processes with exponentially distributed pulse amplitudes, Poisson distribution of pulse events and the double-sided exponential pulse shape. Even though Section 4.2 shows that the waiting time distribution and amplitude distribution of conditionally averaged data cannot be used to conclusively predict the waiting time- and amplitude distribution of the underlying pulses, these assumptions still lead to strong results in other areas, particularly in excess time statistics. Here, we will present the results from applying the methods in this thesis to the experimental data set from TCV.

From the introduction, we have a preliminary estimate of $\gamma = 1.92$ from the PDF of the normalized, detrended ion saturation current $\widehat{J}_{\text{sat}}$. We also have two different sets of rise- and fall time. From conditional averaging, these have the values $\tau_{\text{r}} = 5.14\mu s$ and $\tau_{\text{f}} = 10.7\mu s$. From fitting to the autocorrelation function, we have $\tau_{\text{r}} = 0.615\mu s$ and $\tau_{\text{f}} = 15.3\mu s$. These describe vastly different pulse waveforms, the waveform from conditional averaging is a double sided waveform with $\tau_{\text{f}} \approx 2\tau_{\text{r}}$, while fitting to the autocorrelation function implies that the waveform is close to a one-sided waveform.

Still, both of these estimates give $\tau_{\text{d}} = 15.9\mu s$. And they are not inconsistent;

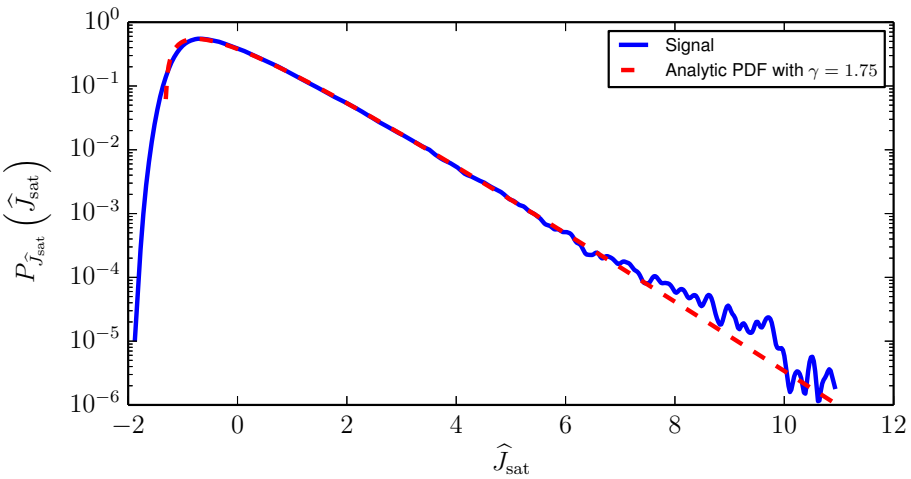

Figure 5.1: PDF of the normalized particle density

from Section 4.2.3, we know that the pulse shape of the conditionally averaged signal is more symmetric than the pulse shape of the original shot noise process, and that this effect increases with γ. This value for $\tau_{\rm d}$ will in the following be kept fixed, and for further parameter fitting we will use $\lambda = \tau_{\rm r}/\tau_{\rm d}$. From conditional averaging, we have $\lambda_{\rm C} = 0.323$, while the fit to the autocorrelation function gives $\lambda_{\rm R} = 0.0387$.

5.1 Moments of the normalized ion saturation current

From the detrended ion saturation current probe time series, we calculate the skewness and kurtosis moments. They are presented below:

$$S_{\widehat{J}_{\rm sat}} = 1.51 \tag{5.1}$$

$$F_{\widehat{J}_{\rm sat}} = 6.65 \tag{5.2}$$

Using $S_\Phi = 2/\gamma^{1/2}$, we estimate γ to have the value 1.75. Figure 5.1 presents the PDF of $\widehat{J}_{\rm sat}$ along with the normalized gamma distribution [see appendix, Eq. (B.25)] with shape parameter $\gamma = 1.75$. Comparing this to Figure 1.6, there is little difference between the analytic expressions with $\gamma = 1.75$ and $\gamma = 1.92$. We will in the following use $\gamma = 1.75$ as our base estimate of the intermittency parameter, since it comes directly from the signal, and not from a fit to a PDF. Note that $\gamma = 1.75$ gives a theoretical flatness of $F_\Phi = 3 + 6/\gamma = 3 + 6/1.75 = 6.43$, which is consistent with the flatness measured from the signal.

5.2 Moments of the derivative of the normalized ion saturation current

To have a unitless time derivative of the ion saturation current, we will use

$$\eta = \tau_{\mathrm{d}} \frac{\mathrm{d}\widehat{J}_{\mathrm{sat}}}{\mathrm{d}t} = \frac{\tau_{\mathrm{d}}}{J_{\mathrm{rms}}} \dot{J}, \tag{5.3}$$

where we have from the introduction that $J_{\mathrm{rms}} = 4.89\mathrm{mA}$, and τ_{d} is given above. In Table 5.1, we present the moments of η. In the first column, the moments are calculated from the signal. In the second column, we have used the analytical values from Section 2.2.2 with $\gamma = 1.75$ and $\lambda = \lambda_{\mathrm{C}}$. In the third column, we have used analytical expressions with the same γ and $\lambda = \lambda_{\mathrm{R}}$. It is evident that neither fit the values from the signal well. Indeed, there is no good fit to these moments for the moments of the derivative of a shot noise process.

	Experimental	λ_{C}	λ_{R}
$\langle\eta\rangle$	$3.04 \cdot 10^{-5}$	0	0
η_{rms}	4.02	2.14	5.19
S_η	1.02	1.13	7.24
F_η	19.3	8.36	85.0

Table 5.1: Comparison of moments of the derivative of the normalized ion saturation current.

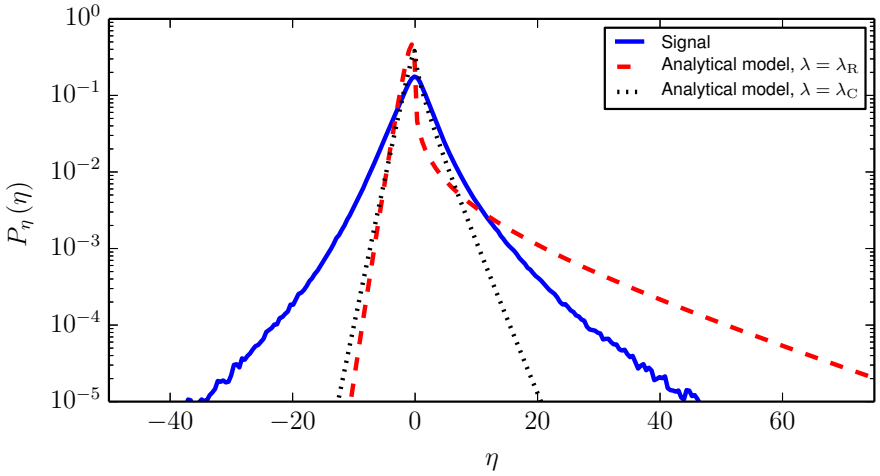

Figure 5.2: PDF of the normalized derivative of the ion saturation current from TCV Discharge 27601. Note the logarithmic scale used for the y-axis.

In Figure 5.2 we present the PDF of η along with the analytical expression from Eq. (2.100) with $\gamma = 1.75$ and both $\lambda = \lambda_{\mathrm{R}}$ and $\lambda = \lambda_{\mathrm{C}}$ [$\langle A\rangle$ has been rescaled away since we divide by J_{rms} in Eq. (5.3)]. From this figure, it is clear why

the moments in Table 5.1 do not fit, as the analytic model is a poor match to the actual shape of the PDF. These differences should not come from either the 5-point polynomial method for differentiation of the signal or from the Gaussian kernel method used for estimating the PDF; both of these methods have been tested against synthetic data. The likeliest source of these differences is the same as for the problems with the PDF estimate of $\widehat{J}_{\text{sat}}$; the signal has negative values not reachable by a shot noise process with positive definite pulse shapes.

Compared to the experimental measurement, the analytic PDF for $\lambda = \lambda_R$ is too low for large negative values of η ($\eta < -5$) and for small positive values for η ($0 < \eta < 15$), while it is too high for small negative and large positive values ($-5 < \eta < 0$ and $\eta > 15$). A possible interpretation is the following: For a signal with small rise time and large fall time, we expect to see a derivative with small negative values (due to the slow decay) and large positive values (rapid growth). When the signal falls to negative values frequently and stays at negative values for extended periods, we expect to see more large negative values for the derivative (to bring the signal value down) and more small positive derivatives (not bringing the signal values up to higher values). By comparison, large, positive derivatives becomes less likely. The peak seen at small negative values for the analytic expression in Figure 5.2, which is not present for the PDF from the experimental signal, is due to the overwhelming amount of time spent at slow decay, compared to the time spent at rapid growth. This disappears when the large negative values and the small positive values become more likely. Note that the fit for $\lambda = \lambda_C$ is no better, with less likelihood of both positive and negative values as compared to the PDF from the signal.

5.3 Excess time statistics for the TCV data

We will now look at excess time statistics of the TCV ion saturation current. With the estimated value $\gamma = 1.75$, we are in the intermediate regime. We will in the following compare the general model found in Section 3.2 to the non-intermittent limit found in Section 3.3, since these two are qualitatively different and the non-intermittent limit is prevalent in the literature [Rice, 1945, Fattorini et al., 2012, Sato et al., 2012]. The strong intermittency model is found by taking the limit $\gamma \to 0$ in the general model, and is therefore not discussed here. Note that since we are using the normalized signal, we are also using the normalized threshold, $\widehat{J}_{\text{sat}} > \zeta$.

It is also important to note that while the problems with the experimental data set and therefore the signal η above may influence comparisons with the analytic, general model (since it depends on the joint PDF between the signal and its derivative), these problems do not affect the calculation of the excess time statistics from the experimental data set itself, since these calculations only use the signal, and not its derivative.

5.3.1 Fraction of time above threshold

In Figure 5.3, the fraction of time spent above threshold, $\mathscr{T}(\zeta)/T$ is presented. The solid blue line is found from the signal itself, the dashed red line is Eq. (3.12), with $\gamma = 1.75$ and the black dotted line is the non-intermittent Gaussian limit, Eq. (3.25). The expression for the general model fits very well, at least for $\zeta < 6$. This is to be expected, as the expression for the general model is simply the complementary cumulative distribution of $\widehat{J}_{\text{sat}}$, and we already know that $\widehat{J}_{\text{sat}}$ is well fitted by a Gamma distribution. The non-intermittent limit does not fit at all. Again, this is to be expected as γ estimated from the experimental data is of order unity.

5.3.2 Rate of positive threshold crossings

The rate of upwards crossings, $\mathscr{N}(\zeta)/N$, with $N = 5.8 \times 10^6$ being the total number of data points in the time series, is presented in Figure 5.4. The blue line is calculated from the signal itself, the red dashed line is for the general model, from Eq. (3.14) with $\tau_{\text{d}} = 15.9\mu\text{s}$, $\gamma = 1.75$ and $\lambda = \lambda_{\text{R}}$, and the black dotted line is the Gaussian model, Eq. (3.26), with the mean and rms-values of $\widehat{J}_{\text{sat}}$ and η calculated from the signal. Again, the non-intermittent limit falls off far too quickly, as expected. Neither does the general model fit exactly, the peak of the general model is too far to the right, it is too low for negative ζ-values and

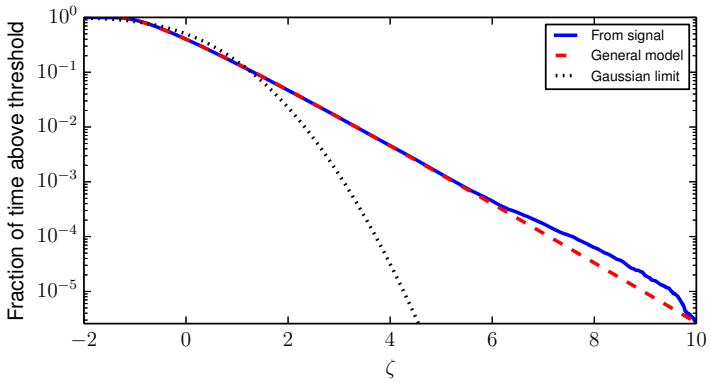

Figure 5.3: TCV Discharge 27601: Fraction of time above threshold as a function of the normalized threshold, compared to the general model and the non-intermittent limit.

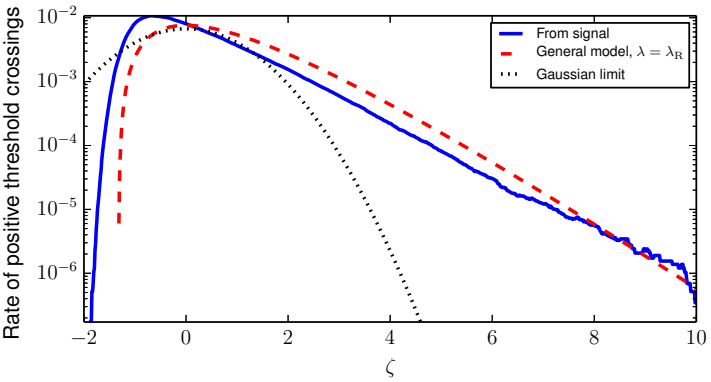

Figure 5.4: TCV Discharge 27601: Rate of positive threshold crossings as a function of the normalized threshold, compared to the general model and the non-intermittent limit.

too high for positive ζ-values. This is because the general model is derived by using the joint PDF of $\widehat{J}_{\text{sat}}$ and η, and we know that the PDF of η does not fit the theoretical PDF from Eq. (2.100). The difference can also be explained from the negative ion saturation current values. Since the signal spends more time at low values, the threshold crossings for $\zeta < 0$ happen more often than is expected from theory. For the same reason, threshold crossings at higher values happens less often than the general model predicts. Still, the qualitative behaviour of the general model is very close to the qualitative behaviour of the calculations from the signal, and is a large improvement over the non-intermittent model.

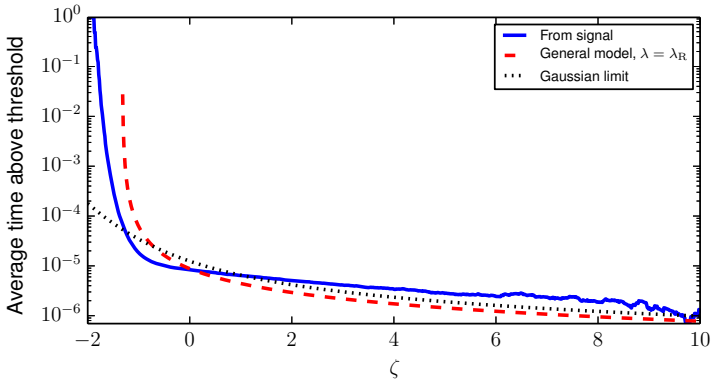

Figure 5.5: TCV Discharge 27601: Average time above threshold as a function of the normalized threshold, compared to the general model and the non-intermittent limit.

5.3.3 Average time above threshold

In Figure 5.5, the average time above threshold, $\langle \mathcal{T} \rangle(C)$, is presented. The blue line is the average time above threshold calculated from the signal, the red dashed line is the general model, from Eq. (3.15), with the same parameter values as above and the black dotted line is the Gaussian limit, from Eq. (3.27), with the same parameters as above. The discrepancy between the general model and the signal values has the same explanation as for $\mathcal{N}(\zeta)$, since the analytic expression for $\langle \mathcal{T} \rangle(\zeta)$ uses the expression for $\mathcal{N}(\zeta)$. Despite the problems with the predictions in the non-intermittent limit in Sections 5.3 and 5.3.2, for $\zeta > 0$ these problems cancel out. The Gaussian limit and the general model predict essentially the same behaviour for these ζ-values, only for $\zeta < 0$ is the behaviour of the Gaussian limit qualitatively different from the general model and the signal values. As in Section 5.3.2, the general model is qualitatively in agreement with the experimental measurements although it predicts lower average time above threshold for large ζ than is found from the TCV data set.

Note that the time above threshold falls very slowly for large threshold values. For $\zeta < 0$, the decrease in $\langle \mathcal{T} \rangle$ is very rapid, but from $\zeta = 0$ (which is threshold at the mean value) to $\zeta = 6$ (threshold equals 6 times the rms-value above the mean value), $\langle \mathcal{T} \rangle$ decreases from $8.28 \cdot 10^{-6}$s to $2.43 \cdot 10^{-6}$s. As the threshold value increases, the time the large bursts spends above threshold decreases, lowering the average time above threshold. But at the same time, the smaller bursts no longer contribute short times above threshold to the average value, increasing the average time above threshold. Evidently, these two effects almost cancel each other, resulting in a slowly decreasing average time above threshold.

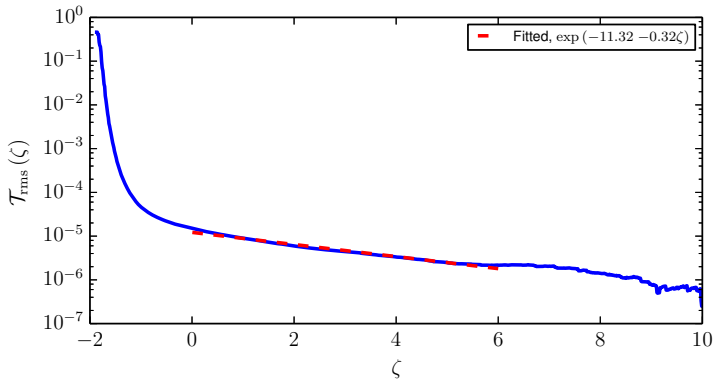

Figure 5.6: TCV Discharge 27601: Rms-value of time above threshold as a function of the normalized threshold.

5.3.4 Rms-value of time above threshold

In Figure 5.6, we present the rms-value of time above threshold, $\mathcal{T}_{\mathrm{rms}}$, as a function of ζ. Included is also an exponential fit in the interval $0 < \zeta < 6$. The rms-value has some of the same basic behaviour as the average time above threshold; as ζ increases from negative values towards zero, the function falls rapidly. This is followed by a slow decay for $\zeta > 0$. At the mean signal value, we have $\mathcal{T}_{\mathrm{rms}}(\zeta = 0) = 1.50 \times 10^{-5}$, while 6 times the rms-value above $\langle \widehat{J}_{\mathrm{sat}} \rangle$, $\mathcal{T}_{\mathrm{rms}}(\zeta = 6) = 2.16 \times 10^{-6}$. The $\mathcal{T}_{\mathrm{rms}}$-value falls less than one decade in this interval. The fitted exponential function suggests exponential behaviour of the rms-value for large threshold values.

5.3.5 PDF of time above threshold

In Figure 5.7, the PDF of $\mathcal{T}$ is presented for some values of ζ, along with exponential fits to these functions. In all cases, the PDF is a monotonically decreasing function with exponential decay for large $\mathcal{T}$. The first data point in all figures is above the exponential fit, suggesting faster than exponential decay for small $\mathcal{T}$-values. This decreases as the threshold ζ increases, although otherwise the shape of the PDFs are universal. This qualitatively fits with the PDFs of $\mathcal{T}$ for synthetic data, see Section 3.6.6, where we concluded that the PDF is a monotonically decreasing function for $\gamma > 1$.

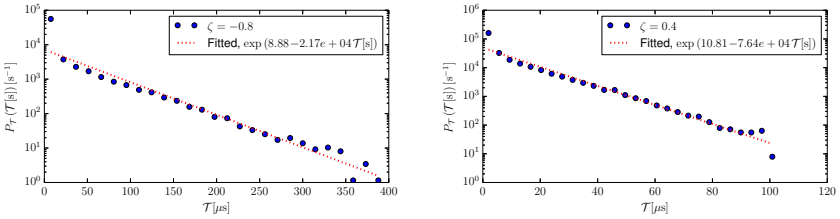

(a) PDF of time above threshold for $\zeta = -0.8$

(b) PDF of time above threshold for $\zeta = 0.4$

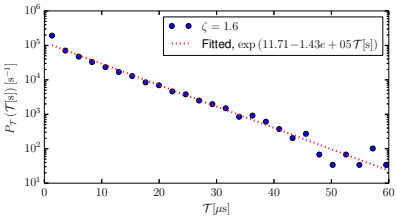

(c) PDF of time above threshold for $\zeta = 1.6$

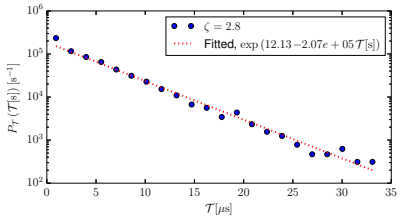

(d) PDF of time above threshold for $\zeta = 2.8$

Figure 5.7: TCV Discharge 27601: PDF of time above threshold as a function of time above threshold for different threshold values.

6

Conclusion

In this thesis, we set out to investigate the statistical properties of the intermittent plasma fluctuations in the tokamak SOL. Our investigation focused on a shot noise process with exponential pulse shapes with exponentially distributed pulse amplitudes, arriving according to a Poisson process, and we will exclusively focus on this process in the summary unless otherwise noted. This particular model was motivated by conditional averaging of the TCV Discharge 27601 ion saturation current, which yielded exponentially distributed waiting times and amplitudes of the conditionally averaged bursts, as well as exponential burst waveforms. In addition, the PDF, autocorrelation function and power spectral density of the ion saturation current coincided well with those predicted by the shot noise process described above, further motivating this particular model.

Chapter 2 focused on the statistical properties of the shot noise model. Campbell's theorem gave the mean and rms-value of a shot noise process and we found that for four different waiting time and amplitude distributions, the relative fluctuation level $\Phi_{\mathrm{rms}}/\langle\Phi\rangle$ primarily scales as $1/\gamma = \tau_{\mathrm{d}}/\tau_{\mathrm{w}}$, justifying this as an intermittency parameter. We found the PDF and moments of Φ, as well as the parabolic relation between skewness and flatness of Φ: $F_\Phi = 3 + 3S_\Phi^2/2$, showing that the flatness of a shot noise process is always greater than or equal to the flatness of a Gaussian process. Φ was shown to be Gamma-distributed, with scale parameter γ and shape parameter $\langle A\rangle$. The autocorrelation function and power spectral density of the shot noise process were also discussed.

Using the double-sided exponential waveform, we were able to compute the moments of the derivative of the shot noise process, Θ, as well as the PDF of Θ. We also found an expression for the joint PDF between Φ and Θ. This joint PDF was then used in Chapter 3 to derive a general model for the excess time statistics of a shot noise process. This general model was compared to the non-intermittent Gaussian limit, the strong intermittency limit and the results presented by Biermé and Desolneux [2012]. It was found that for $\gamma \to \infty$, the general model and the non-intermittent limit are in agreement. It was also show how, in the strong intermittency limit, the probability density function for the time above threshold $P_{\mathcal{T}}(\mathcal{T}|C)$ can be found. These results were compared to computations of excess time statistics from synthetically generated shot noise processes. For synthetically generated time series, the PDF of $\mathcal{T}$ and $\mathcal{T}_{\text{rms}}$ were also discussed. The cases studied suggest that $P_{\mathcal{T}}(\mathcal{T}|C)$ is unimodal for $\gamma < 1$, while it is monotonically decreasing for $\gamma \geq 1$.

In Chapter 4, conditional averaging of synthetically generated shot noise processes with different pulse shapes, pulse waiting times and pulse amplitudes was presented. It was shown that the waiting time between conditionally averaged bursts tends towards an exponential distribution, irrespective of the underlying waiting time distribution for individual pulses. This may come from the loss of information about the underlying distributions, as discussed in Chapter 4. In the same way, the amplitude distribution also tended towards an exponential distribution. For the waveforms tested, conditional averaging does seem to preserve the pulse shape, but not the parameters τ_{r} and τ_{f}. The shapes become more symmetrical with increasing γ.

In Chapter 5, we applied excess time statistics to the TCV Discharge 27601 ion saturation current. It was found that the PDF of the derivative of this current did not fit well with the data, most likely due to the problems with negative values in the original data set. Still, the general model for excess time statistics was in qualitative agreement with the excess time statistics computed from the signal itself. This was compared to the non-intermittent Gaussian limit, which did not fit for $\mathscr{T}(\zeta)$ or $\mathscr{N}(\zeta)$, but coincided well with the general model for $\langle\mathcal{T}\rangle(\zeta)$ with large ζ-values. It was noted how $\langle\mathcal{T}\rangle(\zeta)$ and $\mathcal{T}_{\text{rms}}(\zeta)$ exhibited slow, exponential decay for $\zeta > 0$. The PDF of $\mathcal{T}$ was computed for some values of ζ. All were well fitted to an exponential for large $\mathcal{T}$, and all exhibited faster than exponential decay for small values of $\mathcal{T}$.

The primary results of this thesis, which as far as we know has not been derived before, is extending the one-sided exponential waveform to the continuous double-sided exponential waveform, allowing the computation of the joint PDF between a shot noise process and its derivative. Further, this was used to find a general model for the excess times of the shot noise process. Lastly, it was shown that the predictions of this model agrees better with the excess time statistics of

the TCV Discharge 27601 ion saturation current than the predictions of the non-intermittent Gaussian model, used before in the literature. The general model derived agrees qualitatively with the excess statistics for the ion saturation current.

6.1 Future work and prospects

In this thesis, we have performed excess statistics for the TCV data set. In the future, these methods will be applied to Alcator C-Mod gas puff imaging data [Garcia et al., 2013a,b]. Other future plasma applications include divertor region measurements, including probes and radiation. Previously, excess time statistics has been applied to for instance basic plasma experiments [Fattorini et al., 2012], space plasma [Sato et al., 2012] and concentration fluctuations in the atmosphere [Kristensen et al., 1991, **?**].

Concerning further work on the material in this thesis, exploring other pulse shapes, pulse waiting time and amplitude distributions may be fruitful. The general model should also be tested for robustness concerning changes in these values. The conditional average gave similar results for a wide range of pulse amplitude and waiting time distributions and the general excess time model may prove to do the same. Lastly, the PDF for the time above threshold in the strong intermittency limit has already been found, and the form of the PDF of time above threshold for the TCV Discharge 27601 ion saturation current gives hope that it is possible to find a general expression for this PDF.

A

Special Functions

The appendix contains results from and formulations of some non-elementary functions and statistical distributions in addition to the definition and notation of fourier transform, statisitcal moments and the characterisitc functions used througout this text. Wikipedia and Wolfram Math World have been used extensively as resources.

A.1 The Fourier transform $\mathcal{F}$

For two functions $g(t)$ and $G(\omega)$ defining a Fourier transform pair

$$g(t) \overset{\mathcal{F}}{\leftrightarrow} G(\omega),$$

we will use the asymmetric Fourier transform:

$$G(\omega) = \mathcal{F}[g(t)](\omega) = \int_{-\infty}^{\infty} \mathrm{d}t\, g(t) \exp(-i\omega t), \tag{A.1}$$

$$g(t) = \mathcal{F}^{-1}[G(\omega)](t) = \frac{1}{2\pi} \int_{-\infty}^{\infty} \mathrm{d}\omega\, G(\omega) \exp(i\omega t). \tag{A.2}$$

A.2 The gamma function $\Gamma(s)$

The gamma function is given as:

$$\Gamma(s) = \int_0^\infty \mathrm{d}t\, t^{s-1} \exp(-t). \tag{A.3}$$

The defining properties of the gamma function are:

$$\Gamma(1) = 1, \tag{A.4}$$
$$\Gamma(s+1) = s\,\Gamma(s). \tag{A.5}$$

A.2.1 Large arguments

We will use Stirling's approximation for $\Gamma(s)$ for large s:

$$lim_{s\to\infty} \frac{\Gamma(s+1)}{\sqrt{2\pi s}\, s^s \, \exp(-s)} = 1. \tag{A.6}$$

A.2.2 Small argument

When the argument s of $\Gamma(s)$ is close to zero, we can use properties (A.4) and (A.5):

$$\lim_{s\to 0} s\Gamma(s) = \Gamma(s+1) = \Gamma(1) = 1. \tag{A.7}$$

A.2.3 The incomplete gamma functions

The gamma function can be split into an upper and lower incomplete gamma function,

$$\Gamma(s) = \Gamma_\mathrm{L}(s,x) + \Gamma_\mathrm{U}(s,x), \tag{A.8}$$

where the lower incomplete gamma function is

$$\Gamma_\mathrm{L}(s,x) = \int_0^x \mathrm{d}t\, t^{s-1} \exp(-t), \tag{A.9}$$

and the upper incomplete gamma function is

$$\Gamma_\mathrm{U}(s,x) = \int_x^\infty \mathrm{d}t\, t^{s-1} \exp(-t). \tag{A.10}$$

We will also use the *regularized* gamma functions

$$P(s,x) = \frac{\Gamma_{\mathrm{L}}(s,x)}{\Gamma(s)}, \tag{A.11}$$

and

$$Q(s,x) = \frac{\Gamma_{\mathrm{U}}(s,x)}{\Gamma(s)}. \tag{A.12}$$

Note that $P(s,x) + Q(s,x) = 1$.

A.2.4 The limit of large x

In the case $x \to \infty$, we have

$$\lim_{x\to\infty} frac\Gamma_{\mathrm{U}}(s,x)x^{s-1}\exp(-x) = 1, \tag{A.13}$$

$$\lim_{x\to\infty} \Gamma_{\mathrm{L}}(s,x) = \Gamma(s). \tag{A.14}$$

A.2.5 The limit of small x

For $x \ll 1$, we have

$$\lim_{x\to 0} \frac{\Gamma_{\mathrm{L}}(s,x)}{x^s/s} = 1, \tag{A.15}$$

$$\lim_{x\to 0} \Gamma_{\mathrm{U}}(s,x) = \Gamma(s) - \lim_{x\to 0} \Gamma_{\mathrm{L}}(s,x) = \Gamma(s) - \frac{1}{s}x^s. \tag{A.16}$$

A.3 The error function

The error function and the complementary error function are defined as

$$\mathrm{erf}(x) = \frac{2}{\sqrt{\pi}} \int_0^x \mathrm{d}t\ \exp\bigl(-t^2\bigr), \tag{A.17}$$

$$\mathrm{erfc}(x) = 1 - \mathrm{erf}(x) = \frac{2}{\sqrt{\pi}} \int_x^\infty \mathrm{d}t\ \exp\bigl(-t^2\bigr). \tag{A.18}$$

These functions are related to the incomplete gamma functions by

$$\Gamma_{\mathrm{L}}\left(\frac{1}{2},x\right) = \sqrt{\pi}\,\mathrm{erf}(\sqrt{x}), \tag{A.19}$$

$$\Gamma_{\mathrm{U}}\left(\frac{1}{2},x\right) = \sqrt{\pi}\,\mathrm{erfc}(\sqrt{x}). \tag{A.20}$$

A.3.1 The limit $x \to \infty$

The complementary error fuction has an asymptotic limit for large, real valued x,

$$\lim_{x\to\infty} \operatorname{erfc}(x) = \frac{\exp(-x^2)}{\sqrt{\pi}x} \sum_{n=0}^{\infty} (-1)^n \frac{(2n-1)!!}{(2x^2)^n}. \tag{A.21}$$

A.4 A useful limit

Given a function $f(x)$ such that

$$f(x) = \left(1 + \frac{x}{a^{1/2}}\right)^a \exp\left(-a^{1/2}x\right),$$

where $a > 0$ is a free parameter. The limit $a \to \infty$ turns out to be simple:

$$\begin{aligned}
\lim_{a\to\infty} f(x) &= \exp\left\{ \lim_{a\to\infty} \ln[f(x)] \right\} \\
&= \exp\left\{ \lim_{a\to\infty} -a^{1/2}x + a \ln\left(1 + \frac{x}{a^{1/2}}\right) \right\} \\
&= \exp\left\{ \lim_{a\to\infty} -a^{1/2}x + a\left(\frac{x}{a^{1/2}} - \frac{x^2}{2a} + \frac{x^3}{3a^{3/2}} + \dots\right) \right\} \\
&= \exp\left\{ \lim_{a\to\infty} -\frac{x^2}{2} + \frac{x^3}{3a^{1/2}} + \dots \right\} \\
&= \exp\left(-\frac{x^2}{2}\right).
\end{aligned}$$

B

Statistical Concepts

In the following, X denotes a random variable with the probability density function (PDF) (or, if X only takes on discrete values, the probability mass function) $P_X(X)$ and the cumulative distribution function (CDF) $\text{CDF}_X(X)$. Here and in the following, $\mathcal{P}[A]$ is the probability of A.

B.1 The cumulative distribution function

We define the CDF of a random variable X as

$$\text{CDF}_X(x) = \mathcal{P}[X \leq x], \tag{B.1}$$

and it has the following properites:

- $\text{CDF}_X(\infty) = 1$, $\text{CDF}_X(-\infty) = 0$.
- $\text{CDF}_X(x)$ is a nondecreasing function of x.
- $\text{CDF}_X(x)$ is continous from the right.

B.2 The probability density function

The PDF of X is defined from the CDF of X:

$$P_X(x) = \frac{\mathrm{dCDF}_X(x)}{\mathrm{d}x}. \tag{B.2}$$

It has the properties

- $P_X(x) \geq 0$.
- $\int_{-\infty}^{\infty} \mathrm{d}x\, P_X(x) = 1$.
- $\mathrm{CDF}_X(x) = \int_{-\infty}^{x} \mathrm{d}\xi\, P_X(\xi)$.
- $\mathcal{P}[a \leq X \leq b] = \int_{a}^{b} \mathrm{d}x\, P_X(x)$

If X only takes discrete values, the integrals in the above equations are replaced by sums, such that for instance

$$\sum_{x=-\infty}^{\infty} P_X(x) = 1.$$

B.3 Moments of X

The moments $\langle X^n \rangle$ where n is an integer are used to characterize the PDF of X. Here and in the following, the angular brackets denotes an average of a random variable over all its values. The first four moments are the most important, as they estimate the essential properties of the distribution (location, spread, skewedness and flatness). The *raw* moments are

$$\langle X^n \rangle = \int_{-\infty}^{\infty} \mathrm{d}x\, x^n P_X(x), \tag{B.3}$$

while the *central* moments are

$$\mu_n = \langle (X - \langle X \rangle)^n \rangle, \quad n > 1. \tag{B.4}$$

B.3.1 The mean value $\langle X \rangle$

The mean value is the first raw moment,

$$\langle X \rangle = \int_{-\infty}^{\infty} \mathrm{d}x \, x P_X(x). \tag{B.5}$$

The mean may coincide with, but is not equivalent to, the most likely value in the distribution (called the *mode*) or the value separating the left half of the distribution from the right half (called the *median*).

B.3.2 The variance and rms values

The second central moment is called the variance,

$$\mu_2 = \left\langle (X - \langle X \rangle)^2 \right\rangle = \left\langle X^2 \right\rangle - \langle X \rangle^2. \tag{B.6}$$

This value denotes the spread of the likely values from a PDF; a small variance means that the X-values are close to the mean $\langle X \rangle$, while a large variance means the X-values spread out far from the mean. We will often use the square root of the variance (which we call the rms-value) instead of the variance,

$$X_{\mathrm{rms}} = \left\langle (X - \langle X \rangle)^2 \right\rangle^{1/2}, \tag{B.7}$$

and, if we are referring to the variance, we will use the notation $X_{\mathrm{rms}}^2 = \mu_2$.

B.3.3 Skewness

The skewness is a measure of the asymmetry of the distribution function. Negative skewness indicates that the left tail of the distribution is longer or fatter than the right tail. Positive skewness indicates a longer or fatter right tail. A symmetric distribution has zero skewness. The skewness of X is written as S_X, and we have

$$S_X = \frac{\mu_3}{\mu_2^{3/2}}. \tag{B.8}$$

B.3.4 Kurtosis

The kurtosis (or flatness) is a measure of how peaked a distribution function is, and how heavy its tail is. A sharp distribution or one with fatter tails has a large kurtosis, while a distribution with a rounded peak and thin tails has a low kurtosis. The flatness of X is written as F_X, and is given by

$$F_X = \frac{\mu_4}{\mu_2^2}. \tag{B.9}$$

Excess kurtosis is definded as $F_X - 3$, and a normal distribution has zero excess kurtosis.

B.3.5 Preserving S_X and F_X under normalization

We will sometimes wish to make the normalization

$$\widehat{X} = \frac{X - \langle X \rangle}{X_{\text{rms}}},$$

such that $\langle \widehat{X} \rangle = 0$ and $\widehat{X}_{\text{rms}} = 1$. Thus the central moments of $\widehat{X}$ are

$$\begin{aligned}
\widehat{\mu}_n &= \left\langle \left(\widehat{X} - \left\langle \widehat{X} \right\rangle \right)^n \right\rangle \\
&= \left\langle \left(\frac{X - \langle X \rangle}{X_{\text{rms}}} \right)^n \right\rangle \\
&= \frac{\langle (X - \langle X \rangle)^n \rangle}{X_{\text{rms}}^n} \\
&= \frac{\mu_n}{\mu_2^{n/2}}.
\end{aligned}$$

In this case, we have $S_{\widehat{X}} = S_X$ and $F_{\widehat{X}} = F_X$ since

$$S_{\widehat{X}} = \frac{\widehat{\mu}_3}{\widehat{\mu}_2^{3/2}} = \frac{\mu_3}{\mu_2^{3/2}} = S_X,$$

and

$$F_{\widehat{X}} = \frac{\widehat{\mu}_4}{\widehat{\mu}_2^2} = \frac{\mu_4}{\mu_2^{4/2}} = F_X.$$

B.3.6 Estimation of moments

If $\{x_k\}_{k=1}^K$ is a collection of K data points drawn from the distribution of X, we can estimate the mean value by

$$\langle x \rangle = \frac{1}{K} \sum_{k=1}^{K} x_k, \tag{B.10}$$

and we estimate the central moments by

$$\langle x^n \rangle = \frac{1}{K} \sum_{k=1}^{K} \sqrt{(x_k - \langle x \rangle)^n}. \tag{B.11}$$

The estimate of the mean is unbiased, while the rest of the estimators are biased, although they can be redefined to provide unbiased estimations. It has

previously been found that for a shot noise process with one-sided exponential pulse shapes, exponentially distributed pulse amplitudes and arrivals according to a Poisson process, the mean square error of all estimators are inversly proportional to the number of samples N for $N\Delta t/\tau_\mathrm{d} \gg 1$ [Kube and Garcia, 2015]. In addition, it was demonstrated that the estimated kurtosis has significaltly larger relative error than the estimated skewness.

B.4 The characteristic function

The characteristic function of a random variable X and the PDF of X are a Fourier transform pair [although commonly defined with the $1/(2\pi)$-constant on the other transformation compared to Eq. (A.1) and Eq. (A.2)].

$$\langle \exp(iXu) \rangle = \int_{-\infty}^{\infty} \mathrm{d}X P_X(X) \exp(iXu), \tag{B.12}$$

$$P_X(X) = \frac{1}{2\pi} \int_{-\infty}^{\infty} \mathrm{d}u \, \exp(-iXu) \langle \exp(iXu) \rangle. \tag{B.13}$$

The characteristic function has two properties we will use: If X and Y are two random variables with characteristic functions $\langle \exp(iXu) \rangle$ and $\langle \exp(iYv) \rangle$, then adding the random variables corresponds to multiplying their characteristic functions:

$$Z = X + Y \iff \langle \exp(iZu) \rangle = \langle \exp(iXu) \rangle \langle \exp(iYu) \rangle. \tag{B.14}$$

The second property comes from the Fourier transform nature of the characteristic function: if the characteristic function of a random variable can be separated into two characteristic functions, then the PDF of the random variable is the convolution of the PDFs corresponding to each of the separate characteristic functions. That is, if $P_{X_1}(X) \overset{\mathcal{F}}{\leftrightarrow} \langle \exp(iX_1 v) \rangle$ and $P_{X_2}(X) \overset{\mathcal{F}}{\leftrightarrow} \langle \exp(iX_2 w) \rangle$, then

$$\langle \exp(iXu) \rangle = \langle \exp(iX_1 v) \rangle \langle \exp(iX_2 w) \rangle \overset{\mathcal{F}}{\leftrightarrow} P_X(X) = P_{X_1}(X) * P_{X_2}(X), \tag{B.15}$$

where $P_{X_1}(X) * P_{X_2}(X)$ is the convolution

$$\int_{-\infty}^{\infty} \mathrm{d}\xi \, P_{X_1}(\xi) P_{X_2}(x - \xi).$$

B.5 Commonly used distribution functions

In this section, we present some properties of PDFs frequently appearing in this thesis, namely the exponential distribution, the Rayleigh distribution, the

degenerate distribution and the uniform distribution. We are particuarly interested in one-parameter distributions for positive valued random variables, $X > 0$. In the thesis, we frequently define the distributions by their mean value $\langle X \rangle$, so having one-parameter distributions is desireable. We will also express the raw moments (up to 4th moment) as functions of the mean value.

B.5.1 The exponential distribution

The exponential distribution is a one-parameter distribution defined as:

$$P_X(x;\lambda) = \lambda \exp(-\lambda x), \quad x \geq 0.$$

The mean of the random varialbe is given as

$$\langle X \rangle = \lambda^{-1},$$

so we prefer to write the exponential function as

$$P_X(x) = \frac{1}{\langle X \rangle} \exp\left(-\frac{x}{\langle X \rangle}\right), \quad x \geq 0. \tag{B.16}$$

The raw moments of the exponential distribution are are

$$\langle X^n \rangle = \frac{n!}{\lambda^n} = n! \langle X \rangle^n,$$

giving

$$\begin{aligned} \left\langle X^2 \right\rangle &= 2\langle X \rangle^2, \\ \left\langle X^3 \right\rangle &= 3\langle X \rangle^3, \\ \left\langle X^4 \right\rangle &= 4\langle X \rangle^4. \end{aligned}$$

B.5.2 The Rayleigh distribution

The Rayleigh distribution is another one-parameter distribution in standard form given by

$$P_X(x;\sigma) = \frac{x}{\sigma^2} \exp\left(-\frac{x^2}{2\sigma^2}\right), \quad x \geq 0,$$

where σ is the mode. For the Rayleigh distribution, we have the raw moments

$$\langle X^n \rangle = \sigma^n 2^{n/2} \Gamma\left(1 + \frac{n}{2}\right).$$

This gives the mean value

$$\langle X \rangle = \sigma \sqrt{\frac{\pi}{2}},$$

and we can alternatively write the Rayleigh distribution as

$$P_X(x) = \frac{\pi x}{2\langle X \rangle^2} \exp\left(-\frac{\pi x^2}{4\langle X \rangle^2}\right), \quad x \geq 0. \tag{B.17}$$

The raw moments are given in terms of the mean value as:

$$\left\langle X^2 \right\rangle = \frac{4}{\pi}\langle X \rangle^2,$$
$$\left\langle X^3 \right\rangle = \frac{6}{\pi}\langle X \rangle^3,$$
$$\left\langle X^4 \right\rangle = \frac{32}{\pi^2}\langle X \rangle^4.$$

B.5.3 The degenerate distribution

For the degenerate distribution, only one value of the random variable has nonzero probability:

$$P_X(x) = \delta(x - \langle X \rangle) \tag{B.18}$$

Thus all the values are simply $\langle X \rangle$ and the moments are given by $\langle X^n \rangle = \langle X \rangle^n$. This means that the variance of the degenerate distribution is 0 and that the skewness and kurtosis, which are defined by dividing by the variance, are undefined.

B.5.4 The uniform distribution

The uniform distribution is given as

$$P_X(x) = \begin{cases} 1/(b-a) & a \leq x \leq b \\ 0 & \text{otherwise} \end{cases}. \tag{B.19}$$

The mean value of the uniform distribution is

$$\langle X \rangle = \frac{b-a}{2},$$

and assuming the lowest cutoff point is 0, we have $a = 0$, $b = 2\langle X \rangle$ and the distribution becomes

$$P_X(x) = \begin{cases} \dfrac{1}{2\langle X \rangle} & 0 \leq x \leq 2\langle X \rangle \\ 0 & \text{otherwise} \end{cases}. \tag{B.20}$$

The central moments of this uniform distribution are given by $\mu_k = (2\langle X \rangle)^k/(k+1)$ for $k > 1$.

B.5.5 Other relevant distributions

Here, we present some other relevant distribution functions, used throughout the thesis.

The Poisson distribution

The Poisson distribution is a discrete one-parameter distribution. Its probability mass function is

$$P_X(x;\lambda) = \frac{\lambda^x}{x!}\exp(-x), \quad x \in 1,2,3,/cdots. \tag{B.21}$$

The Poisson distribution has equal mean and variance

$$\langle X\rangle = X_{\text{rms}}^2 = \lambda. \tag{B.22}$$

The Gamma distribution

The gamma distribution is a two-parameter distribution, with shape parameter $k > 0$ and scale parameter $\lambda > 0$:

$$P_X(x;k,\lambda) = \frac{x^{k-1}}{\Gamma(k)\lambda^k}\exp(-x/\lambda), \quad x \geq 0. \tag{B.23}$$

This distribution has mean $\langle X\rangle = k\lambda$ and variance $X_{\text{rms}}^2 = k\lambda^2$. The characteristic function of the Gamma distribution is

$$\langle \exp(iXu)\rangle = (1-\lambda iu)^{-k}. \tag{B.24}$$

The normalized Gamma distribution If we use the normalized random variable $\widehat{X} = X/X_{\text{rms}} - \langle X\rangle/X_{\text{rms}}$, we can get the PDF for this normalized variable Stark and Woods [2012]:

$$P_{\widehat{X}}(\widehat{x};k,\lambda) = X_{\text{rms}}P_X(X_{\text{rms}}\widehat{x} + \langle X\rangle;k,\lambda) = \frac{k^{k/2}}{\Gamma(k)}\left(\widehat{x}+k^{1/2}\right)^{k-1}\exp\left(-k^{1/2}\widehat{x}-k\right). \tag{B.25}$$

Note that this equation is independent of λ, effectively becoming a one-parameter distribution with shape parameter k. This is consistent with $S_{\widehat{X}} = S_X = 2/k^{1/2}$ and $F_{\widehat{X}} = F_X = 3 + 6/k$, where the equivalence of the moments comes fron Section B.3.5.

The mirrored Gamma distribution The gamma distribution is only defined for positive values. We also need a gamma distribution mirrored around $X = 0$ which is only defined for negative values. The shape parameter is the same as above, $k > 0$, while the scale parameter only takes negative values, $\lambda < 0$. The PDF is:

$$P_X(x; k, \lambda) = -\frac{1}{\Gamma(k)\lambda^k} x^{k-1} \exp\left(-\frac{x}{\lambda}\right), \quad x \leq 0. \tag{B.26}$$

This distribution has negative mean $\langle X \rangle = k\lambda$ and positive variance $X_{\text{rms}}^2 = k\lambda^2$.

The normal distribution

The normal distribution is defined in terms of the mean and the rms-value:

$$P_X(x; \langle X \rangle, X_{\text{rms}}) = \frac{1}{\sqrt{2\pi} X_{\text{rms}}} \exp\left[-\frac{1}{2}\left(\frac{x - \langle X \rangle}{X_{\text{rms}}}\right)^2\right]. \tag{B.27}$$

The Laplace distribution

The Laplace distribution is given as

$$P_X(x; k, \lambda) = \frac{1}{2\lambda} \exp\left(-\frac{|x - k|}{\lambda}\right), \tag{B.28}$$

where k is the location parameter and $\lambda > 0$ is the scale parameter. The four first moments of the Laplace distribution are

$$\begin{aligned} \langle X \rangle &= k, \\ X_{\text{rms}}^2 &= 2\lambda^2, \\ S_X &= 0, \\ F_X &= 6. \end{aligned}$$

The Gompertz distribution

This is from `http://www.math.uah.edu/stat/special/Gompertz.html`. The Gompertz distribution is a two-parameter distribution over positive values, with a shape parameter $k > 0$ and a scale parameter $\lambda > 0$:

$$P_X(x; k, \lambda) = \lambda k \exp[\lambda x + k - k \exp(\lambda x)], \quad x \geq 0. \tag{B.29}$$

The mean of the Gompertz distribution is

$$\langle X \rangle = \frac{1}{\lambda} \exp(k) \Gamma_{\text{U}}(0, k), \tag{B.30}$$

and the variance is

$$X_{\text{rms}}^2 = \frac{1}{\lambda^2}\exp(k)\Bigg\{-2k\sum_{n=0}^{\infty}\frac{(-k)^n}{n!(n+1)^3} - [\Gamma'(1)]^2 + \frac{\pi^2}{6} - 2\Gamma'(1)\ln(k) + [\ln(k)]^2 - \exp(k)[\Gamma_{\text{U}}(0,k)]^2\Bigg\}. \quad \text{(B.31)}$$

Note that the mean and variance are often written in terms of the Exponential Integral, Euler-Mascheroni constant and hypergeometric functions. Here, we have related all of these to gamma functions.

B.6 The connection between the Poisson distribution, the uniform distribution and the exponential distribution

Consider a random process where events happens consecutively and where we are interested in the time between events (for example time between alpha particle decay of radium, sea waves over a certain amplitude or pulse events of a shot noise process).

Let $K(T)$ denote the number of events in a time interval $[0, T]$, and the arrival times are ordered as $t_1 < t_2 < \cdots < t_K$. We will make three assumptions regarding this process:

- The probability of events happening at the same time is negligible.
- The PDF of $K(T)$ only depends on the length of the interval $[0, T]$ (and not, for instance, on how many pulses have arrived before the start of the interval).
- The number of pulses in one interval is independent on the number of pulses in other, disjoint, intervals.

In other words, we assume that the process $K(T)$ has independent, stationary, increments. Under these assumptions, $K(T)$ has a Poisson distribution [Walpole et al., 2007] with rate parameter λT,

$$P_K(K;\lambda T) = \frac{(\lambda T)^K}{K!}\exp(-\lambda T), \quad \text{(B.32)}$$

where the rate of arrivals is λ (so the mean time between events is $1/\lambda$). From Section B.5.5 we know that $\langle K(T)\rangle = \lambda T$.

We will now show that if $K(T)$ is a Poisson process, the waiting time between events $\tau_k = t_{k+1} - t_k$ is exponentially distributed with rate λ:

$$P_\tau(\tau) = \lambda \exp(-\lambda\tau) H(\tau) \tag{B.33}$$

t_k is the time until the k'th event. The waiting time until the k'th event is larger than T if and only if there are less than k pulses arriving in the time T:

$$t_k > T \iff K(T) < k. \tag{B.34}$$

Thus these two events must have the same probability:

$$\mathcal{P}[t_k > T] = \mathcal{P}[K(T) < k]. \tag{B.35}$$

If we now look at the waiting time until the first pulse arrives, we have from Eq. (B.32):

$$\mathcal{P}[t_1 > T] = \mathcal{P}[K(T) < 1] = \mathcal{P}[K(T) = 0] = P_K(0; \lambda T) = \exp(-\lambda T), \tag{B.36}$$

giving

$$\mathcal{P}[t_1 \leq T] = 1 - \exp(-\lambda T), \tag{B.37}$$

which is the CDF of an exponential distribution. Thus the waiting time until the first pulse arrives is exponentially distributed with parameter λ:

$$P_{t_1}(T; \lambda) = \lambda \exp(-\lambda T) H(T). \tag{B.38}$$

Since the number of events in one interval is independent of the events in another interval, it follows that the waiting time between t_1 and t_2 is also exponentially distributed, and so on for all waiting times. Thus, the waiting times are all exponentially distributed and Eq. (B.33) holds. Note that the result is one-way: Poisson distributed events leads to exponentially distributed waiting times, but exponentially distributed waiting times can (in theory) arise from other event distributions. It is also possible to show that if $K(T)$ is a Poisson process, the arrival times t_k are uniformly distributed on the interval $[0, T]$ [Boxma and Yechiali, 2007].

B.7 Equivalence of Gamma distribution and Gaussian distribution in the limit of large shape parameter

We will now show that in the limit $k \to \infty$, the gamma distribution (slightly rewritten)

$$G(x; k, \lambda) = \frac{1}{\lambda\Gamma(k)} \left(\frac{x}{\lambda}\right)^{k-1} \exp\left(-\frac{x}{\lambda}\right)$$

approaches the normal distribution

$$N(x;\langle X\rangle, X_{\text{rms}}) = \frac{1}{\sqrt{2\pi}X_{\text{rms}}}\exp\left[-\frac{1}{2}\left(\frac{x-\langle X\rangle}{X_{\text{rms}}}\right)^2\right].$$

From Section B.5.5, we have for the Gamma distribution $\langle X\rangle = k\lambda$ and $X_{\text{rms}} = k^{1/2}\lambda$. Writing

$$\widehat{x} = \frac{x-\langle X\rangle}{X_{\text{rms}}}$$
$$\frac{x}{\lambda} = k^{1/2}\widehat{x} + k,$$

the normal and Gamma distributions can now be written as

$$N(x;\langle X\rangle, X_{\text{rms}}) = \frac{1}{\sqrt{2\pi}X_{\text{rms}}}\exp\left(-\frac{\widehat{x}^2}{2}\right),$$

and

$$\begin{aligned} G(x;k,\lambda) &= \frac{k^{1/2}}{X_{\text{rms}}\Gamma(k)}\left(k^{1/2}\widehat{x}+k\right)^{k-1}\exp\left[-\left(k^{1/2}\widehat{x}+k\right)\right] \\ &= \frac{k^{1/2+k-1}\exp(-k)}{X_{\text{rms}}\Gamma(k)}\left(\frac{\widehat{x}}{k^{1/2}}+1\right)^{-1}\left(\frac{\widehat{x}}{k^{1/2}}+1\right)^{k}\exp\left[-k^{1/2}\widehat{x}\right]. \end{aligned}$$

Now, $\lim_{k\to\infty}\left(1+\widehat{x}/k^{1/2}\right)^{-1} = 1$, $\lim_{k\to\infty}\Gamma[k] = \sqrt{2\pi k}k^{k-1}\exp(-k)$ and from Section A.4, we have that

$$\lim_{k\to\infty}\left(\frac{\widehat{x}}{k^{1/2}}+1\right)^{k}\exp\left(-k^{1/2}\widehat{x}\right) = \exp\left(-\frac{\widehat{x}^2}{2}\right).$$

Thus, we have

$$\lim_{k\to\infty} G(x;k,\lambda) = \frac{1}{\sqrt{2\pi}X_{\text{rms}}}\exp\left(-\frac{\widehat{x}^2}{2}\right) = N(x;\langle X\rangle, X_{\text{rms}}). \tag{B.39}$$

The result in Eq. (B.39) show that the Gamma distribution and the normal distribution are the same in the limit of large scale parameter k. Obviously, this is not true for all values of x. The Gamma distribution is not defined for negative values, but as k increases, so does $\langle X\rangle$, and the probability of getting negative values from the normal distribution diminishes. However, the approximation in the curly brackets does not hold for $\widehat{x} \sim -\sqrt{k}$, and in numerical solutions the gamma function falls quickly to $-\infty$ for such values. In Figure B.1, three Gamma distributions with different scale parameter k are shown together with a normal distribution. The failure of the approximation at $-\sqrt{k}$ is clearly visible for the two smallest values ($\sqrt{5} \approx 2.2$ and $\sqrt{10} \approx 3.2$ respectively). For $k = 150$, the failure is further to the left than the plot limits. As k increases, the approximation becomes better, and at $k \sim 1000$ there is no discernible difference (not pictured).

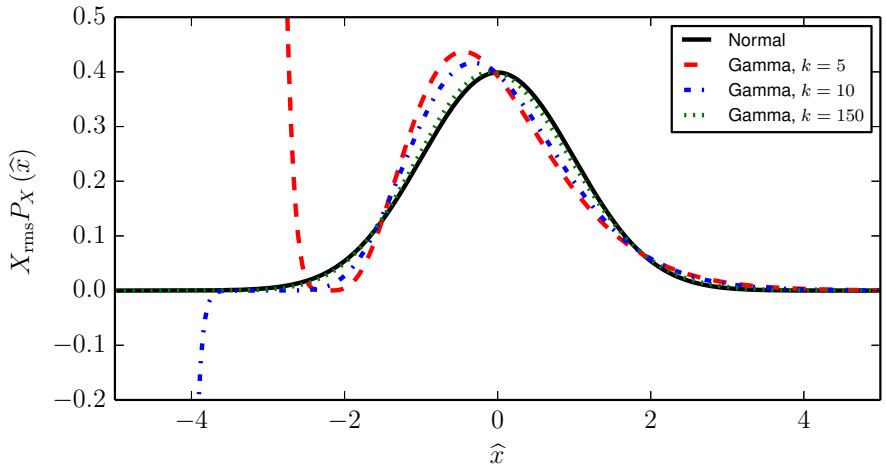

Figure B.1: Comparison of the normal distribution to the Gamma distribution for three different values of the scale parameter k.

B.8 Truncated distributions

In Section 4.1, we encounter the problem of finding $P_X(x|x > a)$ when $P_X(x)$ and $CDF_X(x)$ are known. We have from Stark and Woods [2012] that:

$$\text{CDF}_X(x|x > a) = \frac{\mathcal{P}[X \leq x, x > a]}{\mathcal{P}[x > a]}. \tag{B.40}$$

This equation can be written as

$$\text{CDF}_X(x|x > a) = \frac{\mathcal{P}[X \leq x, x > a]}{\mathcal{P}[x > a]} = \frac{\int_a^x \mathrm{d}\xi\, P_X(\xi) H_0(x-a)}{\int_a^\infty \mathrm{d}\xi\, P_X(\xi)}, \tag{B.41}$$

where the denominator follows directly from the definintion of the CDF and the numerator is the probability of finding X between x and a. The heaviside function $H_0(x-a)$ is needed since we already know that $x > a$. Now, we use

the definition of the PDF, Eq. (B.2), to find the truncated PDF:

$$\begin{aligned} P_X(x|x > a) &= \frac{\mathrm{d}}{\mathrm{d}x}\mathrm{CDF}_X(x|x > a) \\ &= \frac{\dfrac{\mathrm{d}}{\mathrm{d}x}\displaystyle\int_a^x \mathrm{d}\xi\, P_X(\xi)H_0(x-a)}{\displaystyle\int_a^\infty \mathrm{d}\xi\, P_X(\xi)} \\ &= \frac{P_X(x)H_0(x-a)}{1-\mathrm{CDF}_X(a)}. \end{aligned} \tag{B.42}$$

Thus, the truncated distribution is simply the original distribution with no values below a allowed, rescaled to preserve $\int_{-\infty}^{\infty} \mathrm{d}x\, P_X(x) = 1$. To find the truncated CDF, we go back to Eq. (B.41):

$$CDF_X(x|x > a) = \frac{\displaystyle\int_a^x \mathrm{d}\xi\, P_X(\xi)H_0(x-a)}{\displaystyle\int_a^\infty \mathrm{d}\xi\, P_X(\xi)} = \frac{\mathrm{CDF}_X(x) - \mathrm{CDF}_X(a)}{1-\mathrm{CDF}_X(a)}H_0(x-a). \tag{B.43}$$

Truncated exponential distribution

The exponential distribution has the PDF and CDF

$$\begin{aligned} P_X(x;\lambda) &= \lambda \exp(-\lambda x), \\ \mathrm{CDF}_X(x;\lambda) &= 1 - \exp(-\lambda x). \end{aligned}$$

Giving the truncated PDF and CDF

$$P_X(x|x > a;\lambda) = \lambda \exp(-\lambda[x-a])H(x-a), \tag{B.44}$$

$$\mathrm{CDF}_X(x|x > a;\lambda) = [1 - \exp(-\lambda[x-a])]H(x-a). \tag{B.45}$$

Truncated Rayleigh distribution

The Rayleigh distribution has the PDF and CDF

$$P_X(x;\sigma) = \frac{x}{\sigma^2}\exp\left(-\frac{x^2}{2\sigma^2}\right),$$
$$\mathrm{CDF}_X(x;\sigma) = 1 - \exp\left(-\frac{x^2}{2\sigma^2}\right).$$

Giving the truncated PDF and CDF

$$P_X(x|x > a;\sigma) = \frac{x}{\sigma^2}\exp\left(-\frac{x^2 - a^2}{2\sigma^2}\right)H(x-a), \tag{B.46}$$
$$\mathrm{CDF}_X(x|x > a;\sigma) = \left[1 - \exp\left(-\frac{x^2 - a^2}{2\sigma^2}\right)\right]H(x-a). \tag{B.47}$$

C

Source Code

In this chapter, the Python code is listed. We only provide code for generating synthetic time series and performing some analysis on these time series, such as calculating PDF and CDF, the conditional average and excess time statistics. We do not provide code for plotting or evaluating the analytic results, as this is all done using standard and straight forward python libraries and methods.

```
# -*- coding: utf-8 -*-
"""
Created on Thu May 14 11:09:11 2015

@author: ath019

This is a code file generated and summarized for inclusion in the thesis.
It contains code for:
- Generating synthetic shot noise time series
- Performing derivation, calculation of PDF and CDF and auto-correlation
  function and power spectral density
- Performing conditional average
- Performing excess time statistics.

No plotting or analytic computation is present. For printing reasons,
some lines have been split.
"""
import numpy as np
import scipy.stats as sps
import scipy.signal as scs
import scipy.integrate as spi
```

```
def gen_amp_ta(Tdist,Adist,K,tw,mA=1.,
               ST=None,SA=None, randT = False, randA = False):
    """ This function generates the amplitudes and arrival times
        used to make a shot noise signal.
    Tdist, Adist: what type of distribution.
    0: degenerate, 1: exponential, 2:rayleigh, 3: uniform
    K: number of bursts
    tw: average waiting time (1/gamma)

    Output is arrival times Ta, amplitudes A and end time tend

    Advanced options:

    ST and SA are seeds to the random state,
        specify them to have a particular seed.
    randT and randA are used to scramble waiting times and amplitudes.
    Use in conjuration with ST and SA to keep values the same,
            but at different locations.
    """
    # Generate array of arrival times.
    # Random numbers are drawn from the waiting time distribution,
    # the waiting time is added to the last arrival time
    # to get the next arrival time.

    # First, we generate K values Tw=[t1,t2,...,tk-1,tk]
    # Then, we make sure there is a burst at the start:
    # Tw=[0,t1,t2,...,tk-1,tk]
    # We then take the arrival times as the cummulative sum of these,
    # ta0=0, ta1=ta0+t1 etc. up til tak-1=0+...+t(k-1)
    # The last tk is saved to make the end time

    prngT = np.random.RandomState(seed = ST)
    prngA = np.random.RandomState(seed = SA)

    if Tdist==0: # Degenerate distribution
        Tw = tw*np.ones(K)
    elif Tdist==1: #exponential waiting times
        Tw = prngT.exponential(scale=tw,size=K)
    elif Tdist == 2: #
        Tw = prngT.rayleigh(scale=np.sqrt(2./np.pi)*tw, size = K)
    elif Tdist ==3:
        Tw = prngT.uniform(low=0.0, high=2*tw, size=K)
    else:
        print('Invalid Tdist!')
        return None
    if randT == True:
        np.random.shuffle(Tw)
    Tw=np.insert(Tw,0.,0)
```

```
    Ta=np.cumsum(Tw[:-1])
    # Generate amplitudes
    if Adist==0:
        A=mA*np.ones(K)
    elif Adist==1:
        A=prngA.exponential(scale=mA, size=K)
    elif Adist==2:
        A=prngA.rayleigh(scale=np.sqrt(2./np.pi)*mA, size=K)
    elif Adist ==3:
        A = prngA.uniform(low=0.0, high=2.*mA, size=K)
    else:
        print('Invalid Adist!')
        return None
    if randA == True:
        np.random.shuffle(A)
    tend=Ta[-1]+Tw[-1]

    return Ta,A,tend

def make_signal(Ta,A,tend,dt,tr,tf,cutoff=10**-30,
                derivative=False,waveform = 0):
    import numpy as np
    """ This function creates the signal:
    Ta : array of arrival times
    A : array of amplitudes
    N: number of time points
    K: number of bursts
    dt : time resolution
    tr: rise time
    tf: fall time (tr+tf=1)
    cutoff: when to stop calculating
    derivative: Is this the main signal or its derivative?
    waveform: 0: exponential,
              1: box (no dependence on tr/tf)
              2: gaussian (no dependence on tr/tf)

    Return signal and time vector T.

    In the following,
    t_ refers to time in the main signal, s refers to time per burst
    """
    if waveform !=0:
        tr=0.5
        tf=0.5

    T=np.arange(0,tend,dt)
    N=len(T)
    K=len(A)
```

```
# The only thing separating the signal and its derivative
# is a factor in front of the waveform.
if derivative == False:
    pr=1.
    pf=1.
elif derivative == True:
    if tr != 0:
        pr=1/tr
    elif tr == 0:
        pr = 1.
    if tf != 0:
        pf=-1/tf
    elif tf == 0:
        pf = -1

# Define the waveform
if waveform == 0:
    def psi(t):
        psi=np.zeros(len(t))
        if tr != 0 and tf != 0:
            L=np.where(t<=0)[0][-1]
            psi[0:L]=pr*np.exp(t[0:L]/tr)
            psi[L:]=pf*np.exp(-t[L:]/tf)
        elif tr == 0:
            psi = pf*np.exp(-t/tf)
        elif tf == 0:
            psi=pr*np.exp(t/tr)
        return psi

elif waveform == 1:
    def psi(t):
        psi=np.zeros(len(t))
        L=np.where(t<=0)[0][-1] #Midpoint of box
        xmax = L+(tf+tr)/(2*dt)
        xmin = L-(tf+tr)/(2*dt)
        psi[xmin:xmax]=1
        return psi

elif waveform == 2:
    def psi(t):
        psi = np.exp(-np.pi*(t/(tr+tf))**2)
        return psi

sgnl = np.zeros(N) #Main signal array

for k in range(0,K):
    tk= Ta[k]
    a = A[k]
    #How much should we include?
```

```
            #We find the times where the burst falls below cutoff,
            #and remove those.
            #Thus the bursts become significalntly shorter.
            # Also, make sure we don't go uotside the time domain:
            smin = max( -tk, tr * np.log(cutoff/(a*pr)))
            smax = min(tend-tk-dt, - tf * np.log(cutoff/abs(a*pf)))
            # above: - dt to stay inside domain
            S=np.arange(smin,smax,dt)
            sgnl_tmp=psi(S)
            tstart=int(round((tk+smin)/dt))
            tstop=tstart+len(sgnl_tmp)
            sgnl[tstart:tstop] += a*sgnl_tmp

        # There is a problem with the last point going to zero.
        # This is a quick fix to make sure it doesn't
        sgnl = sgnl[:-1]
        T = T[:-1]
        return sgnl, T

def derivative(S,dt,run = None, polyfit = False):
    ''' This function takes the derivative of a given signal S.
    S: the signal
    dt: the time resoultion of the signal
    run: if run is given, a running mean of window run is taken.

    this uses the numpy gradient method. From the website:
        The gradient is computed using second order accurate
        central differences in the interior and either first differences or
        second order accurate one-sides (forward or backwards) differences
        at the boundaries.
        The returned gradient hence has the same shape as the input array.

    returns the derivative dS as a numpy array.
    '''

    def make_pdSn(Sn,dt):
        """
        This function estimates the derivative of Sn by doing the follwing:
        for each point Sn[i]:
            - five points are used to fit the signal Sn to a polynomial
              p(t)=a*t^2+b*t+c at the middle point Sn[i]
              (so two points at each side of Sn[i])
            - This polynomial is then derivated; p'(t)=2at+b.
            - The middle point is stored, pdSn[i] = p'(0) = b
            - First and last points are fitted to a 1.st degree polynomial
              with first and second point. (so p(t)=a*t+b; pdSn[0]=a)
            - Second and next to last points are midpoins of
              2nd. deg polynomial with 3 points (one on each side)
        """
```

```
        N = len(Sn)
        pndSn = np.zeros(N)

        # first point
        pndSn[0]=np.polyfit([0,dt],Sn[:2],1)[0]
        #second point
        pndSn[1]=np.polyfit([-dt,0,dt],Sn[:3],2)[1]
        #next-to last point
        pndSn[-2]=np.polyfit([-dt,0,dt],Sn[-3:],2)[1]
        # last point
        pndSn[-1]=np.polyfit([-dt,0],Sn[-2:],1)[0]

        for i in range(2, N-2):
            pndSn[i]=np.polyfit([-2*dt,-dt,0,dt,2*dt],Sn[i-2:i+3],2)[1]
            #print(i/N)
        return pndSn

    def runmean(values,window):
        import numpy as np
        weigths = np.repeat(1.0, window)/window
        #including valid will REQUIRE there to be enough datapoints.
        #for example, if you take out valid, it will start @ point one,
        #not having any prior points, so itll be 1+0+0 = 1 /3 = .3333

        # OTOH, using 'same' ensures we have the same amount of points
        # as before. There may be boundary issues as stated above
        smas = np.convolve(values, weigths, 'same')
        return smas # as a numpy array
    if polyfit==True:
        dS = make_pdSn(S,dt)
    elif polyfit == False:
        dS=np.gradient(S) / dt

    if run != None and run != 0:
        dS=runmean(dS,run)
    return dS

def distribution(Data,N,kernel=False,ccdf = True):
    """ This function calculates the pdf and ccdf of Data,
        either by histogram or by gaussian kernels.
    N:
    If histogram is used, N is the number of bins to separate the data into.
    If kernel is used, N gives the number of data points.
    ccdf: if true, returns the complementary cdf
    """
    if kernel==False:
        # Calculate waiting time distributions
        hist, edges = np.histogram(Data,N)
        #We are interested in the middle points inside the bins,
```

```
        # not the edges of the bins:
        bin_centers=np.array([(edges[i]+edges[i+1])/2
                              for i in range(0,len(edges)-1)])

        pmf = hist/sum(hist) # Probability mass function (pmf) of T_w

        # Probability density function (pdf) of T_w
        pdf= hist / np.trapz(hist, x=bin_centers)

        # The cummulative distribution function (cdf)
        cdf = np.zeros(N)
        cdf[0] = pmf[0]
        for n in range(1,N):
            cdf[n] = cdf[n-1] + pmf[n]
        if ccdf == True:
            # We want the complementary cummulative distribution function
            cdf=1.0-cdf

        return pdf, cdf, bin_centers
    elif kernel==True:
        X = np.linspace(min(Data),max(Data),N)

        pdf_func=sps.gaussian_kde(Data)
        pdf=pdf_func(X)

        cdf_func = lambda ary:
            np.array([pdf_func.integrate_box_1d(-np.inf, x) for x in ary])
        cdf=1-cdf_func(X)

        return pdf, cdf, X

def RS_make(sgnl,dt):
    """ This function estimates the power spectral density
        and autocorrelation function of a signal.
    The normalized process is used,
    so the normalized autocorr and psd will be given.
    sgnl: The realized process
    dt: sampling time
    """

    sgnl = (sgnl-np.mean(sgnl))/(np.std(sgnl)) # Normalize the signal

    def estimate_autcorrelation(x):
        """
        Modified, the original is found at:
        http://stackoverflow.com/q/14297012/190597
        http://en.wikipedia.org/wiki/Autocorrelation#Estimation
        """
        n = len(x)
```

```
        r = np.correlate(x, x, mode = 'full')[-n:]
        r = r/(np.arange(n, 0, -1))
        return r

    N=len(sgnl)
    T=dt*np.arange(N)
    estR=estimate_autcorrelation(sgnl)
    f,estS=scs.welch(sgnl,fs=1./dt,nperseg=2**13)

    return f, estS, T, estR

def cond_av(signal,time,dt,trig,delta):
    """ This function creates the conditional average of a given signal.
    Input:
    signal: the signal itself
    time: the time vector of the signal
          (assumed to be as long as the signal)
    dt: the time step in the time vector
    trig: trigger treshold. Default is 2.5
    delta: 2*delta is both the width of the recording
          and the minimal distance between two peaks.
    In this implementation, recordings can touch, but can't overlap.
    delta is measured in time.

    Output:
    signal_av: conditionally averaged signal
    time_av: the time scale of the conditional averaging (for plotting)
    peaks: peak amplitudes
    wait: waiting times between peak values
    """
    ''' Lowest order moments of the signal '''
    sgnl_avg = np.mean(signal) # Mean of signal
    sgnl_std = np.std(signal) # Standard Deviation of signal

    '''Conditional averaging of signal'''
    sgnl = (signal-sgnl_avg)/sgnl_std # The rms-normalized signal
    print('(rms/mean)^2 = {}'.format(sgnl_std**2/sgnl_avg**2))
    print('normalization done')

    places=np.where(sgnl>trig)[0]
    print('Length of signal is {}, objects to be checked are {}.'
                                    .format(len(signal),len(places)))
    s_tmp=np.array([signal[places],time[places]])

    # Sort according to amplitudes in signal,
    # keeping time together with signal
    # (also flip, so highest values are first)
    s_tmp=np.take(s_tmp,s_tmp[0,:].argsort(),1)[:,::-1]
    print('assignment and sorting done')
```

```
    index = 0
    # This is the main loop. It picks out peaks,
    # making sure peaks are not close to peaks already chosen.
    while index<len(s_tmp[0,:]):
        #The indexes of those close to the current peak
        # (have to add one as this gives the indexes from the next)
        t_to_close=np.where(abs(s_tmp[1,index+1:]
                        -s_tmp[1,index])<=2*delta)[0]+(index+1)
        s_tmp=np.delete(s_tmp,t_to_close,1)
        index+=1
    # The peaks are the remaining valus after all superflous have been deleted.
    peak_values=s_tmp[0,:]
    time_trig=s_tmp[1,:]
    time_trig=np.sort(time_trig)
    wait=np.array([(time_trig[i+1]-time_trig[i])
                   for i in range(0,len(time_trig)-1)])
    time_trig_ind=np.round((time_trig-time[0])/dt).astype(int)
    print('main loop done, {} bursts recorded'.format(len(s_tmp[0,:])))

    signal_av=np.zeros(2*int(delta/dt)+1)
    # Iterate through the selected instances,
    # registering the required parts of the main signal
    for i in range(0,len(time_trig_ind)):
        # Lowest index of selected part (make sure it is after start)
        low_ind=max(0,time_trig_ind[i]-int(delta/dt))
        # Highest index of selected part (make sure it is before end)
        high_ind=min(len(signal),time_trig_ind[i]+int(delta/dt)+1)
        #In case we don't have an array of the full length, we need to pad it.
        pad=( 2*int(delta/dt) +1) - ( high_ind-low_ind )
        signal_av=signal_av + np.append( signal[low_ind:high_ind]
                                , np.zeros(pad) )/len(time_trig_ind)

    # This is the time vector of the signal, for easier plotting
    time_av=np.array(range(-int(delta/dt),int(delta/dt)+1))*dt

    return signal_av, time_av, peak_values, wait

def excess_stat(S,A,dt):
    ''' This finds the total time spent above threshold Theta,
    number of upwards crossings N and average time above threshold avT.
    It also returns the length of all excess times given A as a dictionary:
    dT_array={A[0]:[t01,t02,t03,...],A[1]:[t11,t12,t13,...]...}, to be used
    for calculating the pdf P(dT|A)
    by looking directly at the array itself.
    S: the signal
    A: a numpy array of threshold values
    dt: time resolution
    '''
```

```
    Theta_array = np.array([])
    N_array = np.array([])
    avT_array = np.array([])
    rmsT_array = np.array([])
    dT_dict={}
    for a in A:
        #This is the basis:
        #    the parts of the signal that are above the threshold.
        places = np.where(S>a)[0]
        if len(places)>0:
            #print('Num, places to check:{}'.format(len(places)))
            Theta = dt*len(places)

            #Find N, avT an distribution of dT
            # Each blob is connected,
            # so discrete blobs have more than one time length between them
            dplaces = places[1:]-places[:-1]
            # split the array
            # at places where distance between points is greater than one
            split = np.where(dplaces!=1)[0]
            lT = np.split(dplaces,split)
             # To get correct length of the first
            lT[0] = np.append(lT[0],1)
            # Number of upwards crossings is equal to number of blobs
            N = len(lT)
            if places[0]==0:
                N+=(-1) #Don't count the first blob if there is no crossing.
            # Array of excess times
            dT = np.array([dt*len(lT[i]) for i in range(0,len(lT))])
            avT = np.mean(dT)
            rmsT = np.std(dT)
        elif len(places)==0:
            Theta = 0
            N = 0
            avT = 0
            rmsT = 0
            dT=np.array([])
        Theta_array = np.append(Theta_array,Theta)
        N_array = np.append(N_array,N)
        avT_array = np.append(avT_array,avT)
        rmsT_array = np.append(rmsT_array,rmsT)
        dT_dict.update({a:dT})
    return Theta_array, N_array, avT_array, rmsT_array, dT_dict

def excess_stat_pdf_dT(dT,dt,A):
    '''
␣␣␣␣Calculate␣the␣pdf␣P(dT|A)␣and␣avT␣from␣this␣pdf.
␣␣␣␣dT:␣dictionary.␣Should␣be␣found␣using␣excess_stat,␣above.
␣␣␣␣A:␣threshold␣values
```

```
    n: length of time array

    Returns the time array t, the array of averages avT_th2,
    and the 2d-array dTpdf, containing the pdfs.
    t and dTpdf are both 2d-arrays storing the values for each
    A along the axis. The pdf for A[i] is dTpdf[i,:], t[i,:].
    '''
    avT_th2 = np.zeros(len(A))
    dTpdf = np.zeros((len(A),32))
    t = np.zeros((len(A),32))

    for i in range(0,len(A)):
        a = A[i]
        if len(dT[a])>=1:
            dTpdf[i,:],bin_edges=np.histogram(dT[a],bins=32,density=True)
            t[i,:] = (bin_edges[1:]+bin_edges[:-1])/2 #Record bin centers
            avT_th2[i] = spi.simps(dTpdf[i,:],t[i,:])
        else:
            continue # Need not do anything, everything is zeroes.
        #print('{} of {} done'.format(i+1,len(A)),flush = True)
    return avT_th2, dTpdf, t
```

Bibliography

G. Y. Antar, G. Counsell, and :-W-Ahn. On the scaling of avaloids and turbulence with the average density approaching the density limit. *Physics of Plasmas (1994-present)*, 12(8), 2005.

H. Biermé and A. Desolneux. A fourier approach for the level crossings of shot noise processes with jumps. *J. Appl. Probab.*, 49(1):100–113, 03 2012. doi: 10.1239/jap/1331216836. URL http://dx.doi.org/10.1239/jap/1331216836.

D. Block, I. Teliban, F. Greiner, and A. Piel. Prospects and limitations of conditional averaging. *Physica Scripta*, 2006(T122):25–33, February 2006.

J. A. Boedo, D. Rudakov, R. Moyer, S. Krasheninnikov, D. Whyte, G. McKee, G. Tynan, M. Schaffer, P. Stangeby, P. West, S. Allen, T. Evans, R. Fonck, E. Hollmann, A. Leonard, A. Mahdavi, G. Porter, M. Tillack, and G. Antar. Transport by intermittent convection in the boundary of the diii-d tokamak. *Physics of Plasmas (1994-present)*, 8(11):4826–4833, 2001.

O. J. Boxma and U. Yechiali. *Poisson Processes, Ordinary and Compound*. Wiley, 2007.

D. A. D'Ippolito, J. R. Myra, and S. J. Zweben. Convective transport by intermittent blob-filaments: Comparison of theory and experiment. *Physics of Plasmas (1994-present)*, 18(6):060501, 2011. doi: http://dx.doi.org/10.1063/1.3594609. URL http://scitation.aip.org/content/aip/journal/pop/18/6/10.1063/1.3594609.

L. Fattorini, Å. Fredriksen, H. L. Pécseli, C. Riccardi, and J. K. Trulsen. Turbulent transport in a toroidal magnetized plasma. *Plasma Physics and Controlled Fusion*, 54(8):085017, 2012. URL http://stacks.iop.org/0741-3335/54/i=8/a=085017.

T. K. Fowler. Nuclear power - fusion. *Reviews of Modern Physics*, 71(2):S456–S459, 1999.

Å. Fredriksen, H. L. Pécseli, and J. Trulsen. Crash and recovery of the potential in a torodial plasma column, as observed by generalized onditional sampling. *New Journal of Physics*, 10(033030):19, March 2008.

J. Freidberg. *Plasma Physics and Fusion Energy*. Cambridge University Press, 2007.

O. E. Garcia. Blob transport in the plasma edge: a review. *Plasma and Fusion Research*, 4(019), 2009.

O. E. Garcia. Stochastic modeling of intermittent scrape-off layer plasma fluctuations. *Physical Review Letters*, 108(26), June 2012.

O. E. Garcia, I. Cziegler, R. Kube, B. LaBombard, and J. L. Terry. Burst statistics in alcator c-mod sol turbulence. *Journal of Nuclear Materials*, 438:S180–S183, 2013a.

O. E. Garcia, S. M. Fritzner, R. Kube, I. Cziegler, B. LaBombard, and J. L. Terry. Intermittent fluctuations in the alcator c-mod scrape-off layer. *Physics of Plasmas (1994-present)*, 20(5), 2013b.

O. E. Garcia, J. Horacek, and R. A. Pitts. Intermittent fluctuations in the tcv scrape-off layer. *Nuclear Fusion*, Forthcoming 2015.

O. Grulke, T. Klinger, and A. Piel. Experimental study of the dynamics of conditionally averaged structures in weakly developed electrostatic turbulence. *Physics of Plasmas (1994-present)*, 6(3):788–796, 1999. doi: http://dx.doi.org/10.1063/1.873318. URL `http://scitation.aip.org/content/aip/journal/pop/6/3/10.1063/1.873318`.

J. Horacek, R. A. Pitts, and J. P. Graves. Overview of edge electrostatic turbulence experiments on tcv. *Czechoslovak Journal of Physics*, 55(3):271–283, 2005. ISSN 0011-4626. doi: 10.1007/s10582-005-0040-z. URL `http://dx.doi.org/10.1007/s10582-005-0040-z`.

T. Huld, A. H. Nielsen, H. L. Pecseli, and J. J. Rasmussen. Coherent structures in twodimensional plasma turbulence. *Physics of Fluids B: Plasma Physics (1989-1993)*, 3(7):1609–1625, 1991.

B.-D. Israel and A. Nemirovsky. Level crossings of nondifferentialbe shot processes. *IEEE Transactions on Information Theory*, 18(1):27–34, January 1972.

L. Kristensen, M. Casanova, M.S. Courtney, and I. Troen. In search of a gust definition. *Boundary-Layer Meteorology*, 55(1-2):91–107, 1991. ISSN 0006-8314.

doi: 10.1007/BF00119328. URL http://dx.doi.org/10.1007/BF00119328.

R. Kube and O. E. Garcia. Convergence of statistical moments of particle density time series in scrape-off layer plasmas. *Physics of Plasmas (1994-present)*, 22 (1), 2015.

M. R. Leadbetter and G. V. Spaniolo. Reflections on rice's formulae for level crossings - history, extensions and use. *Australian & New Zealand Journal of Statistics*, 46(1):173–180, 2004.

R. J. Maqueda, D. P. Stotler, S. J. Zweben, and The NSTX Team. Intermittency in the scrape-off layer of the national spherical torus experiment during h-mode confinement. *Journal of Nuclear Materials*, 415:S459–S462, 2011.

A. H. Nielsen, H. L. Pecseli, and J. J. Rasmussen. Turbulent transport in low plasmas. *Physics of Plasmas (1994-present)*, 3(5):1530–1544, 1996.

F. J. Øynes, O.-M. Olsen, H. L. Pécseli, Å. Fredriksen, and K. Rypdal. Experimental study of low-frequency electrostatic fluctuations in a magnetized toroidal plasma. *Phys. Rev. E*, 57:2242–2255, Feb 1998. doi: 10.1103/PhysRevE.57.2242. URL http://link.aps.org/doi/10.1103/PhysRevE.57.2242.

H. L. Pécseli. *Fluctuations in Physical Systems*. Cambridge University Press, 2000.

S. O. Rice. Mathematical analysis of random noise. *Bell System Technical Journal*, 23(3):282–332, July 1944.

S. O. Rice. Mathematical analysis of random noise. *Bell System Technical Journal*, 24(1):46–156, 1945.

E. N. Rowland. The theory of the mean square variation of a function formed by adding known functions with random phases, and applications to the theories of the shot effect and of light. *Mathematical Proceedings of the Cambridge Philosophical Society*, 32(04):580–597, 1936.

D. L. Rudakov, J. A. Boedo, R. A. Moyer, S. Krasheninnikov, A. W. Leonard, M. A. Mahdavi, G. R. McKee, G. D. Porter, P. C. Stangeby, J. G. Watkins, W. P. West, D. G. Whyte, and G. Y. Antar. Fluctuation-driven transport in the diii-d boundary. *Plasma Physics and Controlled Fusion*, 44(6), 2002.

H. Sato, H. L. Pécseli, and J. Trulsen. Fluctuations in the direction of propagation of intermittent low-frequency ionospheric waves. *Journal of Geophysical Research*, 117(A03329):20, March 2012.

P. C. Stangeby. *The Plasma Boundary of Magnetic Fusion Devices*. Plasma Physics Series. Institute of Physics Publishing, 2000a.

P. C. Stangeby. A tutorial on some basic aspects of divertor physics. *Plasma Physics and Controlled Fusion*, 42:B271–B291, 2000b.

H. Stark and J. W. Woods. *Probability, Statistics and Random Processes for Engineers*. Pearson Education, 4. edition, 2012.

R. E. Walpole, R. H. Myers, S. L. Myers, and K. Ye. *Probability and Statistics for Engineers and Scientists*. Pearson Education, 8. edition, 2007.

A. J. Wootton. Edge turbulence. *Journal of Nuclear Materials*, 176-177(C):77–88, 1990.